Control Methods for Fail-Safety in Cooperative Automated Driving

G. Koudijs

DC 2016.001

Master's Thesis

Coach: ir. E. van Nunen

Supervisor: prof. dr. H. Nijmeijer

Eindhoven University of Technology
Master Automotive Technology
Department of Mechanical Engineering
Dynamics & Control

TNO
Technical Sciences
Department Integrated Vehicle Safety

Eindhoven, December, 2015

Abstract

Heavy-duty vehicle platooning potentially reduces labour costs, optimizes the road capacity, improves road safety, reduces emissions and reduces the vehicle idle times. To maximally exploit the fuel saving potential of vehicle platooning, the vehicles are aimed to drive at a time gap as small as possible. Hence the driver view is blocked and lateral automation is required. While driving fully automatically, the driver reaction time can be 1.5 upto 10s. Therefore, the driver cannot serve as backup in case of a failure, so the system should have its own backup: the fail-safety mode. The goal of this master's thesis is to propose control methods which bring the vehicle to a safe state in case of a threat applying longitudinal and/or lateral control and thereby improve the system availability. The considered safety scenario is a communication failure in combination with possible braking actions of the lead vehicle. Inter-vehicular communication of the actual vehicle acceleration enables the vehicles to drive at small time gaps, which is unsafe in case only on-board sensors are used. Hence, a communication failure brings the vehicle in a potential unsafe state. To validate the system behaviour in this scenario, 23 test cases are defined in which the system behaviour is evaluated based on five key performance indicators: for instance the number of collisions in the test cases. For evaluation of the system by simulations, a non-linear vehicle model of a tractor semi-trailer combination is used. To properly control the vehicle to a safe state, first some safety measures are defined to assess the threat for emergency braking and an evasive manoeuvre. Second, two emergency braking controllers are proposed: a controller assuming the system behaviour is known accurately and a sliding mode control approach. The first controller shows smoother behaviour at the cost of robustness compared to the sliding mode controller. The sliding mode controller is more robust to system uncertainties and disturbances. For the nominal system, both controllers are able to avoid collisions in all defined test cases in the communication failure scenario in simulations. In case of uncertain system parameters, collisions occur in the worse case scenario. However the impact speed is always limited to 20km/h. Experiment results show a high consistency with the simulation results. To increase the system availability, it is desired to activate a collision avoidance controller as late as possible. Therefore, evasive manoeuvring is investigated. For steering control in an evasive manoeuvre, also a sliding mode control approach is proposed. The controller robustness is evaluated in case of for instance sensor noise. Evasive manoeuvring by only steering avoids collisions in all defined test cases in simulation, but has to be activated before emergency braking to ensure rear-end collisions with the lead vehicle can be avoided. Hence, evasive manoeuvring will not increase the system availability compared to emergency braking. Combined braking and steering in an evasive manoeuvre potentially increases the system availability significantly. The developed techniques can be applied to control a combined manoeuvre. However, the influence of combined braking and steering on the vehicle dynamic behaviour has to be investigated further.

Acknowledgements

This master's thesis is the result of an interesting and educational graduation period. I want to express my gratitude to all people that contributed to this thesis. Special thanks go to my graduation professor Henk Nijmeijer for the useful comments and remarks on my work. This definitely contributed to the final level of this thesis and to my personal development. Next, I would like to express my gratitude to TNO for giving me the opportunity to perform the research in their organization and to use their expertise. Special thanks go to my TNO coach Ellen van Nunen. In spite of her busy schedule, she always found time to guide the process and to give helpful feedback. Furthermore, I want to thank all colleagues and fellow students at TNO, in particular ASD trainee Dimitrios Tzempetzis. Our interesting discussions and collaboration contributed to the level of the final product. Finally, I want to thank my family for supporting me throughout my study time.

December 2015.

Notation

Definitions

Failure	Event that occurs when the delivered service deviates from correct service (system function). Can also occur because the specification did not adequately describe its function.
Threat	Faults, errors and failures
Fail-safety	In the event of failure, no harm is caused, or at least a minimum of harm, to other devices or danger to personnel.
Fault-tolerance	The property that enables a system to continue operating properly in the event of the failure of (or one or more faults within) some of its components. If its operating quality decreases at all, the decrease is proportional to the severity of the failure.
False negative	The system was intended to intervene but it did not.
False positive	The system performs an intervention which was not required to ensure safety.
Finite time stability	The system trajectories remain within prescribed bounds for a finite time interval.
Lyapunov stability	Lyapunov stability proves the stability of an equilibrium point by proving that all trajectories in the vicinity of the equilibrium point converge to the equilibrium point.
Practical stability	The system trajectories remain within prescribed bounds for infinite time.

Abbreviations

BTN	Brake Threat Number
CACC	Cooperative Adaptive Cruise Control
CAD	Cooperative Automated Driving
MF	Magic Formula
SMC	Sliding Mode Controller
TTC	Time To Collision
TTS	Time To Steer

Symbols

Symbol	Description	Unit
$\underline{A}$	system state matrix	
a	acceleration	[m/s^2]
b	input scalar	[m/(s^{2}rad)]
C	cornering stiffness/differential inclusion limit	[N/rad]/[-]
d	inter-vehicle distance	[m]
F	force	[N]
f_{tyre}	normalized cornering stiffness	[1/rad]
g	gravitational acceleration	m/s^2]
$\underline{H}$	matrix containing the centripetal and Coriolis terms	
$\mathcal{H}$	host trajectory	
h_{cog}	height of the centre of gravity	[m]
J	moment of inertia	[kgm^2]
K	boundary layer gain	[-]
k	sliding surface gain	[-]
j	jerk	[m/s^3]
$\underline{L}$	observer gain matrix	
L	wheelbase	[m]
LW	lane width	[m]
l	length or distance	[m]
$\underline{M}$	mass-matrix	
M	moment	[Nm]
m	mass	[kg]
P	probability	[-]
$\underline{Q}$	matrix containing the applied forces	
$\underline{q}$	array of generalized coordinates	
r_{eff}	effective tyre radius	[m]
$\underline{S}$	matrix representing the generalised force directions	
s	track width/sliding variable	[m]/[-]
$\mathcal{T}$	lead trajectory	
t	actual time	[s]
t_{brake}	time of braking event	[s]
t_{ev}	evasive time of an evasive path	[s]
t_{fail}	time since failure occurred	[s]
t_{imp}	expected time of impact	[s]
t_p	prediction time	[s]
t_{reach}	time to reach the sliding surface	[s]
t_{trans}	transition time of a lane change path	[s]
$\underline{u}$	system input array	
u	control effort	[-]
V	Lyapunov candidate	
v	velocity in local tractor coordinate frame	[m/s]
$\underline{x}$	system state array	
x	longitudinal position in global coordinate frame	[m]
y	lateral position in global coordinate frame	[m]
y_{ev}	lateral displacement required to avoid a collision	[m]
α	tyre slip angle	[rad]
β	body slip angle	rad]
δ	steering angle of the front wheels	[rad]
ϵ	uncertainty factor	[-]
θ	time delay	[s]
κ	longitudinal slip	[-]
σ	relaxation length	[m]
τ	time constant	[s]
Φ	tractor heading angle	[rad]
ϕ	articulation angle between tractor and trailer	[rad]
ω	rotational velocity	[rad/s]

Subscripts and superscripts

Symbol	Description
0	value at t=t_0
b	braking system
ca	collision avoidance
e	error
H	host vehicle
f	front axle
fb	front bumper
$\mathcal{H}$	host vehicle trajectory
h	hitch point
i	arbitrary vehicle axle $i \in [f, r, t]$
j	vehicle side $j \in [r, l]$
L	lead vehicle
LL	preceding vehicle of the lead vehicle
l	left vehicle side
lat	lateral load transfer
lim	limit of an absolute value
$long$	longitudinal load transfer
$margin$	margin for safety
max	upper saturation limit of a value
min	lower saturation limit of a value
obs	observer
$pred$	variable belonging to the prediction-based controller
r	rear axle/right vehicle side
$radar$	radar
req	required to avoid a collision
ref	reference value
s	steering system
$stop$	stopping point
SMC	variable belonging to the sliding mode controller
$\mathcal{T}$	lead vehicle (predicted) trajectory
t	semi-trailer (axle)
$wifi$	communication
wh	rotational direction of the wheel
x	longitudinal direction of the global or vehicle frame
y	lateral direction of the global or vehicle frame
z	vertical vehicle axis
zz	around the vertical vehicle axis
$-$	lower limit
$+$	upper limit

Contents

Chapter 1

Introduction

TNO is the Dutch organization for applied scientific research. The Integrated Vehicle Safety department of TNO Automotive performs research in safety issues that arise in the field of cooperative automated driving (CAD). One of the internal projects is the development of a safety concept for CAD, focussed on heavy-duty vehicle platooning. In vehicle platooning, a set of vehicles is driving automatically at close following distances. This master's thesis contributes to a *fail-safety* algorithm in vehicle platooning. In this chapter, first a motivation for the research performed in this field is given. Second, the problem statement will be presented. Then, an overview of the available literature and the outline of the report will be given.

1.1 Motivation

The scope of this report is heavy-duty vehicle platooning. Motivators for heavy-duty vehicle platooning are:

- Decrease fuel consumption: For heavy-duty vehicle platooning, the fuel saving potential is 5-20% [5][15][20]. According to research of the NEA/Niwo (organization for Dutch transportation companies), expenditures on fuel account for 30% of all expenses of Dutch transportation companies. Hence, reducing fuel consumption is of major interest for heavy-duty vehicle owners.
- Labour cost reduction: If the vehicle performs the driving task fully automated for a period of time, the driver can take his rest improving time efficiency.
- Road capacity optimization: Arem et al. [10] investigate the influence of vehicle platooning on the traffic flow. The results show an improvement of traffic flow stability and a slight increase in traffic flow efficiency; consequently traffic throughput.
- Improvement of the road safety: According to the European Research and Safety report [54], 90% of the accidents in manual driving are caused by human error. This implies automation of the driver tasks has a huge potential in accident reduction (in case these systems are fail-safe).
- Emission reduction: Fuel consumption is directly related to the CO_2 emissions. Since vehicle platooning potentially decreases fuel consumption significantly, substantial reduction of the CO_2 emissions is expected when applying vehicle platooning.
- Asset utilisation optimization: Since the driver can take his rest when driving fully automated, the idle time of the vehicle can potentially be decreased.

To maximally exploit the fuel saving potential of vehicle platooning, the inter-vehicle time gap should be as small as possible [5]. An approach enabling these small time gaps is Cooperative Adaptive Cruise Control (CACC) [42]. This controller is an extension of Adaptive Cruise Control. In Adaptive Cruise Control the time gap is controlled based on the relative distance and relative velocity to the preceding vehicle, measured by on-board sensors. In CACC the acceleration information of the vehicles is communicated, enabling time gaps down to 0.3s. When driving at such short following distances, the driver view is blocked. Hence, the CAD system also includes lateral automation.

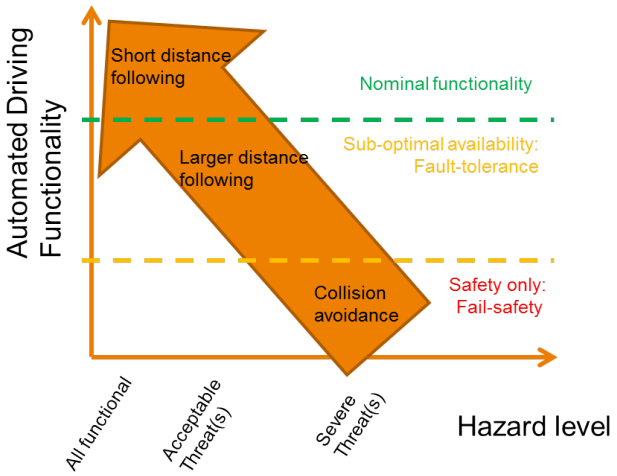

Fig 1.1: Safety approach

When proving technical feasibility in CAD, considering the occurrence of *threats* is usually not the first priority. A possible *threat* is a *failure*: an event that occurs when the delivered service deviates from the correct service. There are multiple events that can cause a deviation in the system behaviour, such as unexpected behaviour of other road users. Since the CAD system is not designed to ensure safety in all hazardous situations due to other traffic, this is referred as a *failure*. Further, hardware and software *failures* can occur. In vehicle platooning, the driver cannot serve as backup in case of a *failure* because of two reasons. First, the vehicles are driving at small time gaps down to 0.3s; consequently the driver view is blocked. Second, when driving fully automatically the driver does not have a driving task any more. Hence, the driver reaction time can be 1.5 upto 10s depending on the driver state [33]. If the following vehicle drives at a 0.3s time gap, the driver is incapable to intervene in time to avoid a collision [58]. Therefore, the system should have its own reliable backup in case a *failure* occurs: the *fail-safety* mode. In order to increase the system availability, the system should keep its functionality, or part of its functionality, as long as possible. A possible approach is illustrated in Fig 1.1. The following levels of remaining system functionality can be distinguished:

- *Nominal functionality*: short distance following is possible without endangering a collision.
- *Fault-tolerance*: in case of one or more *failures*, the system keeps its functionality. Based on the severity of the *threat*, the operating quality decreases accordingly.
- *Fail-safety*: in the event of *failure*, no harm is caused, or at least a minimum of harm, to other devices or danger to personnel.

The approach in Fig 1.1 is very general. The detailed system behaviour in presence of *threats* has to be defined. This report will contribute to the system behaviour definition.

1.2 Problem statement

To add safety functionality to the CAD system, the goal of this master's thesis is to contribute to the *fail-safety* algorithm. As mentioned in the previous section, the focus is on heavy-duty vehicle platooning. There are multiple possible *threats*; this thesis concentrates on a specific *threat*: a wireless communication *failure*. The reasons for considering this specific safety scenario are:

- *Failure* of the wireless link is a regular occurring *failure* based on experience.
- The inter-vehicular communication enables the vehicles to drive at small time gaps, which is not safe without communication [42]. Hence, a communication *failure* is potentially a significant *threat* to the system.
- It is expected that the *fail-safety* techniques for this specific safety scenario can be extended towards other safety scenarios.

The communication *failure* safety scenario shown in Fig 1.2 can be described as follows:

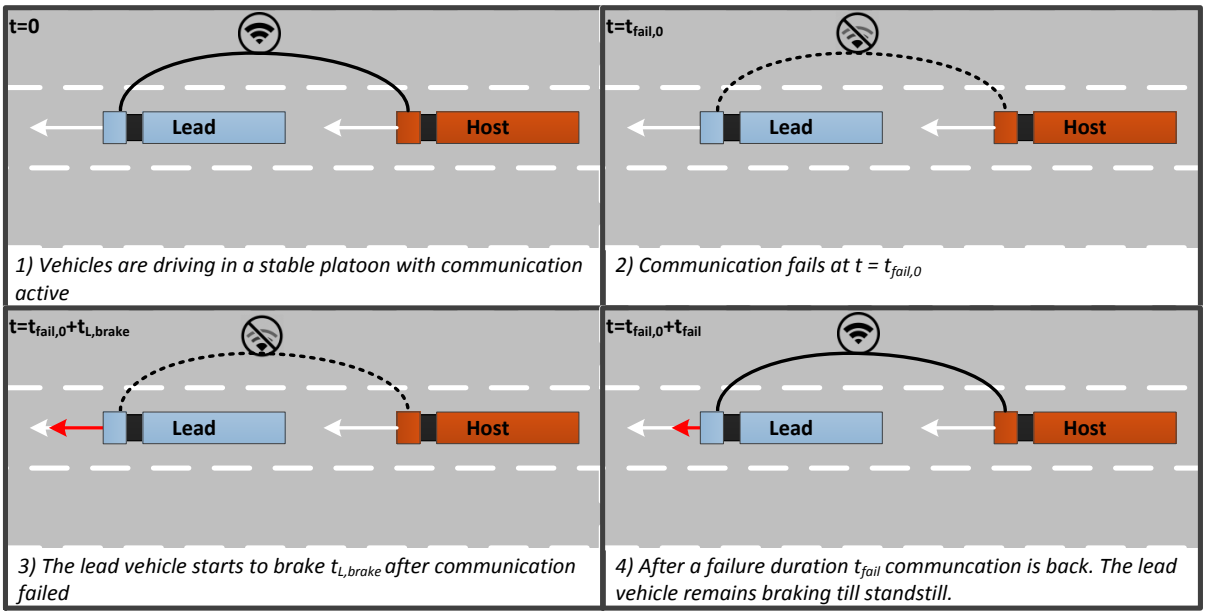

Fig 1.2: Illustration of the safety scenario

Scenario Attributes		Simulations	
Failure duration	Lead acceleration	Collision	Impact
0.1s	-6m/s^2	No	0km/h
1s	-6m/s^2	Yes	20km/h
10s	-4m/s^2	Yes	8km/h
10s	-6m/s^2	Yes	21km/h

Table 1.1: Simulation results of the nominal controller for specific test cases. The lead vehicle brakes exactly at the moment the communication failure occurs.

Two heavy-duty vehicles are driving 80km/h on the highway in a platoon with a time gap of 0.3s. Suddenly a communication *failure* occurs: for a certain duration no communicated data is available. In case the lead vehicle would decide to brake this situation is potentially unsafe. Table 1.1 shows the simulation results of the current TNO CAD system, without added safety functionality, for some safety critical use cases within this safety scenario. The first column shows the communication *failure* duration, the second column the intended braking effort of the lead vehicle from the moment communication fails, the third column shows whether a collision occurs and the fourth column the impact speed of the possible collision. There are several cases where collisions occur with upto 21km/h impact.

The research question related to this safety scenario is:

- When and how to bring a heavy-duty vehicle driving in a platoon on the highway towards a safe state in case of a communication *failure* applying longitudinal and/or lateral control?

In the research question, a communication *failure* is considered as specific *threat*. However, the developed *fail-safety* techniques for the communication *failure* potentially can be applied to a wide range of other *threats*. Since the objective is to bring the vehicle to a safe state, (steady) safe states have to be defined. The steady safe states that will be considered in this report are:

- drive at an increased following distance,
- standstill in the same lane,
- driving in the adjacent lane,
- standstill in the emergency lane.

The complete list of pre-defined steady safe states for the CAD system can be found in the report of Tzempetzis [56], Table 5-1. The following delimitations and assumptions are considered during the research:

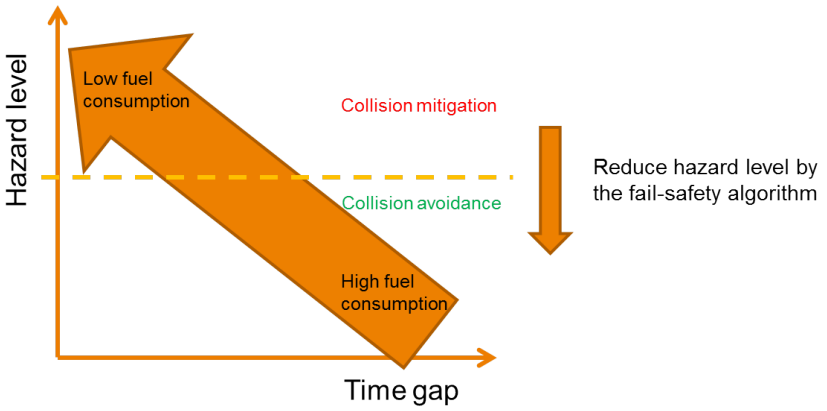

Fig 1.3: Problem definition

1. The low-level controllers are outside the scope of the project. The *fail-safety* algorithm will give a reference value for steering angle and longitudinal acceleration to the low-level controllers.
2. The required software and hardware for obtaining the input signals are outside the scope of the project.
3. The algorithms will be tested in simulation and partly in experiments. Because the heavy-duty vehicles are not fully equipped yet, experiments have to be performed with passenger cars.
4. No *failures* in the braking and steering actuation are considered.
5. Only control of the host vehicle will be considered. Evasive actions of the lead vehicle in parallel can be investigated in future research.
6. It is assumed that the vehicle acts fully autonomous in *fail-safety* mode: the driver is assumed to be outside the control loop.
7. A tractor semi-trailer combination is considered, because this is the most common heavy-duty vehicle combination.
8. Highway platooning is assumed, since driving on the highway with relatively high velocities platooning has the largest fuel saving potential. On the highway, cornering radii will be small.
9. The vehicle platoon is assumed to be stable when a *threat* occurs: no initial control errors.
10. The weather conditions are assumed to be such that the road surface is dry and the visibility of the camera is not limited by sunlight, fog, etc.
11. A homogeneous platoon is assumed: the vehicles in the platoon are identical.

In Fig 1.3, the objective of this thesis is illustrated. A possible hazard (*threat*) to the system is a communication *failure*. For smaller time gaps the hazard level increases. However, to achieve maximum fuel consumption reduction, the time gap should be as small as possible. Above a certain hazard level avoidance of collisions cannot be guaranteed. In that case, the objective of the *fail-safety* algorithm is to mitigate the severity of a possible collision. The objective of this thesis is to keep the hazard level as low as possible when vehicles are driving at a nominal time gap of 0.3s, in combination with a communication *failure*. The applied techniques can be braking, steering or a combination of braking and steering.

1.3 Related work

To maximally exploit the fuel saving potential of vehicle platooning, the time gap between the vehicles should be as small as possible [5]. The smallest possible time gap for which a vehicle platoon with an arbitrary number of vehicles is stable is by Ploeg [42] referred as string stable time gap. Here, also a CACC approach is proposed. In CACC the acceleration of the vehicles is communicated, enabling the vehicles to drive at short following distances. In case communication fails, graceful degradation to an increased time gap is proposed, which is string stable without communicated acceleration data. However, the safety in the transition phase is not assessed. For passenger cars, in [37] the safe following distance between the vehicles in a platoon is evaluated by a particle model, considering three possibilities in collision avoidance: only braking, evasive manoeuvring by only steering and evasive manoeuvring by

integrated braking and steering. In case the platoon is driving with 80km/h, emergency braking requires the largest safe following distance (4m), then evasive manoeuvring by only steering (2m) and evasive manoeuvring by integrated braking and steering requires the shortest safe following distance (1m). In case the vehicle velocity is below 40km/h, braking is always more beneficial. In [37] also evasive actions of the preceding vehicle are considered. In case the lead vehicle steers to the one side and the following vehicle to the other side of the lane, the safe following distance can be decreased even further. However, all previous mentioned literature is on passenger cars. Calculation of a safe following distance by only braking for heavy-duty vehicles is discussed in [6]. Here, a differential game approach is used to calculate safe sets from which a safe following distance is determined.

Collision avoidance systems that are on the market currently focus on braking only. Over the last years these systems have become available in middle and high end cars. The prediction of the heavy-duty vehicle stopping distance and directional behaviour in a brake event is evaluated in [17]. This report concludes that parameters influencing the brake torque are e.g. the applied pressure, vehicle speed and brake temperature. As mentioned by [34], heavy-duty vehicle braking actuators are slow, which degrades the braking performance significantly. Next, literature on collision avoidance of standstill objects will be mentioned. The distance needed for an emergency action will be referred as the safety distance; a shorter safety distance implies collision avoidance by braking and/or steering can be activated at a later moment, resulting in an increased system availability. For passenger cars is proven in [3], [37] and [49] that at higher velocities the safety distance can be decreased by evasive manoeuvring compared to only braking. The lateral acceleration of passenger cars is limited by tyre grip; for heavy-duty vehicles this is limited by the roll-over limit which limits the potential of evasive manoeuvring. A collision avoidance controller using lateral and longitudinal control for a heavy-duty vehicle is developed in [27] and [38]. First step in these citations is comparing the possibilities for braking and steering by an optimal control definition of the system. The considered system is a particle model with constrains on the longitudinal and lateral accelerations. One of the results is shown in Fig 1.4. Note that this figure shows the safety distance for a standstill object and not for a platoon. It is found that the break-even point for only braking and only steering is at 78km/h. Combining braking and steering in an evasive manoeuvre could reduce the break-even point for only braking and an evasive manoeuvre to 68km/h. In case of a low friction coefficient road surface, which is not shown in the figure, steering has already a shorter safety distance from 35km/h. The control algorithms are designed for a rigid truck, not for an articulated vehicle.

Based on the previous paragraph, it is expected that an evasive manoeuvre is beneficial in some cases. However, an evasive manoeuvre adds new challenges, since other traffic participants or barriers can obstruct the region to steer to. Heavy-duty vehicles add another challenge: lateral vehicle instability. Fig 1.5 shows that a significant part of the accidents are due to jackknifing or roll-overs, which are usually the result of lateral vehicle instability. Volvo research [54] concludes 15% of the fatal accidents involving heavy-duty vehicles are due to lateral instability, of which 12% are jackknifing and 88% are roll-over accidents. Hence, it can be concluded that caution has to be taken when performing a lateral manoeuvre with a heavy-duty vehicle. To investigate and evaluate the vehicle behaviour in possible strategies, the vehicle should be modelled. Modelling of a truck for collision avoidance purposes is discussed in [14]. This model includes non-linear tyre behaviour and vehicle roll dynamics for a rigid truck. The behaviour and modelling of articulated vehicles is discussed in [36] based on [40]. However, in these citations vertical vehicle dynamics and non-linear (tyre) behaviour are not included. Control strategies for lateral truck stabilization are presented in for instance [46] and [59].

Only braking, only steering and integrated braking and steering are possible actions in collision avoidance. This section will evaluate some possible control strategies to perform these manoeuvres. Focussing on braking first, in [18] an automatic emergency braking system is described. It calculates the required deceleration to avoid a collision and applies this required deceleration to the system. Braking system dynamics, a stop distance and vehicle dynamics are taken into account for the required deceleration calculation. Alternatively, the relative velocity to the lead vehicle or an object in front of the vehicle can be controlled. In [23] and [28] a sliding mode controller is designed to control the relative velocity to the preceding vehicle. These two sources propose a sliding mode controller to control steering actions as well. A similar sliding mode control approach for steering is proposed in [4], [53] and [57]. In [27] a classical PID-controller is used to control evasive manoeuvring with heavy-duty vehicles. The sliding mode controller and PID-controller control objective is to follow a path determined by a path planning algorithm. An evaluation of different lane change trajectories for path generation can be found in [53]. Path planning in more complex environments using polynomial fitting is proposed in [21]. Here a path

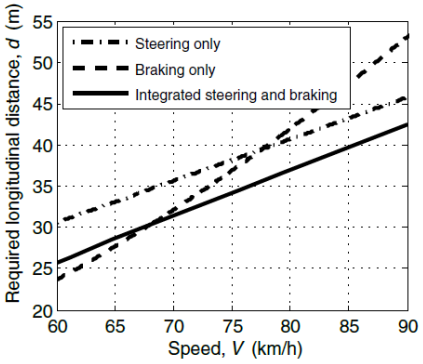

Fig 1.4: A comparison of different evasive manoeuvres [27]

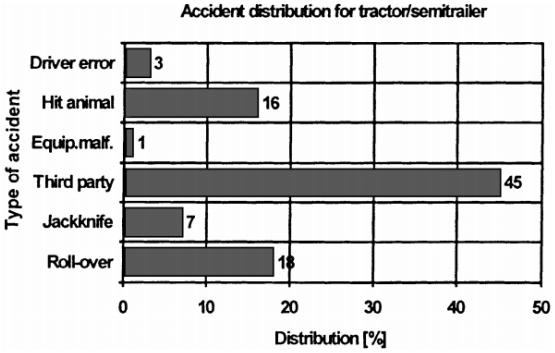

Fig 1.5: The results of heavy-duty vehicle accident analysis [52]

with constant lateral acceleration segments is proposed. Since constant acceleration profiles are not realizable for a vehicle, an extension using constant jerk segments is proposed in [22]. Alternatively to the PID-controller and sliding mode controller, a model predictive control approach can be applied. In model predictive approaches for lateral control, predicted position maps or reachability maps are used to determine a safe corridor. The safe corridor is the region in the environment that is collision free. Within the safe corridor an optimal path is searched by optimization methods. The optimization can be based on for instance slip angles, lateral acceleration or steering wheel angle rate. Constraints on for example lateral acceleration and jerk are possible as well. Examples of model predictive control applied to lateral vehicle control in automotive applications can be found in [11], [51] and [55]. The most significant disadvantage of model predictive control methods is the computational load, especially in case the complexity of the models (e.g. non-linear models) and environment increases. For safety critical applications, the complexity of the optimization function is challenging for system certification [30]. Moreover, the constraints posed on the system are time varying. Hence, the calculated optimal control input for the actual time instant might not be the optimal control input over the full manoeuvre. A model predictive controller for emergency braking is presented in [47]. Instead of the methods based on path planning, also reactive control methods are investigated. Reactive control is fast and easy to implement. It determines for every time step a control effort based on virtual forces. Virtual forces can be derived from for instance vehicle dynamics and road hazards. Most significant disadvantage is that there is no pre-determined path. Since obstacles can change position during the manoeuvre, there is no guarantee that the path where the vehicle ends up is collision free. A possible reactive control method is presented in [48], referred as a virtual bumper controller. Here, a virtual force is added to environmental obstacles forcing the vehicle to a safer region. The longitudinal and lateral dynamics are controlled separately and the vehicle dynamic bounds are considered. The principle of virtual forces is used in potential field methods as well, discussed in for instance [24] and [25]. Repelling forces are added to environmental hazards and the vehicle dynamic limitations, forcing the trajectory of the vehicle to a safer region. An interesting alternative potential field method is presented in [50]. Fluid dynamics are used to determine the vehicle heading and velocity. A complete different approach not requiring path planning is *finite time stability*. *Finite time stability* is not yet applied to collision avoidance purposes. This approach prescribes bounds on the system trajectories for a finite time interval. For collision avoidance purposes these bounds can describe a safe region which the system trajectories should not exceed in order to be safe. A review on *finite time stability* is presented in Appendix F.

Summarizing, based on the literature the time gap between the vehicles should be as small as possible to maximally exploit the fuel saving potential of vehicle platooning. CACC is a possible technique enabling these short following distances. In case the communication between the vehicles fails, the short following distance is potentially unsafe. Hence, collision avoidance techniques have to be developed to ensure safety when communication fails. Braking is the most trivial collision avoidance action. However, it is expected that evasive manoeuvring can reduce the safety distance in some cases, especially when combined braking and steering is considered. Caution has to be taken when performing a lateral manoeuvre with a heavy-duty vehicle, since there is a high risk on lateral instability. There are several possible techniques to control an emergency braking action or an evasive manoeuvre, such as classical PID-control, sliding mode control, model predictive control and potential field methods.

1.4 Structure of the report

The methodology to approach the problem statement will be discussed in Chapter 2. Moreover, the system architecture which complies to the ISO26262 standard [1] will be presented, in which the proposed techniques are aimed to be implemented. To develop and validate the proposed techniques, a vehicle model is needed. The used vehicle models are presented in Chapter 3. The system architecture can be divided into three parts. The detection mechanism, the decisions and the actions. The detection mechanism and decisions will be discussed in Chapter 4. The applied controllers to perform the longitudinal and lateral actions will be discussed in Chapter 5 and 6 respectively. Finally, Chapter 7 will give the conclusions and recommendations for future work.

Chapter 2

Methodology

In this chapter, the approach towards the proposal for a *fail-safety* algorithm is discussed. First, the proscess followed during this research is presented. The techniques that will be developed in this thesis are aimed to be implemented in a defined system architecture which complies to the ISO26262 standard [1], which is discussed in the second part of this chapter.

2.1 Development process

The development process towards the *fail-safety* algorithm can be divided into the several steps. First, to develop and evaluate the control methods proposed in this study, a vehicle model is needed. Using the vehicle model, techniques can be developed. The research will consist of the following steps:

1. **Development of a vehicle model:** To develop and analyse the control methods proposed in this study, a vehicle model is needed. In Section 1.3 is concluded based on literature that evasive manoeuvring could be beneficial compared to only braking as collision avoidance technique. Since integrated braking and steering is expected to have the highest potential in avoiding accidents, the model should be able to incorporate braking and steering simultaneously. However, there is a high risk on lateral instability for heavy-duty vehicles. Hence, only braking and only steering are considered as a first step towards integrated braking and steering. Therefore, decoupled models for longitudinal and lateral dynamics will be developed, since this simplifies the controller development significantly because design techniques aimed for linear systems can be used.

2. **Definition of safety measures to assess the *threat* and determine a strategy corresponding to the *threat* level:** To evaluate which intervention is preferable, safety measures have to be developed. Based on these safety measures, system modes can be selected accordingly. System modes could be for instance emergency braking, evasive manoeuvring or a *fault-tolerant* mode. Requirement for the safety measures is that they need to be accurate, such that *false positive* and *false negative* interventions can be prevented by the system. *False-negatives* might lead to collisions; *false positives* are undesired for comfort and are potentially hazardous for traffic approaching from behind. Moreover, the system should maintain its functionality, or part of its functionality, as long as possible to increase the system availability. Therefore a strategy has to be defined, which ensures safety and intervenes corresponding to the *threat* level.

3. **Longitudinal and lateral controller design:** This thesis concentrates on the vehicle control during the emergency braking and evasive manoeuvring actions in *fail-safety*. Since in most situations braking is expected to be sufficient to avoid an accident, first two controller types for emergency braking will be proposed and compared based on key performance indicators. After that, an evasive manoeuvring controller applying only steering will be developed. This is a first step towards an integrated braking and steering approach for evasive manoeuvring, which is expected to have a high potential to increase the system availability. Requirement for the lateral controller is that it should be robust to

- varying operating conditions considering the delimitations in Section 1.2,
- initial condition errors upto 30cm,
- and sensor noise with an amplitude upto 10cm.

Since no final decision is made with respect to the sensor set-up that will be applied for lateral control, the values to evaluate the robustness of the lateral controller are arbitrary chosen. In case the sensors are able to deliver the desired accuracy, the robustness analysis in this thesis is sufficient. In case a proposed sensor set-up is not able to deliver the desired accuracy, the robustness study has to be adapted to evaluate the feasibility of the proposed sensor set-up.
General requirements for the longitudinal and lateral controllers are that they should ensure safety and the interventions should correspond to the *threat* level. For instance, severe braking in case the *threat* is relatively low is undesired for comfort and safety. The key performance indicators for assessment of these requirements are:

- Number of collisions: the number of collisions in the test cases, that will be defined, should be minimized.
- Impact speed: in case a collision occurs, the accident severity can be rated by the impact speed.
- Minimum inter-vehicle distance: In case this distance is large, the controller might be too conservative. In case the inter-vehicle distance is very small, the controller might be too risky. The minimum inter-vehicle distance in case of lateral manoeuvring is defined as the distance between the front corner of the host vehicle and rear corner of the lead vehicle that are the closest to each other.
- Maximum deceleration: The maximum deceleration is seen as measure for comfort. Less deceleration is assumed to be more comfortable. *False positive* interventions can be evaluated with this indicator, since *false positives* will lead to an unnecessary high deceleration.
- Maximum lateral acceleration: This is only relevant in case an evasive manoeuvre is performed. Less lateral acceleration is assumed to be more comfortable. Besides that, a high lateral acceleration might lead to roll-overs. Hence, the maximum lateral acceleration is a measure for comfort and safety.

4. **Evaluation by simulations and experiments**. Evaluation of the longitudinal and lateral collision avoidance controllers will be done by simulations. When possible by time constraints, the longitudinal controllers will be validated by experiments. Experiments to evaluate the lateral controller cannot be performed, since the vehicles are currently insufficiently equipped to apply lateral control in collision avoidance. The controllers will be evaluated in the communication *failure* scenario presented in Section 1.2. To evaluate the key performance indicators listed at the previous step, a set of test cases is defined by the following steps:
   (a) Assumptions: The assumption is that both vehicles have the same braking capacity (upto -6m/s^2) and drive with 80km/h at a following distance of 10m.
   (b) Safety scenario parameters:
      - *Failure* duration.
      - Start time of lead vehicle deceleration with respect to the *failure*: When communication fails the behaviour of the lead vehicle is crucial.
      - The lead vehicle deceleration. The values for the lead vehicle acceleration are in the range from -6m/s^2 to 0m/s^2.
      - Traffic density: The system might adapt its behaviour to the traffic conditions.
   (c) Test case derivation: The test cases are derived from a combination of the safety scenario parameters. For safety related functionality, the test cases cover all the critical combinations. Beside that, the test cases incorporate non-hazardous cases to evaluate the system sensitivity to *false positives*. Based on that, a set of 23 test cases is defined as shown in Appendix E.2.

   Since no sufficiently equipped heavy-duty vehicle is available, the experiments will be performed with passenger cars. Hence, only the general system behaviour can be validated in practice.

These four steps will be performed to come to a proposal to control the vehicle to a safe state in case of a communication *failure*.

2.2 System architecture

This master's thesis is part of a larger project in TNO: the Safety Concept Approach. In close collaboration a system architecture is defined, in which the techniques proposed in this report will be implemented. For more detailed information about the system architecture, the reader is referred to the report of Tzempetzis [56]. In this section, first the global system architecture will be explained. Then, the relevant sub-blocks will be discussed in more detail.

Fig 2.1 illustrates the current TNO CAD system. The system hardware is depicted by the bottom two blocks; the software by the top four blocks. The central unit is the Supervisor, which is responsible for the decisions in the system. Actions are performed by the High-level Controllers and Low-level Controllers. The controllers and Supervisor require measurement data of the current host vehicle state and environmental perception. Measurement data is obtained from sensors and wireless communication, which is processed in the Sensor Processing Unit. A more detailed illustration of the Supervisor is shown in

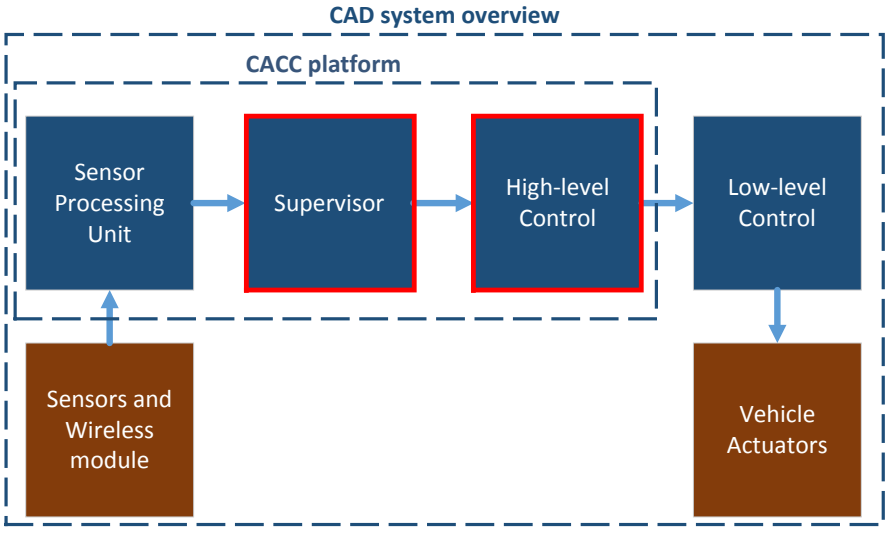

Fig 2.1: TNO CAD system overview [56]

Fig 2.2. In the Supervisor, Safety and Performance related decisions are split into the Safety Decision Unit and Performance Decision Unit respectively. The *fail-safety* functions belong to the safety mechanism in the Safety Decision Unit, which includes the following components required by the ISO26262 standard [1]:

1. Detection mechanism (Situation Awareness).
2. Decisions (Safety Mode Selection).
3. Actions (Safety Algorithm).

These blocks will be discussed in more detail in the following paragraph. This thesis will contribute mainly to the Situation Awareness, Safety Algorithm and High-level Control blocks.

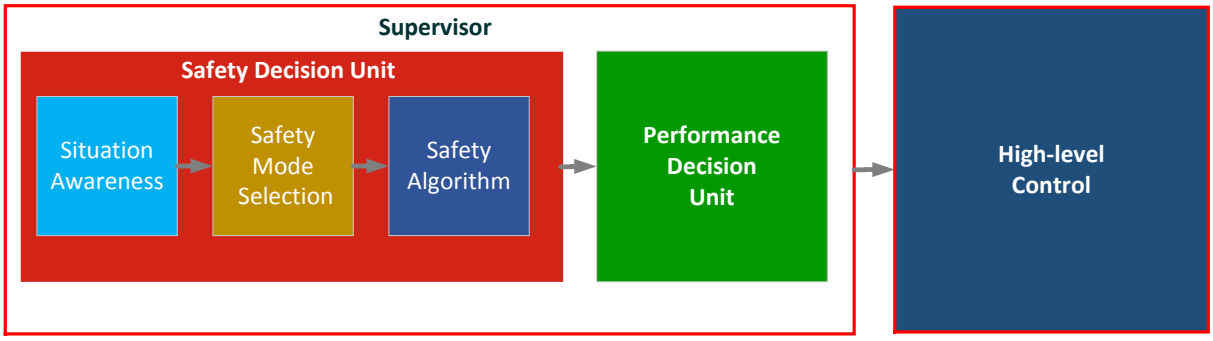

Fig 2.2: The Supervisor block with Decision Units and High-level control block [56]

Situation Awareness consists of several components, for instance object classification and *threat* assessment. This thesis contributes to the *threat* assessment task of the Situation Awareness block by defining some safety measures, which will be used by the Supervisor and controllers. The Safety Mode Selection is able to select modes, corresponding to the *threat* severity as illustrated in Fig 1.1. For each safety scenario, a statechart diagram has to be defined that brings the vehicle to one of the steady safe states defined in Section 1.2. The Safety Algorithm and High-level Controllers both determine how a task selected by the Safety Mode Selection will be performed. Task of the Safety Algorithm is for example the calculation of a safe following distance. The control of the system to achieve the safe distance or follow an escape path is the task of the High-level Controllers. The actions will also be influenced directly by the Situation Awareness outputs.

2.3 Summary

First the methodology followed in this thesis is presented. The first step in the methodology will be the development of a vehicle model to evaluate vehicle manoeuvres. Based on this, some safety measures will be defined. These safety measures will be used to select a system mode, one of which is collision avoidance. In collision avoidance, emergency braking and evasive manoeuvring are possible actions, for which controllers have to be designed. All controllers will be evaluated in simulations and when possible by experiments. The evaluation will be based on five key performance indicators in 23 predefined test cases. The defined key performance indicators are:

- Number of collisions: the number of collisions in the test cases.
- Impact speed: in case a collision occurs, the accident severity can be rated by the impact speed.
- Minimum inter-vehicle distance: A large distance might indicate the algorithm is too conservative; a short distance might indicate too risky behaviour.
- Maximum deceleration: Less deceleration is assumed to be more comfortable.
- Maximum lateral acceleration: Lateral acceleration is only relevant for evasive manoeuvring. More lateral acceleration is considered as uncomfortable and dangerous, since heavy-duty vehicles are sensible for lateral instability.

The second part of this chapter presented the system architecture in which the *fail-safety* algorithms will be implemented. The safety measure calculation will be implemented in the Situation Awareness block. Based on the safety measures, the Safety Mode Selection block will select a system mode corresponding to the *threat* level. How the actions selected by the Safety Mode selection will be performed is determined by the Safety Algorithm and High-level Controllers.

Chapter 3

Dynamic vehicle model

To evaluate and develop control methods for *fail-safety*, a vehicle model is needed. The applied vehicle model has been selected considering the application of the *fail-safety* algorithm mentioned in Section 1.2:

– A tractor semi-trailer combination heavy-duty vehicle will be considered (Fig 3.1).

– The scenario is highway platooning at 80km/h. The corner radii on highways are generally small.

First, a non-linear model will be presented. Next, linearised versions for only longitudinal and only lateral dynamics will be derived. The linearised models cannot incorporate integrated braking and steering, since constant longitudinal velocity needs to be assumed to linearise the lateral vehicle model. The models will be compared with measurement data. The parameter values used in the simulations can be found in Appendix A.1.

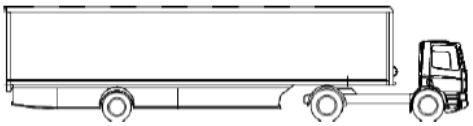

Fig 3.1: Tractor semi-trailer combination [36]

3.1 Non-linear model

The basics of the non-linear model are derived from the linearised bicycle model presented by Pacejka [40] and applied by Luijten [36]. Since the model will be used for collision avoidance purposes, it is expected that the limits in which linear tyre behaviour can be assumed will be exceeded. Therefore, non-linear tyre characteristics and load transfer have been added to the model in this thesis. Further, the Pacejka model only included lateral dynamics; longitudinal dynamics have been added in this thesis. First, the assumptions and approximations applied in the model are listed. Then the equations of motion for the chassis will be stated and the non-linear tyre characteristics will be discussed. The final section will discuss the braking and steering actuator dynamics.

3.1.1 Assumptions

The assumptions for the non-linear model are:

1. Pitch and roll dynamics are neglected. For calculation of longitudinal and lateral load transfer rigid bodies are assumed.
2. Because of the highway application, the small angle assumption for heading angles, steering angle, articulation angle and slip angles is applied: $\sin(x) \approx x$ and $\cos(x) \approx 1$. The small angle assumption is valid since according to TNO research [44] a roll-over will occur with 60km/h at a steering angle of 2°.

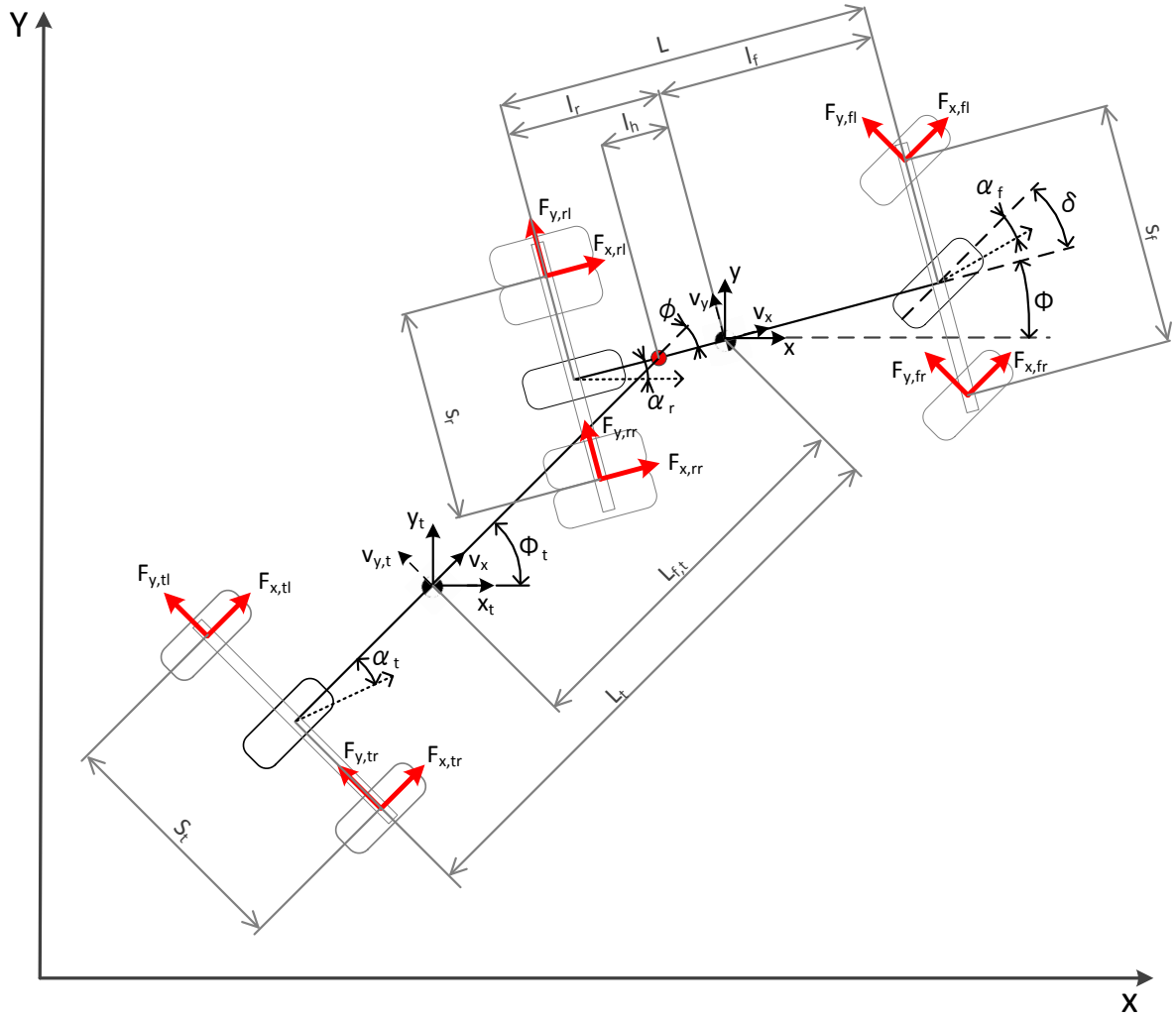

Fig 3.2: Illustration of the vehicle model

This value decreases quadratically with increasing velocities. Similar values hold for the articulation angle.

3. Longitudinal and lateral control can be applied for collision avoidance. Hence, the model should accept steering and braking input.
4. The left and right tyres on the same axle have the same steering and slip angle. The elasticity in the steering system is neglected.
5. The hitch point is assumed to be in the ground plane. Hence the hight of the hitch point does not influence the longitudinal and lateral load transfer.
6. Centre point steering is assumed; there is no pneumatic or mechanical trail.
7. No aerodynamic drag, gradient resistance and influence of side winds is modelled.
8. A constant effective tyre radius is assumed and the tyre rolling resistance is neglected.
9. In case of dual tyres, both carry half of the load on that particular wheel, as in e.g. [14] and [27].

3.1.2 Equations of motion for the chassis

The derivation of the equations of motion for the vehicle chassis using Lagrange is elaborated in Appendix A.2. It is possible to write the system in the following form:

$$\underline{M}\ \underline{\ddot{q}}(t) + \underline{H}\left(\underline{\dot{q}}(t)\right) = \underline{S}\left(\underline{q}(t), t\right) \underline{Q}(t), \tag{3.1}$$

where $\underline{q}$ are the generalised coordinates, $\underline{M}$ is the mass matrix, the matrix $\underline{H}$ contains the Coriolis and centripetal terms, $\underline{S}$ represents the force directions and $\underline{Q}$ the applied forces. The generalized coordinates

are chosen to be independent:

$$\dot{q}(t) = \left[v_x(t),\ v_y(t),\ \dot{\Phi}(t),\ \dot{\phi}(t)\right]^T, \tag{3.2}$$

where v_x is the forward velocity of the tractor in the local tractor coordinate frame, v_y the lateral velocity, Φ the tractor heading angle in the global coordinate frame and ϕ the articulation angle between the tractor and the trailer. The matrices for (3.1), assuming small heading angles, slip angles, steering angle and articulation angle (Assumption 2), are defined as

$$\underline{M} = \begin{bmatrix} m+m_t & 0 & 0 & 0 \\ 0 & m+m_t & -m_t(l_h+l_{f,t}) & -m_t l_{f,t} \\ 0 & -m_t l_h & J_{zz}+m_t l_h(l_h+l_{f,t}) & m_t l_h l_{f,t} \\ 0 & -m_t l_{f,t} & J_{zz,t}+m_t l_{f,t}(l_h+l_{f,t}) & J_{zz,t}+m_t l_{f,t}^2 \end{bmatrix} \quad \underline{H}(\underline{\dot{q}}(t)) = \begin{bmatrix} -(m+m_t)v_y(t)\dot{\Phi}(t) \\ (m+m_t)v_x(t)\dot{\Phi}(t) \\ -m_t l_h v_x(t)\dot{\Phi}(t) \\ -m_t l_{f,t} v_x(t)\dot{\Phi}(t) \end{bmatrix}$$

$$\underline{S}(\underline{q}(t),t) = \begin{bmatrix} 1 & 1 & 1 & 1 & 1 & 1 & -\delta(t) & -\delta(t) & 0 & 0 & -\phi(t) & -\phi(t) \\ \delta(t) & \delta(t) & 0 & 0 & \phi(t) & \phi(t) & 1 & 1 & 1 & 1 & 1 & 1 \\ l_f\delta(t)-\frac{s_f}{2} & l_f\delta(t)+\frac{s_f}{2} & -\frac{s_r}{2} & \frac{s_r}{2} & -l_h\phi(t) & -l_h\phi(t) & l_f+\frac{s_f}{2}\delta(t) & l_f-\frac{s_f}{2}\delta(t) & -l_r & -l_r & -l_h & -l_h \\ 0 & 0 & 0 & 0 & -\frac{s_t}{2} & \frac{s_t}{2} & 0 & 0 & 0 & 0 & -L_t & -L_t \end{bmatrix}$$

$$\underline{Q}(t) = \begin{bmatrix} F_{x,fl}(t) & F_{x,fr}(t) & F_{x,rl}(t) & F_{x,rr}(t) & F_{x,tl}(t) & F_{x,tr}(t) & F_{y,fl}(t) & F_{y,fr}(t) & F_{y,rl}(t) & F_{y,rr}(t) & F_{y,tl}(t) & F_{y,tr}(t) \end{bmatrix}^T, \tag{3.3}$$

An illustration of the vehicle model is shown in Fig 3.2. Subscripts f, r and t are used for the front axle, rear axle and trailer respectively. When referring to a specific wheel on an axle, l and r are added to the subscript to denote the left or right wheel on that axle. In (3.3), m is the body mass, J_{zz} the moment of inertia around the vertical axis, l_f the distance of the centre of mass of the tractor to the front axle, $l_{f,t}$ the distance from the centre of mass of the trailer to the hitch point, l_h the distance from the tractor centre of mass to the hitch point, L the wheelbase of the tractor, s_i the track width of axle i, $F_{x,ij}$ the longitudinal tyre force at wheel ij, $F_{y,ij}$ the lateral tyre force and δ the steering angle of the front wheels. How the tyre forces in $\underline{Q}$ are obtained will be discussed in the next section.

3.1.3 Tyre forces

For calculation of the tyre forces, at each wheel the same method is applied. The tyre forces are calculated using the magic formula (MF) [40], which is a function for calculating the tyre forces:

$$[F_{x,ij}(t),\ F_{y,ij}(t),\ M_{zz,ij}(t)] = MF\left(\alpha_i'(t),\ \kappa_{ij}'(t),\ \mu,\ \tilde{F}_{z,ij}(t)\right). \tag{3.4}$$

Input for the function are the lateral slip angle α_i, longitudinal slip κ_{ij}, tyre to road friction coefficient μ and dynamic vertical force $\tilde{F}_{z,ij}$. The tyre to road friction coefficient is assumed to be constant. The other input variables will be elaborated on in the following paragraphs. The accents on α_i and κ_{ij} denote the slip including tyre relaxation, which will be discussed as well. Output of the magic formula are the longitudinal force $F_{x,ij}$, the lateral force $F_{y,ij}$ and the self-aligning moment $M_{zz,ij}$. The self-aligning moment is neglected since centre point steering is assumed (Assumption 6).

Lateral slip angle

Note that the slip angles for the left and right wheels are assumed to be identical (Assumption 4). Hence the slip angles are calculated per axle. Moreover, the longitudinal velocity of all axles is assumed to be equal. The linearised equations for the slip angles around $\alpha_i = 0$ yield:

$$\begin{aligned} \alpha_f(t) &= \delta(t) - \left(\frac{v_y(t) + l_f\dot{\Phi}(t)}{v_x(t)}\right) \\ \alpha_r(t) &= -\left(\frac{v_y(t) - l_r\dot{\Phi}(t)}{v_x(t)}\right) \\ \alpha_t(t) &= \phi(t) - \left(\frac{v_y(t) - (l_h+L_t)\dot{\Phi}(t) + L_t\dot{\phi}(t)}{v_x(t)}\right). \end{aligned} \tag{3.5}$$

The derivation of these linearised slip angle equations can be found in Appendix A.3.

Longitudinal slip

The moment equilibrium for a rotating wheel is described by:

$$\dot{\omega}_{wh,ij}(t) = \frac{1}{J_{wh,ij}} \left(-F_{x,ij}(t) r_{eff,ij} + M_{wh,ij}(t)\right), \tag{3.6}$$

where $\omega_{wh,ij}$ is the rotational velocity of the wheel, $J_{wh,ij}$ the wheel inertia, $r_{eff,ij}$ the constant effective tyre radius (Assumption 8) and $M_{wh,ij}$ the moment acting on the wheel. The longitudinal slip κ_{ij} is defined as:

$$\kappa_{ij}(t) = \frac{v_{x,ij}(t) - \omega_{ij}(t)\, r_{eff,ij}}{|v_{x,ij}(t)|}, \tag{3.7}$$

where $v_{x,ij}$ are local forward velocities at the tire contact points.

Relaxation

The tyre forces cannot be generated instantly. The lag in the tyre force generation is controlled by a relaxation length (σ) [40]. This phenomenon can be described by the following equations:

$$\dot{\kappa}'_{ij}(t) = \frac{v_{x,ij}(t)}{\sigma_x} \left(\kappa_{ij}(t) - \kappa'_{ij}(t)\right), \quad \dot{\alpha}'_i(t) = \frac{v_x(t)}{\sigma_y} \left(\alpha_i(t) - \alpha'_i(t)\right). \tag{3.8}$$

Remark. Note that for the slip angles, the longitudinal velocity is assumed to be equal for all axles. In contrast, local velocities at the wheels are used for the longitudinal slip calculation.

Weight transfer

The longitudinal and lateral accelerations are assumed to be decoupled (Assumption 1). Hence, the longitudinal load transfer can be calculated first as per axle loads. For visualization, see Fig 3.3. The longitudinal load transfers are:

$$\Delta F_{z,long}(t) = m a_x(t) \frac{h_{cog}}{L}, \quad \Delta F_{z,long,t}(t) = m_t a_x(t) \frac{h_{cog,t}}{L_t}, \tag{3.9}$$

where a_x is the longitudinal acceleration, which is assumed to be equal for the tractor and trailer, and h_{cog} the height of the centre of gravity. The following equations for the dynamic per axle loads can be derived:

$$\begin{aligned} \tilde{F}_{z,f}(t) &= F_{z,f} - \Delta F_{z,long}(t) + \tilde{F}_{z,h}(t) \frac{L - l_h}{L}, & \tilde{F}_{z,r}(t) &= F_{z,r} + \Delta F_{z,long}(t) + \tilde{F}_{z,h}(t) \frac{l_h}{L}, \\ \tilde{F}_{z,h}(t) &= F_{z,h} - \Delta F_{z,long,t}(t), & \tilde{F}_{z,t}(t) &= F_{z,t} + \Delta F_{z,long,t}(t), \end{aligned} \tag{3.10}$$

where tilde denotes the dynamic loads. $F_{z,h}$ is the load on the hitch point. Note that the hitch point is assumed to be in the ground plane (Assumption 5). Hence longitudinal and lateral forces in the hitch point are not influencing the load transfer. The lateral load transfers can be calculated by:

$$\Delta F_{z,lat,f}(t) = \frac{h_{cog}}{s_f} \frac{\tilde{F}_{z,f}(t)}{g} a_y(t), \quad \Delta F_{z,lat,r}(t) = \frac{h_{cog}}{s_r} \frac{\tilde{F}_{z,r}(t)}{g} a_y(t), \quad \Delta F_{z,lat,t}(t) = \frac{h_{cog,t}}{s_t} \frac{\tilde{F}_{z,t}(t)}{g} a_{y,t}(t), \tag{3.11}$$

where g is the gravitational acceleration; a_y and $a_{y,t}$ are the lateral acceleration of the truck and trailer respectively. Based on this, the per wheel loads can be calculated:

$$\begin{aligned} \tilde{F}_{z,fl}(t) &= \frac{1}{2}\tilde{F}_{z,f}(t) - \Delta F_{z,lat,f}(t) & \tilde{F}_{z,fr}(t) &= \frac{1}{2}\tilde{F}_{z,f}(t) + \Delta F_{z,lat,f}(t) \\ \tilde{F}_{z,rl}(t) &= \frac{1}{2}\tilde{F}_{z,r}(t) - \Delta F_{z,lat,r}(t) & \tilde{F}_{z,rr}(t) &= \frac{1}{2}\tilde{F}_{z,r}(t) + \Delta F_{z,lat,r}(t) \\ \tilde{F}_{z,tl}(t) &= \frac{1}{2}\tilde{F}_{z,t}(t) - \Delta F_{z,lat,t}(t) & \tilde{F}_{z,tr}(t) &= \frac{1}{2}\tilde{F}_{z,t}(t) + \Delta F_{z,lat,t}(t). \end{aligned} \tag{3.12}$$

Since the rear axle of the truck has dual tyres, the calculated vertical load has to be divided over the two rear tyres because it is assumed that both tyres carry exactly half of the load (Assumption 9).

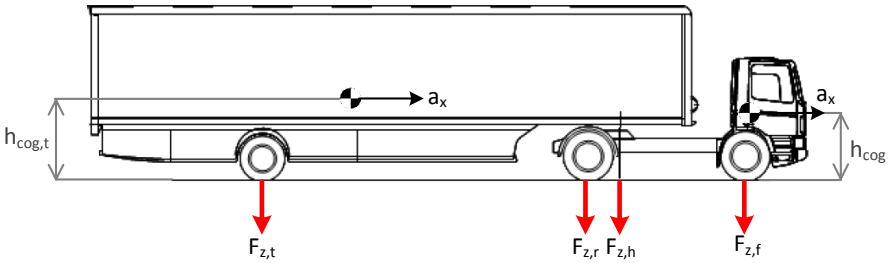

Fig 3.3: Side view of the vehicle to illustrate the longitudinal weight transfer

3.1.4 Actuator dynamics

The braking actuator is approximated with a time constant τ_b and a time delay θ_b:

$$\dot{M}_{wh,ij}(t) = \frac{1}{\tau_b}\left(M_{b,ij}(t-\theta_b) - M_{wh,ij}(t)\right), \tag{3.13}$$

where $M_{b,ij}$ is the applied braking moment and $M_{wh,ij}$ the moment applied to the wheel, which is the input for (3.6). Equivalent to the braking actuator, the steering actuator is modelled as a time constant τ_s and a time delay θ_s:

$$\dot{\delta}(t) = \frac{1}{\tau_s}\left(\delta_{ref}(t-\theta_s) - \delta(t)\right), \tag{3.14}$$

where δ_{ref} is the reference steering angle. The low-level controller will ensure behaviour of the actuators according to these differential equations. Changes to the low-level controllers are outside the scope of the project.

3.2 Linearised decoupled models and model validation

The model presented in the previous section is non-linear. For controller design it is desirable to have a linear approximation of the non-linear model, since it enables the possibility to analyse the system by useful tools, like pole-zero maps and bode diagrams. A linear approximation of the vehicle model for only longitudinal and only lateral dynamics is derived. For linearisation of the lateral vehicle model, a constant longitudinal velocity and a constant cornering stiffness are assumed; all angles are linearised around the origin. The linear models cannot incorporate combined braking and steering. For the longitudinal and lateral model, a comparison between the measurement data, the non-linear model and linear model will be performed.

3.2.1 Longitudinal model

When considering only longitudinal dynamics, the vehicle dynamic model can be simplified. The eigen-frequencies of the tyre are relatively high (>20Hz [40]). Noticing that the relaxation length is relatively small, it can be concluded that the influence of the longitudinal tyre relaxation is small. Hence the tyre dynamics can be neglected, implying the longitudinal vehicle dynamics can be approximated by only the braking system dynamics:

$$\dot{a}_x(t) = \frac{1}{\tau_b}\left(a_{x,ref}(t-\theta_b) - a_x(t)\right), \tag{3.15}$$

where $a_{x,ref}$ is the reference value for the longitudinal acceleration. A comparison between measurement data, the non-linear model and linearised model is shown in Fig 3.4. Both models represent the measurements well. The linearised longitudinal model is not able to incorporate lateral manoeuvring.

Remark. Only measurements upto -1m/s^2 are available. For collision avoidance purposes it is desired to perform additional tests with heavier braking to validate the model.

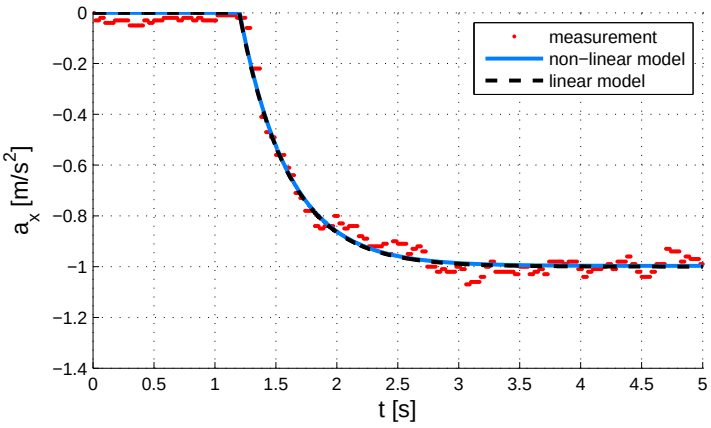

Fig 3.4: A comparison between measurement and simulation results for longitudinal dynamics

3.2.2 Lateral model

For describing only the lateral dynamics, system (3.1) can be linearised. Two assumptions have to be made:

1. The longitudinal velocity v_x is constant. Hence this model cannot incorporate braking.
2. No longitudinal forces are applied ($F_{x,ij} = 0$) and the magic formula calculating the lateral tyre forces can be approximated by:
$$F_{y,i}(t) = C_i \alpha_i(t), \tag{3.16}$$
where C_i is a constant cornering stiffness, defined for each axle i.

Remark. Note that because the magic formula is approximated by a constant cornering stiffness, no weight transfer is included in the linearised equations. For analysis a parameter space with $C_{i,min} \leq C_i \leq C_{i,max}$ could be investigated.

With these assumptions, system (3.1) can be rewritten using the coordinate frame

$$\underline{x}(t) = \begin{bmatrix} v_y(t), & \dot{\Phi}(t), & \dot{\phi}(t), & \phi(t) \end{bmatrix}^T \tag{3.17}$$

to a linear form

$$\underline{\tilde{M}}\ \underline{\dot{x}}(t) = \underline{\tilde{A}}\ \underline{x}(t) + \underline{\tilde{B}}\ \underline{u}(t) \tag{3.18}$$

with

$$\underline{\tilde{M}} = \begin{bmatrix} m+m_t & -m_t(l_h+l_{f,t}) & -m_t l_{f,t} & 0 \\ -m_t l_h & J_{zz}+m_t l_h(l_h+l_{f,t}) & m_t l_h l_{f,t} & 0 \\ -m_t l_{f,t} & J_{zz,t}+m_t l_{f,t}(l_h+l_{f,t}) & J_{zz,t}+m_t l_{f,t}^2 & 0 \\ 0 & 0 & 0 & 1 \end{bmatrix}, \quad \underline{\tilde{B}} = \begin{bmatrix} C_f \\ l_f C_f \\ 0 \\ 0 \end{bmatrix}, \quad \underline{u}(t) = \delta(t),$$

$$\underline{\tilde{A}} = -\frac{1}{v_x} \begin{bmatrix} C_f+C_r+C_t & l_f C_f - l_r C_r - C_t(l_h+L_t) + (m+m_t)v_x^2 & -C_t L & -C_t v_x \\ l_f C_f - l_r C_r - C_t l_h & l_f^2 C_f + l_r^2 C_r + C_t l_h(l_h+L_t) - m_t l_h v_x^2 & C_t l_h L & C_t l_h v_x \\ -C_t L_t & C_t L_t(l_h+L_t) - m_t l_{f,t} v_x^2 & C_t L_t^2 & C_t L_t v_x \\ 0 & 0 & -v_x & 0 \end{bmatrix} \tag{3.19}$$

Now by choosing $\underline{A} = \underline{\tilde{M}}^{-1}\underline{\tilde{A}}$ and $\underline{B} = \underline{\tilde{M}}^{-1}\underline{\tilde{B}}$, equation (3.18) can be rewritten as a time invariant state space system:

$$\underline{\dot{x}}(t) = \underline{A}\ \underline{x}(t) + \underline{B}\ \underline{u}(t). \tag{3.20}$$

As mentioned by Luijten [36], heavy-duty vehicles are generally neutrally steered. Hence, the cornering stiffnesses can be calculated using a constant normalized cornering stiffness f_{tyre} for all axles:

$$C_f = f_{tyre} F_{z,f}, \quad C_r = f_{tyre} F_{z,r}, \quad C_t = f_{tyre} F_{z,t}. \tag{3.21}$$

A comparison between measurement and simulation results of a lane change at 65km/h is shown in Fig 3.5. More information about the measurements and how they are performed can be found in [44]. The

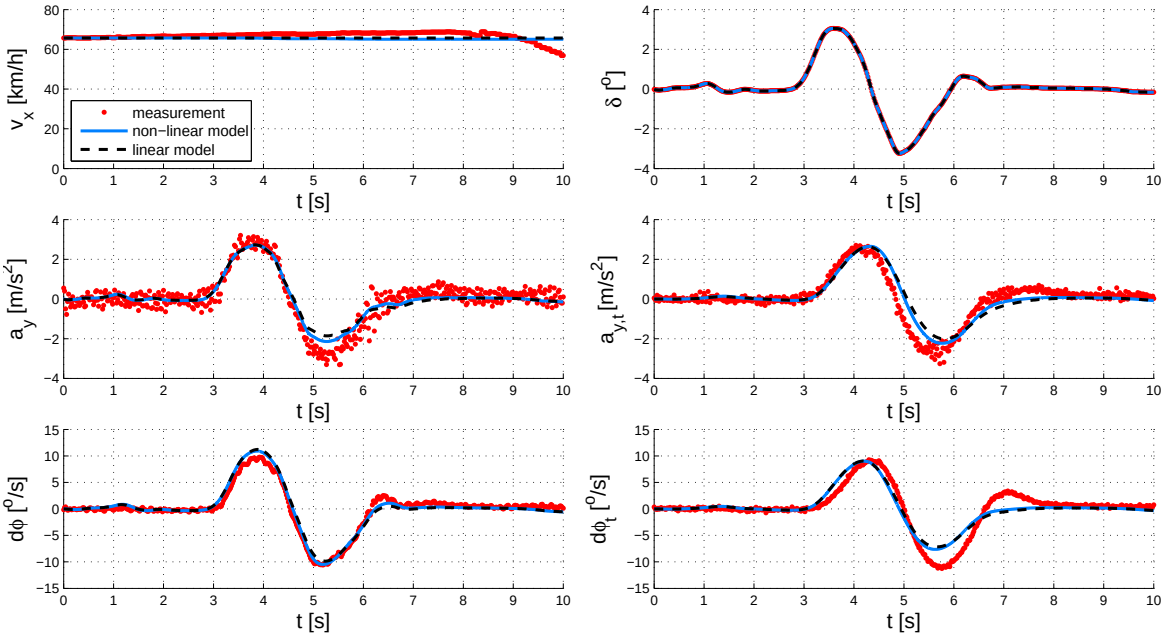

Fig 3.5: A comparison between measurements and simulation results for lateral dynamics

velocity and steering angles from the measurements are given as input to the simulation models (top plots). The lateral acceleration response of the truck and trailer is depicted in the middle plots. Both models are close to the measurements for the first part of the manoeuvre. For the second part of the manoeuvre, the simulation results and measurements start to deviate. The performance of the non-linear model for that part of the manoeuvre is better. The deviations are due to the load transfer (linear model) and unmodelled roll dynamics (both models). The yaw rate of the truck and trailer are shown in the bottom plots. The yaw rate of the truck is simulated accurately. Especially for the second part of the manoeuvre, the yaw rate of the trailer deviates. Apart from the unmodelled roll dynamics, it should also be noted that the simulation model includes a one axle trailer, whereas the tests are performed with a three axle trailer. This possibly explains the phase difference between the simulation results and measurements.

3.3 Summary

A non-linear heavy-duty vehicle model is presented in this chapter that is able to incorporate integrated braking and steering in a highway scenario. Non-linear tyre dynamics are included by the magic formula. Moreover, the model includes tyre relaxation and load transfer. The braking and steering actuators are modelled by a time constant and time delay. For only longitudinal dynamics, the non-linear model can be approximated by only the braking system dynamics. This fits the measurement data for a deceleration of 1m/s^2 well. For only lateral dynamics, the non-linear model can be approximated by a linear model, assuming a constant longitudinal velocity and a constant cornering stiffness. Simulation and measurement results are compared in a lane change manoeuvre. The lateral and non-linear models simulate the first part of the manoeuvre accurately. In the second part of the manoeuvre, the measurement and simulation results start to deviate due to the unmodelled roll-dynamics. The performance of the non-linear model is slightly better for the second part of the manoeuvre because it includes the load transfer.

Chapter 4

Situation Awareness and Safety Mode Selection

A CAD system, and especially its safety mechanism, is very dependent on its environmental perception. To determine which level of functionality can be kept (nominal behaviour, *fault-tolerance* or *fail-safety*), the severity of the *threat* needs to be assessed, as shown in Fig 1.1. Assessment of the *threat* is the task of the Situation Awareness block illustrated in Fig 2.2. For *threat* assessment, the behaviour of other traffic participants needs to be predicted, which will be discussed in Section 4.1. Because in the considered scenario vehicles are driving in a platoon, this thesis is restricted to prediction of the lead vehicle behaviour. The *threat* level is represented by safety measures, which will be defined in Section 4.2. In Section 4.3, the selection of the system modes based on the safety measures in the communication *failure* scenario is discussed.

4.1 Prediction of the worse case lead vehicle trajectory

The prediction of the lead vehicle trajectory is based on a worse case scenario, which is assumed to be an emergency stop of the lead vehicle. No steering actions of the lead vehicle are considered. The prediction of the worse case lead vehicle trajectory consists of two parts: first, estimating the actual lead vehicle state (Section 4.1.1) and second the prediction of the worse case future trajectory (Section 4.1.2). The final section will discuss the acceleration estimation during a communication *failure*.

4.1.1 Actual state estimation

Estimation of the actual lead vehicle state is based on measured and communicated data. An overview of the measured and communicated variables and how they are obtained is shown in Table 4.1. The inter-vehicle distance is given by variable d and the vehicle acceleration by a. Variables related to the lead vehicle will be denoted with subscript L. Signals measured by radar are denoted with subscript $radar$, signals obtained by communication with subscript $wifi$ and the reference values (desired values) with subscript ref. The time delay on the communicated variables and variables measured by radar is different. The values assumed for the time delays (θ) are shown in Table 4.2. The communication time delay is in practice 20ms, but it is assumed negligible in this section. Since the inter-vehicle distance and its derivative are obtained by radar measurements carrying time delay, prediction to the actual state is needed.

The actual state estimation is based on a worse case actual lead vehicle acceleration estimate ($\hat{a}_{L,x}$): if there is no acceleration data available, it is assumed that the lead vehicle is full braking. A distinction has to be made between two cases: first there is communication between the vehicles and second there is no communication. In case there is communication, the obtained signals are not synchronised because of the

Variable	Source	Description
$d_{L,radar}$	radar	inter-vehicle distance
$\dot{d}_{L,radar}$	radar	relative velocity
$a_{L,x,wifi}$	communication	actual acceleration
$a_{L,x,ref}$	communication	reference acceleration

Table 4.1: Sources for obtaining the lead vehicle state variables

different time delays on radar measurements and communicated data. Hence, the relative position and relative velocity of the lead vehicle for the current time step should be estimated by extrapolation from the measured data. A constant relative acceleration model between the host and lead vehicle is applied. In case there is no communication, no accurate information about the actual and reference acceleration of the lead vehicle is available, since no on-board sensor of the host vehicle is able to measure the actual lead vehicle acceleration accurately. The previous discussion results in the following equations to estimate the actual lead vehicle state:

$$\begin{aligned}
\hat{d}_L(t) &= d_{L,radar}(t) + \dot{d}_{L,radar}(t)\theta_{radar} + \frac{1}{2}\left(\hat{a}_{L,x}(t) - a_{H,x}(t)\right)\theta_{radar}^2, \\
\dot{\hat{d}}_L(t) &= \dot{d}_{L,radar}(t) + \left(\hat{a}_{L,x}(t) - a_{H,x}(t)\right)\theta_{radar}, \\
\hat{a}_{L,x}(t) &= \begin{cases} a_{L,x,wifi}(t) & \text{if communcation is active} \\ a_{L,x,min} & \text{if communcation is inactive,} \end{cases} \\
\hat{a}_{L,x,ref}(t) &= \begin{cases} a_{L,x,ref}(t) & \text{if communcation is active} \\ a_{L,x,min} & \text{if communcation is inactive,} \end{cases}
\end{aligned} \tag{4.1}$$

where hats denote estimated values. The host vehicle acceleration $a_{H,x}$ is assumed to be measured accurately and $a_{L,x,min}$ is the minimum acceleration of the lead vehicle. In (4.1) the communication is assumed to be always active or inactive. The transition phase between the active and inactive state will be discussed in Section 4.1.3.

4.1.2 Trajectory prediction

In the previous section the actual lead vehicle state estimation is discussed. This section will present a worse case future trajectory prediction for the lead vehicle given the actual state. The prediction starts at $t = t_0$. The prediction time is denoted with t_p. Note that this is a virtual prediction time, not the actual time. The dependence on the actual time t is omitted in the equations for readability in this section. The predicted trajectory is used for *threat* assessment later in this chapter. The worse case behaviour of the lead vehicle is assumed to be an emergency stop. Since a homogeneous platoon is assumed (Section 1.2), the host vehicle model for longitudinal behaviour can be adopted for the lead vehicle trajectory prediction. This model is presented in Section 3.2.1:

$$\dot{\hat{a}}_{L,x}(t_p) = \frac{1}{\tau_b}\left(\hat{a}_{L,x,ref}(t_p - \theta_b) - \hat{a}_{L,x}(t_p)\right). \tag{4.2}$$

In case a homogeneous platoon is assumed, the time delay θ_b and time constant τ_b are chosen equal to the host vehicle parameters shown in Appendix A.1. However, the method can easily incorporate a heterogeneous platoon by adjusting the parameters. The lead vehicle trajectory prediction $\mathcal{T}$ and the actual state estimation at t_0 ($\mathcal{T}(t_0) = \mathcal{T}_0$) are defined in the host vehicle coordinate frame:

$$\mathcal{T}(t_p) = \left[\hat{x}_{\mathcal{T}}(t_p), \quad \hat{v}_{\mathcal{T}}(t_p), \quad \hat{a}_{\mathcal{T}}(t_p)\right]^T, \quad \mathcal{T}_0 = \left[\hat{d}_{L,0} - d_{margin}, \quad v_{H,x,0} + \dot{\hat{d}}_{L,0}, \quad \hat{a}_{L,x,0}\right]^T, \tag{4.3}$$

where the lead vehicle rear bumper position prediction $\hat{x}_{\mathcal{T}}$ is equal to the inter-vehicle distance at t_0 by taking the host vehicle front bumper position at t_0 as origin. An illustration of the coordinates is shown in Fig 4.1. To obey a small safety margin between the vehicles and compensate for sensor noise, an offset d_{margin} is subtracted from the target trajectory positions. Variable $\hat{v}_{\mathcal{T}}$ is the longitudinal lead vehicle velocity prediction and $\hat{a}_{\mathcal{T}}$ the acceleration. These are all virtual future estimates. The actual host vehicle velocity $v_{H,x}$ is assumed to be measured accurately. The predicted future values, assuming

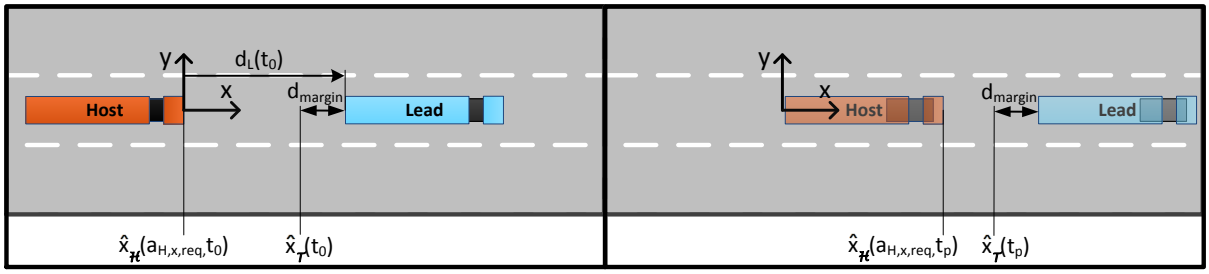

Fig 4.1: On the left the actual (t_0) coordinate definition is illustrated, on the right the predicted (t_p) coordinates.

Variable	Description	Value
θ_{wifi}	Communication time delay	0s
θ_{radar}	Radar time delay	0.2s
d_{margin}	Safety margin	0.5m
$a_{L,x,min}$	Minimum lead deceleration	-6m/s^2
τ_b	Actuator time constant	0.4s
θ_b	Actuator time delay	0.2s

Table 4.2: Parameters for the lead vehicle trajectory prediction

the lead vehicle will perform an emergency stop from t_0, can be calculated based upon the linear model (4.2):

$$\begin{aligned} \mathcal{T}(t_p) &= e^{\underline{A}_{\mathcal{T}} t_p}\mathcal{T}_0 + \int_{t_0}^{t_p} e^{\underline{A}_{\mathcal{T}}(t_p-\xi)}\underline{B}_{\mathcal{T}}\,\hat{a}_{L,x,ref}(\xi-\theta_b)d\xi, \\ \text{with}\quad \hat{a}_{L,x,ref}(t_p) &= \begin{cases} a_{L,x,ref}(t_p) & \text{if}\quad t_p < t_0, \\ a_{L,x,min} & \text{if}\quad t_p \geq t_0, \end{cases} \\ \underline{A}_{\mathcal{T}} = \begin{bmatrix} 0 & 1 & 0 \\ 0 & 0 & 1 \\ 0 & 0 & -\frac{1}{\tau_b} \end{bmatrix}, &\quad \underline{B}_{\mathcal{T}} = \begin{bmatrix} 0 \\ 0 \\ \frac{1}{\tau_b} \end{bmatrix}, \quad t_p \in \{t_p' \geq t_0 : \hat{v}_{\mathcal{T}}(t_p') \geq 0\}. \end{aligned} \tag{4.4}$$

The only input for the trajectory prediction is the reference acceleration time sequence $\hat{a}_{L,x,ref}$. Reference values for $t_p \in [-\theta_b + t_0, t_0]$ are stored following the procedure in (4.1). Since an emergency stop is considered, all future ($t_p \geq t_0$) reference values are set to the minimum achievable acceleration $a_{L,x,min}$.

4.1.3 Acceleration estimation during a communication failure

If communication fails, no actual and reference acceleration data of the lead vehicle is available. In (4.1) it was suggested to put the actual and reference acceleration to $a_{L,x,min}$ when communication is not available to obtain a worse case estimate of the actual lead vehicle acceleration. However, the vehicle model (4.2) shows that the actual acceleration cannot change instantly, but according to the time constant and time delay. Hence, the prediction of the actual acceleration ($\hat{a}_{L,x}$) can be less conservative:

$$\begin{aligned} \hat{a}_{L,x}(t,t_{fail}) &= e^{-t_{fail}/\tau_b}a_{L,x,wifi}(t-t_{fail}) + \int_{t-t_{fail}}^{t} e^{(\xi-t)/\tau_b}\frac{1}{\tau_b}\,\hat{a}_{L,x,ref}(\xi-\theta_b)d\xi, \\ \text{with}\quad \hat{a}_{L,x,ref}(t) &= \begin{cases} a_{L,x,ref}(t) & \text{if}\quad t_{fail} = 0, \\ a_{L,x,min} & \text{if}\quad t_{fail} > 0, \end{cases} \quad \forall t_{fail} \geq 0, \end{aligned} \tag{4.5}$$

where t_{fail} is the time since communication failed. For short *failure* durations, $\lim_{t_{fail}\to 0}\hat{a}_{L,x} = a_{L,x,wifi}$, which is equivalent to active communication in (4.1). For long *failure* durations, noticing that $\hat{a}_{L,x,ref}(t)$ is set to $a_{L,x,min}$ when communication fails, $\lim_{t_{fail}\to\infty}\hat{a}_{L,x} = a_{L,x,min}$, which is equivalent to inactive communication in (4.1).

Example 4.1.1. This example will show the behaviour of the estimated reference and actual acceleration of the lead vehicle when communication fails. The illustration of this example is shown in Fig 4.2. A

communication *failure* occurs at $t = 0$, when the lead acceleration $a_{L,x} = 0$ and the reference acceleration has some arbitrary varying value. For the actuator delay time $\theta_b = 0.2s$ after the *failure*, the reference values $\hat{a}_{L,x,ref}$ can be derived from before the *failure* occurred. After that, the reference value is set to $a_{L,x,min}$. Based on this the worse case estimate for the actual longitudinal acceleration $\hat{a}_{L,x}$ can be calculated based on (4.5). Note that this is not the real behaviour of the lead vehicle acceleration, but a worse case estimate. □

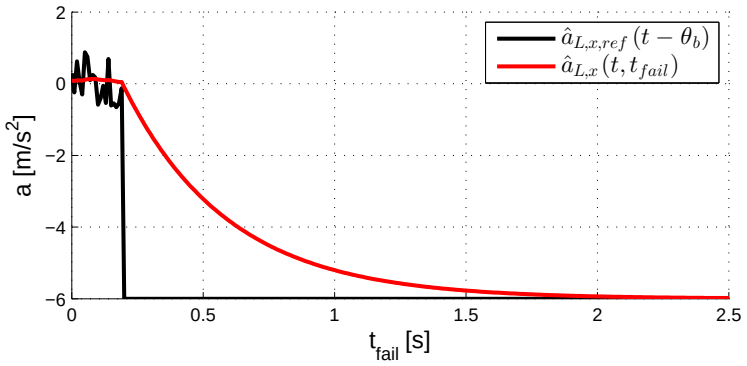

Fig 4.2: Example of the worse case lead vehicle acceleration estimate in case of a communication *failure*

4.2 Safety measures

In the previous section, a method to predict the worse case lead vehicle trajectory is proposed. This information is used to calculate the safety measures for *threat* assessment, which will be discussed in this section. The Safety Mode Selection will make its decisions based on the safety measures. To be sure collisions (*false negatives*) and *false positive* interventions are avoided, it is important to deliver accurate measures to the Safety Mode Selection. In this section, first a brief overview of possible safety measures is given. Then, the safety measures for emergency braking and for evasive manoeuvring are discussed. Finally, an illustrative example is given.

4.2.1 Safety measures in literature

An overview of possible safety measures can be found in [29]. Towards a collision, the following states can be distinguished illustrated by Fig 4.3:

1. Nominal operation: There is no *threat* or risk of a collision. *Fail-safety* or *fault-tolerance* is not activated.
2. Collision avoidable: There is a *threat* and *fail-safety* or *fault-tolerance* is activated, but there exists a possibility to avoid the collision.
3. Collision unavoidable: A collision cannot be avoided by any action, however the severity can be reduced by mitigating actions.
4. Collision: The state when a collision occurs.
5. Post collision: When a collision occurred and the *fail-safety* algorithm is still operational, actions to avoid secondary collisions can be performed.

The two states that will be considered are collision avoidable and collision unavoidable. In collision unavoidable state, the expected host vehicle velocity at the moment a collision is expected to occur could be a safety measure [29]. In case a collision is avoidable, several measures to assess the *threat* are possible. For instance:

1. Headway and Headway Time: The headway is the distance to the obstacle on the path ahead. Assuming both vehicles are driving at a constant speed, a headway time can be calculated.

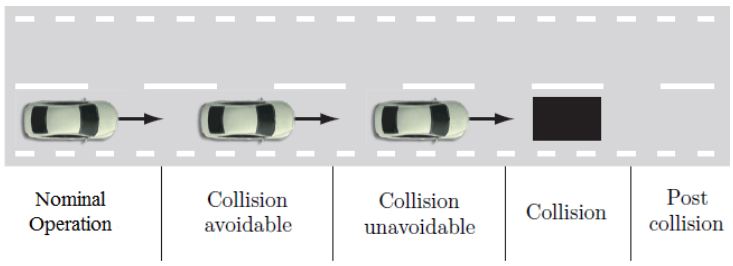

Fig 4.3: The five possible states of a vehicle approaching an obstacle [29]

2. Time to Collision: Time to Collision is the time till a collision is expected to occur. When calculating the time to collision, the relative velocity is often assumed to be constant. Alternatively a constant acceleration model can be used.
3. Closest Point of Approach: The Closest Point of Approach gives the minimum predicted distance to an obstacle. The Closest Point of Approach can be a measure for longitudinal and lateral collision avoidance.
4. Potential force: In this method, all objects in the environment produce a repulsive potential force. This force can be used for calculation of a control input. For potential field control methods applied to vehicles, see e.g. [25]. Drawback of the potential force measure is that if it would be used for vehicle control, there is no guarantee that the path where the vehicle ends up is collision free.
5. Required Longitudinal Acceleration and Required Lateral Acceleration: This is the required longitudinal or lateral acceleration to avoid an accident. The required longitudinal acceleration is the acceleration which brings the velocity difference with the oncoming object to zero at the time a collision is expected to occur. For the required lateral acceleration, the vehicle should have travelled enough lateral distance (integrating the required lateral acceleration twice) at the time a collision is expected to occur. This approach is applied in [18].
6. Last Point to Brake and Last Point to Steer: The latest point to intervene by braking and steering to avoid a collision respectively.

The first two methods are measures to rate the longitudinal *threat*. However, these are no direct measures whether a collision is really avoidable. The Closest Point of Approach and Potential force can incorporate the longitudinal and lateral *threat* in one number. The Required Acceleration and Last Point to Brake/Steer methods make a clear distinction between longitudinal and lateral collision avoidance. The Last Point to Brake/Steer method is most effective to wait for the latest possible moment to intervene and then activate the collision avoidance controller. The Required Acceleration method can be used to adapt the manoeuvre during the action.

Based on the previous literature review, the following safety measures are applied in this thesis. For heavy-duty vehicles there is a significant risk on lateral instability, as presented in literature (Section 1.3). Therefore, it is assumed to be desirable to wait with performing the evasive manoeuvre till the latest possible moment, and then perform a well tuned specific manoeuvre. Hence, the Latest Point to Steer is used to evaluate the possibility to avoid an accident by lateral manoeuvring. When using the latest point to brake, the vehicle is committed to an emergency stop until the *threat* is below a threshold. However, for the object in front (lead vehicle) worse case behaviour is assumed in the previous section. If the lead vehicle does not behave according to the worse case prediction, the lead vehicle will decrease the *threat* as well. Therefore a more adaptive measure for longitudinal control is applied: the Required Longitudinal Acceleration. The following section will elaborate on the chosen safety measures for emergency braking and evasive manoeuvring.

4.2.2 Brake Threat Number and Impact speed

This section will discuss the safety measures assuming the host vehicle is only able to apply the brakes. As mentioned in the previous section, the Required Longitudinal Acceleration to avoid a collision is used to assess the *threat* in case braking would be applied. Therefore a specific number incorporating the Required Longitudinal Acceleration is defined, as by Eidehall [21].

Definition 4.2.1. The Brake Threat Number (BTN) is defined as:

$$\text{BTN}(t) = \frac{a_{H,x,req}(t)}{a_{H,x,min}}, \quad a_{H,x,req}(t) \leq 0 \tag{4.6}$$

where $a_{H,x,req}$ is the required longitudinal acceleration of the host vehicle to avoid an accident assuming worse case behaviour of the lead vehicle. Variable $a_{H,x,min}$ is the lower acceleration limit. Hence, in case the BTN ≤ 1 a collision is avoidable; for a BTN > 1 there is no guarantee a collision can be avoided. □

The required acceleration is calculated using the longitudinal vehicle model presented in Section 3.2.1: a time constant and time delay. In case a homogeneous platoon and equal initial conditions for the host and lead vehicle are assumed, the braking distance of the vehicles can be considered to determine the required acceleration. But since these assumptions might not always hold, the full host vehicle trajectory is considered and compared with the worse case lead trajectory to find the required acceleration. Similar to the lead vehicle trajectory prediction (4.3), the predicted host vehicle front bumper trajectory is calculated in the host vehicle coordinate frame. The prediction starts at $t = t_0$. The prediction time is denoted with t_p. Note that this is a virtual prediction time, not the actual time. The dependence on the actual time t is omitted in the equations for readability. The following definition of the predicted host vehicle trajectory $\mathcal{H}$ is used:

$$\begin{aligned} \mathcal{H}(a_{H,x,req}, t_p) &= \begin{bmatrix} \hat{x}_{\mathcal{H}}(a_{H,x,req}, t_p), & \hat{v}_{\mathcal{H}}(a_{H,x,req}, t_p), & \hat{a}_{\mathcal{H}}(a_{H,x,req}, t_p) \end{bmatrix}^T, \\ \mathcal{H}_0 &= \begin{bmatrix} 0, & v_{H,x,0}, & a_{H,x,0} \end{bmatrix}^T, \end{aligned} \tag{4.7}$$

where the initial velocity $v_{H,x,0}$ and acceleration $a_{H,x,0}$ are measured accurately. The host vehicle front bumper position at t_0 is chosen as origin. An illustration of the coordinates is shown in Fig 4.1. The estimates for the future trajectory are dependent on the reference acceleration set at the actual time instant, which is assumed to be equal to the required acceleration $a_{H,x,req}$:

$$\begin{aligned} \mathcal{H}(t_p, a_{H,x,req}) &= e^{\underline{A}_{\mathcal{H}} t_p} \mathcal{H}_0 + \int_{t_0}^{t_p} e^{\underline{A}_{\mathcal{H}}(t_p - \xi)} \underline{B}_{\mathcal{H}} \, \hat{a}_{H,x,ref}(\xi - \theta_b) d\xi, \\ \text{with} \quad \hat{a}_{H,x,ref}(t_p) &= \begin{cases} a_{H,x,ref}(t_p) & \text{if} \quad t_p < t_0, \\ a_{H,x,req} & \text{if} \quad t_p \geq t_0, \end{cases} \\ \underline{A}_{\mathcal{T}} = \begin{bmatrix} 0 & 1 & 0 \\ 0 & 0 & 1 \\ 0 & 0 & -\frac{1}{\tau_b} \end{bmatrix}, \quad \underline{B}_{\mathcal{H}} &= \begin{bmatrix} 0 \\ 0 \\ \frac{1}{\tau_b} \end{bmatrix}, \quad t_p \in \{t_p' \geq t_0 : \hat{v}_{\mathcal{H}}(a_{H,x,req}, t_p') \geq 0\}, \end{aligned} \tag{4.8}$$

where the reference values $\hat{a}_{H,x,ref}$ for all time instants $t_p \in [-\theta_b + t_0, t_0]$ are stored. For the future time instants ($t_p \geq t_0$) the value is assumed to be $a_{H,x,req}$. An iterative algorithm has been developed calculating $a_{H,x,req}$ such that the relative velocity is brought to zero at the time that the relative distance between the vehicles is zero. In case the found required acceleration is less than the minimum achievable acceleration, an impact speed is calculated.

Definition 4.2.2. The impact speed is defined as:

$$\begin{aligned} v_{imp} &= \hat{v}_{\mathcal{H}}(a_{H,x,min}, t_{imp}) - \hat{v}_{\mathcal{T}}(t_{imp}), \\ t_{imp} &= min(t_p), \qquad\qquad t_p \in \{t_p' \geq t_0 : \hat{x}_{\mathcal{H}}(a_{H,x,min}, t_p') \geq \hat{x}_{\mathcal{T}}(t_p')\}, \end{aligned} \tag{4.9}$$

where the time of impact t_{imp} is defined as the first time instant that the full braking host trajectory crosses the worse case lead trajectory. □

The definitions of BTN and v_{imp} are intuitive, but the implementation is not trivial because the full vehicle trajectories are considered. The activity diagrams for calculating the BTN and v_{imp} are shown in Appendix B.

4.2.3 Time To Steer

In this section the safety measure for evasive manoeuvring is discussed. To find the last possible moment to activate an evasive manoeuvre, first a valid evasive path has to be found. The proposed method to

determine the Last Point to Steer can also incorporate integrated braking and steering, but this is not yet considered since more research is required on the vehicle dynamic behaviour in that case. Chee and Tomizuka [16] did a comparison of several possible vehicle lane change paths:

1. Circular trajectory: A path with constant acceleration segments.
2. Cosine trajectory: A path description by trigonometric functions.
3. 5^{th}-order polynomial trajectory: A 5^{th}-order polynomial is fitted given some initial and terminal conditions.
4. Trapezoidal acceleration trajectory: A path with a trapezoidal shape in lateral acceleration. In contrast to the circular trajectory, this trajectory limits the jerk in the transition between the constant acceleration segments.

The first two possibilities do not limit the lateral jerk. As mentioned by [22], high jerk paths are not feasible to follow for a vehicle, so the latter two possibilities are preferred and will be further compared. Therefore the transition time of the trajectories will be evaluated: the time a generated trajectory requires to perform a full lane change. By limiting the lateral acceleration and jerk, the transition time for a trapezoidal lane change trajectory is approximately less compared to the 5^{th}-order polynomial [16]. For an increasing transition time, the time to evade a collision will increase which is not preferred. Therefore, the trapezoidal lane change path is selected to generate a path, from which the Last Point to Steer is determined.

Next step is defining the bounds on lateral acceleration and lateral jerk. The maximum feasible lateral acceleration for heavy-duty vehicles is determined by the roll-over limit of the vehicle. TNO research [44] proved that the roll-over limit of a tractor semi-trailer combination is generally around a lateral acceleration of 3-4m/s^2, depending on the loading conditions. In vehicle controllers, which should prevent the vehicle for a roll-over, start to intervene from 2.5m/s^2 [43]. Hence, the lateral acceleration limit on the generated path is chosen to be 2.5m/s^2. According to the TNO research [43], the lateral jerk can be upto 5m/s^3 in case the driver applies a step steer input. The steering actuator has to be designed such that this jerk can be achieved.

An illustration of a possible path generated by the path generator is shown in Fig 4.4. The transition time t_{trans} is the time needed to complete the full lane change with the lane width denoted by LW. However, a collision is already avoided when enough lateral distance is travelled to evade the oncoming object. This distance is referred as evasive distance y_{ev}. The time at which the evasive distance is reached is referred as t_{ev}. In Appendix C the trajectory generation is discussed in more detail. For more information about the path description, also with non-zero initial lateral velocity and position, the reader is referred to [13]. All trajectory segments can be described by functions, such that the obstacle and lane width can vary. Using the parameters in Table 4.3, the evasive time would be 2.05s without taking actuator delay into account. To evaluate the Last Point to Steer, actuator delay should be taken into account as well. Before defining the safety measure for evasive manoeuvring, first the Time to Collision will be defined, which will be used in the evasive manoeuvring safety measure.

Definition 4.2.3. Time to Collision (TTC) is defined as the first time instant that the host and lead vehicle trajectories cross. The dependency on the actual time t is omitted for readability.

$$\begin{aligned} \text{TTC} = min(t_p) \quad t_p \in \{t'_p \geq t_0 : \hat{x}_{\mathcal{H}}(\hat{a}_{H,x,ref}(t'_p), t'_p) \geq \hat{x}_{\mathcal{T}}(t'_p)\}, \\ \text{with} \quad \hat{a}_{H,x,ref}(t_p) = \begin{cases} a_{H,x,ref}(t_p) & \text{if} \quad t_p < t_0, \\ 0 & \text{if} \quad t_p \geq t_0. \end{cases} \end{aligned} \tag{4.10}$$

The host vehicle reference acceleration $\hat{a}_{H,x,ref}$ is assumed to be zero. □

Remark. For integrated braking and steering, the host vehicle reference acceleration could be chosen smaller than zero. However, this will not be considered in this thesis. □

Definition 4.2.4. The time till the Last Point to Steer is reached, is defined as Time To Steer (TTS):

$$\text{TTS}(t) = \text{TTC}(t) - \theta_s - t_{ev}, \tag{4.11}$$

where θ_s is the steering actuator delay and t_{ev} the evasive time based on the trapezoidal lane change path description shown in Appendix C. If the TTS ≥ 0, a collision can be avoided by steering. □

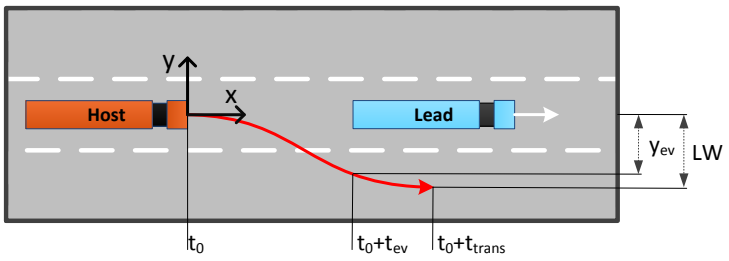

Fig 4.4: Illustration of the path generation for an evasive manoeuvre

Variable	Description	Value
$a_{y,lim}$	Lateral acceleration limit	2.5m/s^2
$j_{y,lim}$	Lateral jerk limit	5m/s^3
LW	Lane width	3.5m
y_{ev}	Evasive distance	2.9m

Table 4.3: Parameter example for an evasive manoeuvre

4.2.4 Probability of the lead vehicle braking

To be more adaptive to traffic conditions, a probability of the lead vehicle braking is used as safety measure, which was presented by Tzempetzis [56]. This probability is calculated as follows. When the lead vehicle has communicated its environmental perception, the last communicated values for the distance (d_{LL}) and range rate ($\dot{d}_{LL}$) between the lead and its preceding vehicle could be used to determine a probability of the lead vehicle performing a braking action. This probability is based on a weighted Poisson distribution with weight w:

$$P_{brake}(d_{LL}(t), \dot{d}_{LL}(t)) = wP_{\dot{d}_{LL}}(\dot{d}_{LL}(t)) + (1-w)P_{d_{LL}}(d_{LL}(t)), \tag{4.12}$$

with

$$P_{\dot{d}_{LL}}(\dot{d}_{LL}(t)) = \lambda_{\dot{d}_{LL}} e^{-\beta_{\dot{d}_{LL}}(\dot{d}_{LL}(t)-\dot{d}_{LL,min})}\Delta t \tag{4.13}$$

and

$$P_{d_{LL}}(d_{LL}(t)) = \lambda_{d_{LL}} e^{-\beta_{d_{LL}}(d_{LL}(t)-d_{LL,min})}\Delta t. \tag{4.14}$$

Variables $\beta_{d_{LL}}$ and $\beta_{\dot{d}_{LL}}$ are configurable. Variables $d_{LL,min}$ and $\dot{d}_{LL,min}$ are tunable parameters defining the thresholds for which the probability is 1. Variables $\lambda_{\dot{d}_{LL}}$ and $\lambda_{d_{LL}}$ are calculated such that $P_{\dot{d}_{LL}}$=1 for $\dot{d}_{LL} < \dot{d}_{LL,min}$ and $P_{d_{LL}}$=1 for $d_{LL} < d_{LL,min}$. Variable Δt is the time period in which the probability of an event is calculated. The selected parameter values are shown in Table 4.4. In case there is a high probability of the lead vehicle performing a braking action the interventions can be more severe, while in case there is a low probability of the lead vehicle braking the interventions can be softer.

Remark. For future work, the probability of the lead vehicle braking can be used to 'soften' the BTN calculation. Currently, maximum braking of the preceding vehicle is used to calculate the BTN, but the probability of this scenario is often negligible. The accident severity in the highly unlikely worse case scenario can be limited to acceptable levels by the impact speed safety measure. □

Variable	Value
w	0.7
$d_{LL,min}$	10m
$\dot{d}_{LL,min}$	-0.1m/s
$\beta_{d_{LL}}$	3
$\beta_{\dot{d}_{LL}}$	2
Δt	0.5s

Table 4.4: Variable values used for the probability calculation, chosen based on [56].

Example 4.2.1. The behaviour of three out of the four presented safety measures when the host vehicle approaches a standing object with a constant velocity of 80km/h is shown in Fig 4.5. Here no braking will be applied by the host vehicle, so this will lead to a collision. The parameters mentioned in the

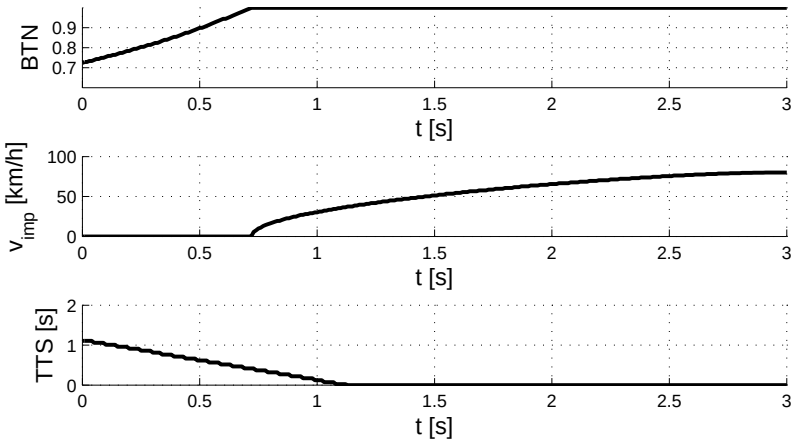

Fig 4.5: Behaviour of safety measures as a vehicle approaches a standing object with 80km/h

previous paragraphs are used. The top plot shows the BTN, the middle plot the impact speed and the bottom plot the TTS. The simulation starts 3 seconds before the collision. The BTN is 0.72, implying an accident can be avoided when at least 72% of the maximum braking capacity is applied. The vehicle keeps approaching with a constant velocity. At time 0.74s, (2.26s before impact) the BTN reaches 1, which implies a collision can just be avoided by an emergency stop. After that the impact speed starts to increase. The BTN would exceed one, but since values above 1 are irrelevant, the function is saturated in the top plot of Fig 4.5. At 1.06s (1.94s before the impact) the TTS becomes zero, implying the Last Point to Steer is reached. The impact speed by applying full braking at that point is already 32km/h. When the Last Point to Steer is passed, only collision mitigation is possible. At the time the collision occurs (3s), the impact speed is 80km/h. □

From the previous example it can be concluded that there is a small period in which steering possibly avoids a collision where braking cannot. At higher speeds the period will be longer; at low speeds shorter. Integrated braking and steering is expected to increase the period where evasive manoeuvring is beneficial, as already mentioned in Section 1.3.

4.3 Safety Mode Selection

To bring the system to a steady safe state as defined in Section 1.2, a strategy has to be defined. Therefore, for each safety scenario a statechart diagram has to be defined in the Safety Mode Selection block (Fig 2.2). Definition of the statechart diagrams was not the focus of this thesis. More details about the statechart diagrams can be found in the report of Tzempetzis [56]. This section will concentrate on the statechart diagram for the communication *failure* scenario illustrated in Fig 4.6 and show how the safety measures influence the decisions. In the statechart diagram, the following four states or modes are defined:

- **Nominal controller**: there is no *threat*. The CAD system can behave as it is designed.
- **Adaptive Headway Time**: the *fault-tolerant* mode. The Adaptive Headway Time functionality increases the headway time with the nominal controller active. More information about the Adaptive Headway Time algorithm can be found in [39].
- **Collision Avoidance**: a *fail-safety* mode. In the Collision Avoidance mode either emergency braking or an evasive manoeuvre will be selected, based on the safety measures. The actions performed in the Collision Avoidance sub-states will be discussed in the next chapters.
- **Intermediate Braking**: a *fail-safety* mode, but for less severe *threats* than Collision Avoidance. In Intermediate Braking, medium braking effort is applied; the braking severity in Intermediate Braking is designed in between the Adaptive Headway Time and Collision Avoidance, giving an

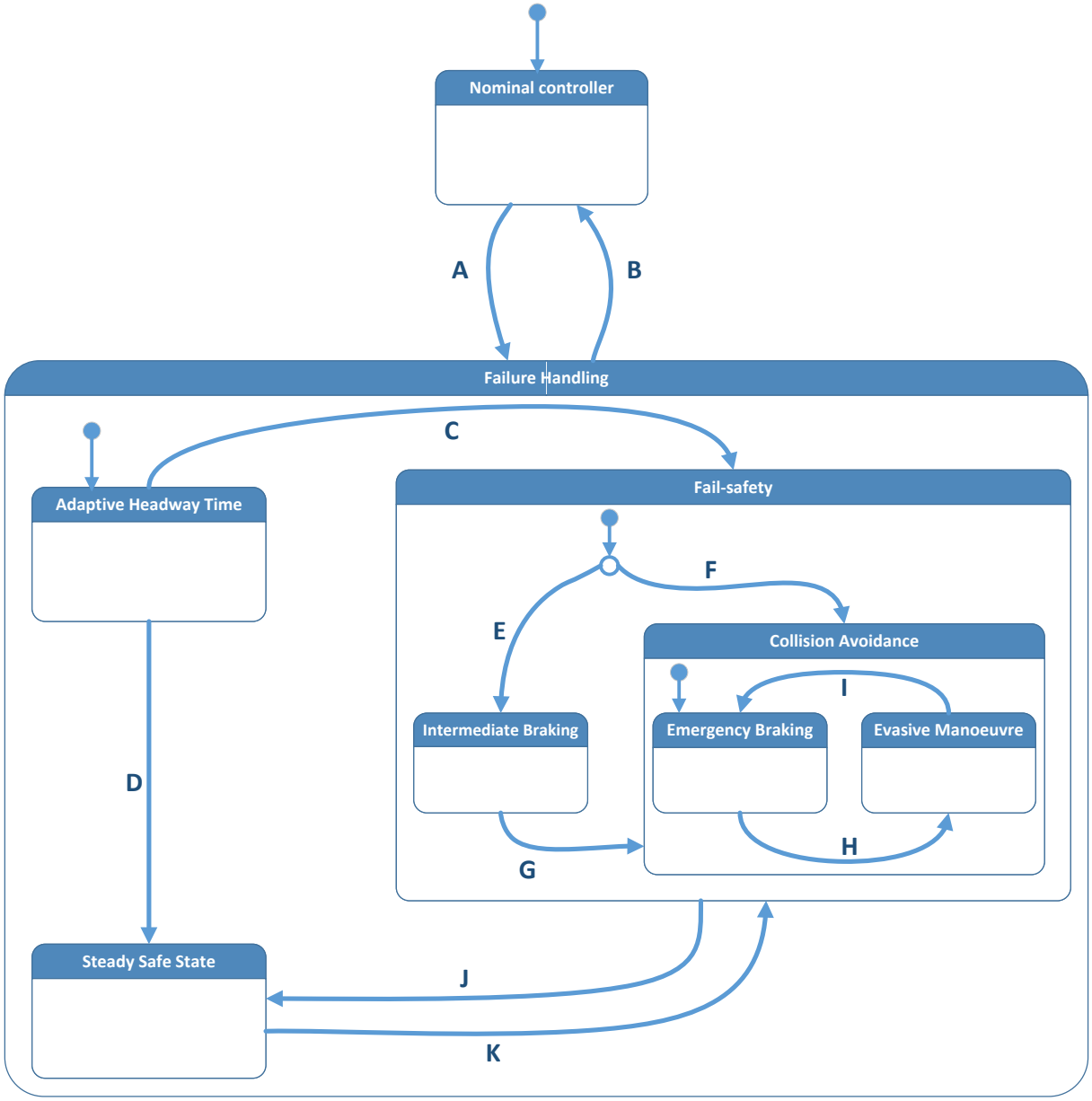

Fig 4.6: Safety Mode Selection

additional possibility to control the vehicle comfortable and safe to a safe state. The deceleration is limited to 3.5m/s^2 and the jerk to 2.5m/s^3, based on the ISO 15622 standard [2] for Adaptive Cruise Control.

Next, the transitions in the statechart diagram based on the safety measures will be discussed:

A Detection of the communication *failure*. In case no message is received for a period of 0.1s the *failure* handling is activated.

B Communication is functional AND it is safe to switch back to the nominal controller. It is not always safe to activate the nominal controller in case communication becomes active, e.g. the host vehicle is approaching the lead vehicle fast. In that case collisions can occur. Therefore the following conditions are added to ensure it is safe to activate the nominal controller:
   - The control errors should be larger than zero.
     * the difference between the measured inter-vehicle distance and desired inter-vehicle distance should be positive.
     * the derivative of the previous should be positive.
   - The second derivative of the inter-vehicle distance should be positive.

C The *failure* duration is longer than the *fault-tolerant* time t_{FT} AND the BTN is above 0.85. The *fault-tolerant* time is defined as the maximum communication *failure* duration for which the Adaptive Headway Time can ensure no collisions occur. This time is vehicle dependent. For the heavy-duty vehicle considered in this report the nominal *fault-tolerant* time $t_{FT,nom}$ is 0.5s based on simulations. The *fault-tolerant* time is reduced with increasing probability that the lead vehicle brakes: $t_{FT} = (1 - P_{brake})t_{FT,nom}$, where P_{brake} is calculated using (4.12).

D The system has reached a Steady Safe State as defined in Section 1.2.

E Two conditions should hold before switching to intermediate braking:
- The Fail-safety state is activated for the first time since the activation of Failure Handing state. It has to be noted that Intermediate Braking state is not aimed to prevent collisions, but to bring the system to a 'safer' state in a comfortable way. This mode is added to prevent severe braking in the transition from driving in a platoon with active communication to a platoon without communication and an increased following distance. Hence, this state should only be activated the first time Fail-safety is activated in the Failure Handling state.
- The probability of the lead vehicle braking P_{brake} is below 0.85. In case there is a high probability of the lead vehicle braking, Intermediate Braking is not activated.

F When the conditions for Transition E are not true, Collision Avoidance is directly activated when Fail-safety mode is entered.

G In case the BTN is above 0.95 AND the distance between the vehicles decreases ($\dot{d}_{L,meas} < 0$) OR the impact speed is above 20km/h, the transition from Intermediate Braking to Collision Avoidance is made.

Remark. Note that if the gap is opening between the two vehicles, an impact speed upto 20km/h is allowed to stay longer in Intermediate Braking and consequently soften the intervention. The impact speed is calculated assuming worse case behaviour of the lead vehicle, which is unlikely to happen. Although there is no guarantee a collision can be avoided, the impact speed is limited to 20km/h by this condition.

H The default path in Collision Avoidance is Emergency Braking. As mentioned in [38], the best initial response for heavy-duty vehicles is braking, since by braking kinetic energy is subtracted from the system where for steering the kinetic energy remains approximately the same. Evasive manoeuvring is only activated in case the system can guarantee the evasive path is collision free. In case the BTN>1 and TTS>0, braking can not ensure avoidance of an accident where an evasive manoeuvre can. Hence the transition is made from Emergency Braking to Evasive Manoeuvre state.

Remark. Besides the lead vehicle, no other traffic participants are considered yet. In practice it should be evaluated if an emergency stop could risk a collision with approaching traffic from behind. For an evasive manoeuvre it should be checked if the lanes are free to perform such a manoeuvre. These conditions are however not considered in this thesis.

I A time period t_{trans} after Evasive Manoeuvre is activated, the manoeuvre is finished and the system will switch back to Emergency Braking.

Remark. Currently, in case the system switches to Evasive Manoeuvre it is committed to this action. In the future conditions can be added, such that the system is able to transit to Emergency Braking in more cases when desired (abort the evasive manoeuvre).

J The transition to Steady Safe State is made when the conditions for a steady safe state are met. This is the case if the host vehicle is in standstill OR drives at a speed less or equal to the lead vehicle AND the inter-vehicle distance is safe.

K In case the system is in Steady Safe State AND the BTN exceeds the threshold of 0.85 AND the vehicles are approaching each other, the system will transit back to Fail-safety mode.

An elaboration on the process towards the statechart diagram can be found in [56].

4.3.1 Collision avoidance strategy

As mentioned, in Collision Avoidance mode there are two sub-states: Emergency braking and Evasive Manoeuvre. The transitions in the statechart diagram (Transition H and I) are made based on the safety measures defined previously. In this section a comparison is made between emergency braking and evasive manoeuvring based on a safe following distance. The safe following distance is defined as

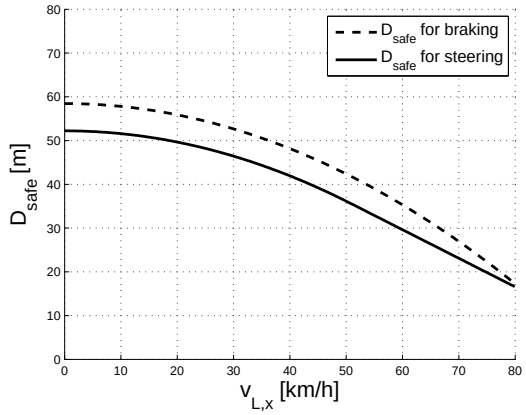

Fig 4.7: Safe following distance comparison for braking and an evasive manoeuvre with different lead velocities. The host vehicle is driving at a constant velocity of 80km/h.

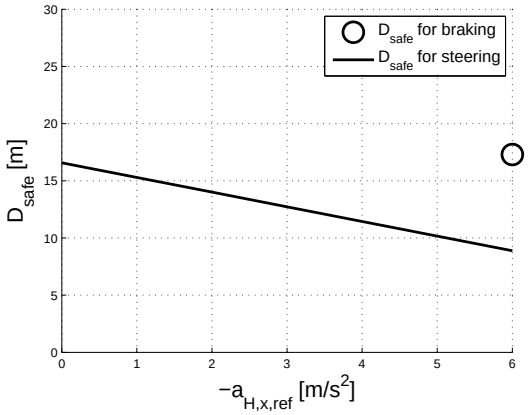

Fig 4.8: Adding braking to an evasive manoeuvre is expected to decrease the safe following distance.

the minimum safe initial distance between the vehicles. The smaller the safe following distance, the later Collision Avoidance can be activated, implying the system availability can be increased. With active communication, it is safe to drive with a time gap of 0.3s, which corresponds to approximately 10m at 80km/h. Fig 4.7 depicts the safe following distance D_{safe} without communication between the host and the lead vehicle in case the host vehicle drives at a velocity of 80km/h and different constant lead velocities. A lead vehicle velocity of zero indicates a standstill object and a velocity of 80km/h a stable platoon. The dotted line is the safe following distance for only braking and the solid line is the safe following distance for only steering. In case of a standstill object an evasive manoeuvre has clearly a shorter safe following distance. In a stable platoon, there is hardly any difference in the safe following distance between emergency braking and an evasive manoeuvre. Note that no braking is applied in the evasive manoeuvre. In both cases the safe following distance in a stable platoon is larger than the nominal following distance with active communication (10m). Hence, if a communication *failure* occurs the distance gap has to be increased to at least the safe following distance illustrated in the figure. In the transition phase, a trade-off between comfort and safety has to be made. In case the safe following distance without communication is closer to the following distance with communication, the intervention in the transition can potentially be smoother and more comfortable without endangering a collision.

For evasive manoeuvring no integrated braking and steering is considered yet. However, this paragraph will show the potential to reduce the safe following distance by adding braking to an evasive manoeuvre based on kinematic calculations. Fig 4.8 shows a comparison of the safe following distance for maximum braking and an evasive manoeuvre in a stable platoon: both vehicles are driving at a constant velocity of 80km/h. The circle indicates the safe following distance for braking and the line an evasive manoeuvre with varying decelerations. Clearly, adding braking in the evasive manoeuvre will decrease the safe following distance. In case the host vehicle is able to brake with more than 5.2m/s^2, the safe following distance is within 10m, which is the inter-vehicle distance in nominal behaviour. Hence the gap could be opened more gradual, if it should be opened at all. However, if such heavy braking during steering is feasible from a vehicle dynamics perspective has to be further investigated. The longitudinal acceleration is limited by the tyre to road friction coefficient. For passenger cars the lateral acceleration is limited by the tyre to road friction coefficient as well. Hence adding braking to an evasive manoeuvre will limit the maximum lateral acceleration and thereby the potential of integrated braking and steering. That is possibly the reason why there is very little literature on integrated braking and steering manoeuvres in collision avoidance. However, for a heavy-duty vehicle the lateral acceleration is limited by the roll-over limit of the vehicle. This implies the tyres have reserve capacity to decelerate without reducing the lateral acceleration limit. The exact values of this reserve capacity have to be investigated further. Moreover, the influence on vehicle roll and pitch should be investigated. Note that the vehicle model presented in Section 3.1 assumes rigid bodies without pitch and roll dynamics (Section 3.1.1, Assumption 1). Therefore, the vehicle model should possibly be extended to evaluate an evasive manoeuvre with combined braking and steering.

Example 4.3.1. Within the communication *failure* scenario, the use case where the lead vehicle does not brake will be elaborated in this example (Test 10 in Appendix E.2). For this test case, the system should remain in Intermediate Braking or Adaptive Headway Time. Activation of Collision Avoidance in case the lead vehicle remains at a constant speed is assumed to be undesired for comfort and safety. Fig 4.9 shows a simulation where the communication *failure* occurs at t=1s in a stable vehicle platoon driving at 80km/h. The inter-vehicle distance is shown in the top left plot. The distance is increased over the simulation to the following distance defined by the ISO 15622 standard [2] for Adaptive Cruise Control. The top right plot shows the system modes. WiFiStatus 0 means no *failure*. At 1s the *failure* occurs; the system switches to WiFiStatus 1: The Adaptive Headway Time. After the *fault-tolerant* time, set to 0.5s, Intermediate Braking is activated (WiFiStatus 2). As the Steady Safe State is reached, the nominal controller is activated with an increased following distance (WiFiStatus 2). The behaviour of the vehicle speeds and host vehicle reference and actual acceleration is shown in the bottom left plots. The bottom right plots show the behaviour of the safety measures. The BTN, in a stable platoon with an inter-vehicle distance of 9.2m, is already quite high (0.83). In case the communication fails, the lead trajectory cannot be estimated accurately (Section 4.1), which causes an increase of the BTN. When the BTN becomes 1, there is no guarantee a collision can be avoided by braking. Hence the impact speed v_{imp} starts to increase. For this use case the maximum impact speed, when the lead would perform an emergency stop is 12km/h. The bottom right plot shows the TTS. Initially with communication active the TTS is 0.14s. When the *failure* occurs, the Last Point to Steer is past (TTS<0) before the BTN exceeds 1. In this case an evasive manoeuvre has no added value above only braking. □

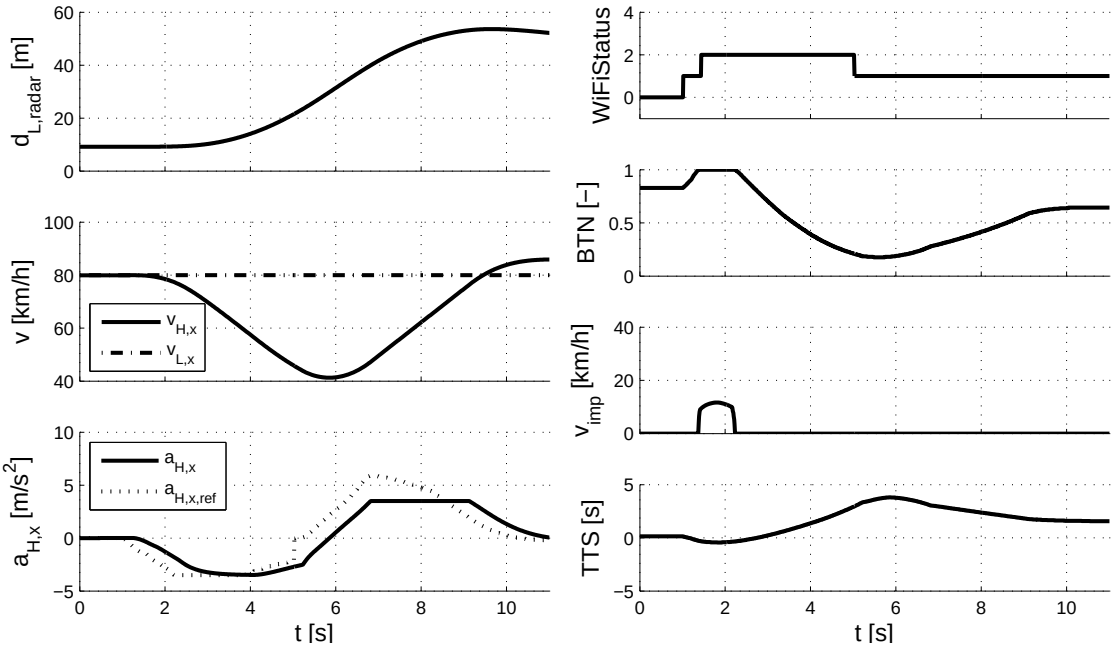

Fig 4.9: Example of the system behaviour in case of a communication failure with no braking of the lead vehicle

4.4 Summary

Summarizing, four safety measures are presented in this chapter. These safety measures are calculated assuming worse case behaviour of the lead vehicle, which is assumed to be an emergency stop. Based on literature, first the Brake Threat Number (BTN) is defined, which is the required longitudinal acceleration to avoid a collision over the maximum achievable longitudinal acceleration of the host vehicle. A BTN$\leq$ 1 reflects a collision can be avoided; a BTN>1 reflects there is no guarantee a collision can be avoided. In the latter case a worse case impact speed is calculated. For the BTN and impact speed calculation, the longitudinal behaviour of the host and lead vehicle is approximated by a time constant and time

delay. For lateral manoeuvring a Last Point to Steer is used. The Last Point to Steer is calculated by a trapezoidal lane change path to evade a rear-end collision. The time till the Last Point to Steer is reached, assuming constant velocity of the host vehicle, is referred as Time To Steer (TTS). The last safety measure is a probability of the lead vehicle braking based on traffic conditions. The safety measures are applied in the Safety Mode Selection to select the desired system modes, which are aimed to bring the system to a steady safe state. The safety measures presented in this thesis contributed to the development of the Safety Mode Selection. In collision avoidance, the safe following distances for only braking and only steering are approximately equal for a stable platoon. The safe following distance can potentially be decreased by adding braking to an evasive manoeuvre.

Chapter 5

Longitudinal collision avoidance control

For longitudinal collision avoidance functionality in the CAD system, two controller types are investigated. The controllers are evaluated in the communication *failure* scenario presented in Section 1.2. In the previous chapter the longitudinal vehicle behaviour is assumed to be known accurately (a prediction-based controller). Therefore, first a controller related to the required acceleration to avoid a collision is designed and validated in Section 5.1, referred as prediction-based controller. Validation is done by simulations and experiments. Section 5.2 will demonstrate that the system model parameters might be uncertain. This limits the performance of the prediction-based controller, which might lead to collisions. Hence, a robust control alternative is investigated in Section 5.3. In Section 5.4 both approaches will be compared using simulations. Evaluation of the controllers in the experiments will be based on the key performance indicators stated in Section 2.1.

5.1 Prediction-based controller

In Section 4.2.2 a detailed calculation of the required reference acceleration to avoid a collision is presented. Since the longitudinal vehicle behaviour is assumed to be well described by the calculation model, a controller applying a braking effort related to the required acceleration is proposed in this section. First the controller design is discussed and an illustrative example of the controller behaviour in case the vehicle approaches a standing object is shown. Finally, simulation and test results in the communication *failure* scenario are presented.

5.1.1 Controller design

The proposed control scheme is illustrated in Fig 5.1. The worse case (WC) lead vehicle trajectory predictor and BTN calculation are based on the algorithms proposed in the previous chapter. Note that the required acceleration to avoid a collision is directly related to the BTN (Definition 4.2.1). There are two reasons to not directly apply the required reference acceleration to the system:

1. In case the required acceleration to avoid a collision is applied directly to the system, the BTN will remain constant. However, if there is a *threat* it is desired to reduce the *threat*. So the BTN should be reduced. Hence the strategy is to apply more braking to reduce the BTN during an emergency braking event.
2. Experiments proved there is regularly an offset between the reference and actual acceleration. Note that open loop braking is applied; there is no feedback to compensate for deviations between the desired and actual acceleration. To compensate for the acceleration offset, it is desired to apply more deceleration than required to guarantee the vehicle brakes with at least the required acceleration.

The amount of additional applied braking can be tuned by compensation parameter λ_{pred}. This is the percentage of the maximum braking capacity that is applied on top of the required acceleration. Experiments proved an upper bound $a_{ca,max}$ on the reference acceleration is needed to compensate for

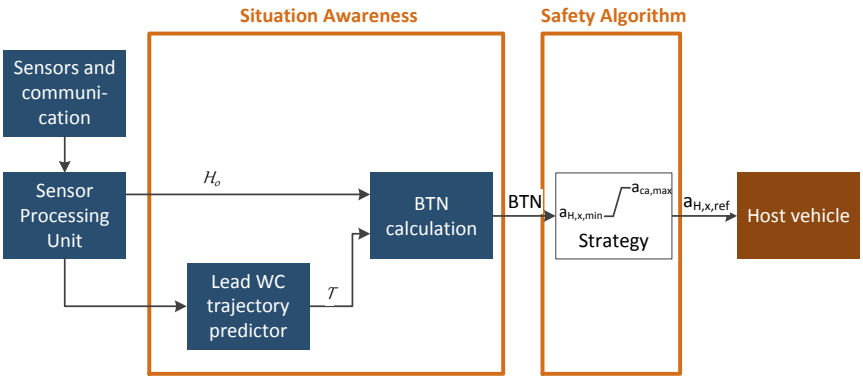

Fig 5.1: Control scheme of the longitudinal prediction-based controller

the unmodelled system behaviour. A lower bound $a_{H,x,min}$ is determined by the saturation of the low-level controllers in the vehicle. This results in the following description of the strategy:

$$a_{x,ca}(t) = a_{H,x,req}(t) + \lambda_{pred}\ a_{H,x,min},$$
$$a_{H,x,ref}(t) = \begin{cases} a_{ca,max} & \text{if } a_{x,ca}(t) \geq a_{ca,max}, \\ a_{x,ca}(t) & \text{if } a_{H,x,min} < a_{x,ca}(t) < a_{ca,max}, \\ a_{H,x,min} & \text{if } a_{x,ca}(t) \leq a_{H,x,min}, \end{cases} \tag{5.1}$$

where $a_{H,x,ref}$ is the reference acceleration applied to the system and $a_{H,x,req}$ the required acceleration to avoid a collision derived from the BTN. The used parameter values are shown in Table 5.1. Based on the value of the compensation factor ($\lambda_{pred} = 0.15$), the strategy is to apply 15% of the maximum braking capacity on top of the required acceleration. This value is determined based on simulations and experiments. The reference value is saturated by an upper and lower bound, as discussed previously.

Variable	Description	Value
λ_{pred}	Compensation factor	0.15
$a_{ca,max}$	Maximum acceleration in Collision Avoidance	-2m/s^2
$a_{H,x,min}$	Minimum acceleration	-6m/s^2

Table 5.1: Parameters for the prediction-based controller

Example 5.1.1. In Fig 5.2, the simulation results are shown of a vehicle driving initially 80km/h approaching a standing object with an initial distance of 70m. This standstill object example is illustrative, since the lead vehicle worse case trajectory predictor will give a constant position as predicted trajectory. Hence, the trajectory predictor does not influence the system response. The top left plot shows the required acceleration to avoid a collision and reference acceleration, the top right plot the actual acceleration, the bottom left plot the vehicle velocity and the bottom right plot the distance to the object. Note that the required acceleration is directly related to the BTN in Definition 4.2.1. The vehicle comes to a standstill at the safe stopping distance d_{margin} (Section 4.1.2) before the standing object. The initial required acceleration is 4.2m/s^2. The braking strategy (5.1) applies more braking effort to the system. Because more braking is applied than required, the required acceleration decreases over time. The strategy could be summarized by applying heavy braking effort in case Collision Avoidance is activated, which will reduce the threat. When the threat is reduced, the braking effort is reduced accordingly. □

5.1.2 Validation

As shown in Table 1.1, collisions are not always prevented by the nominal controller in case of a communication *failure*. The prediction-based controller presented in the previous section is validated in all 23 defined test cases described in Appendix E.2 by simulations and experiments. In this section, the controller performance in the test cases is evaluated based on the key performance indicators defined in Section 2.1.

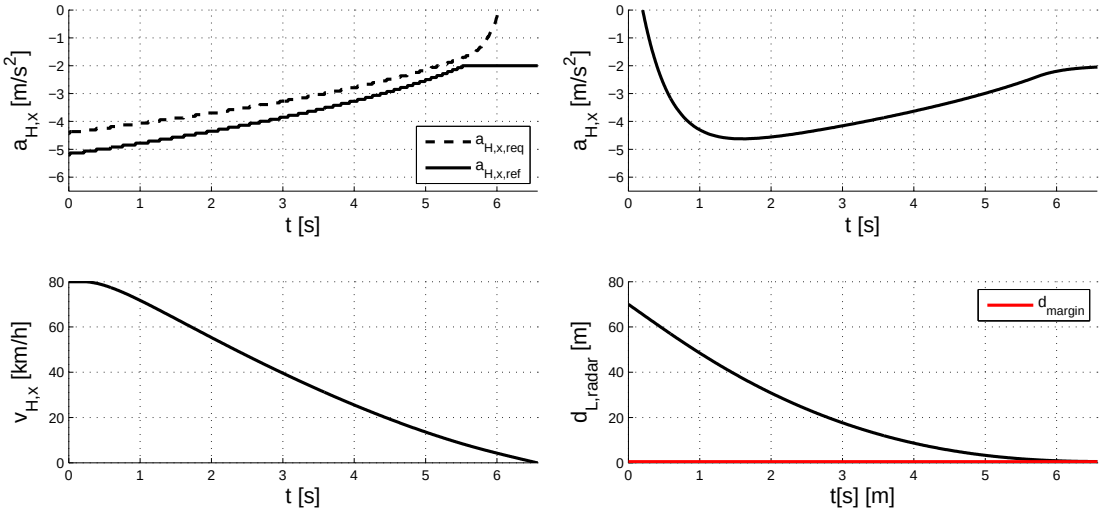

Fig 5.2: Simulation of a vehicle equipped with the prediction-based controller approaching a standing object

Remark. During the experiments, a margin is added to the following distance for safety. Hence, the collisions that will be mentioned are only virtual collisions that would occur if the safe margin is not added.

– **Number of collisions**: From the 23 test cases, in simulation 0 collisions occur; in the experiments 1 virtual collision occurs in Test 13. This is due to the low-level controller of the host vehicle which is not able to achieve the reference acceleration. This is illustrated in Fig 5.3. The reference acceleration is given by the dotted line and the solid line represents the actual acceleration. The spikes in the reference acceleration are because the platform does not allow to apply a low constant reference acceleration for more than 1.5s. More importantly, the actual acceleration is not matching the reference acceleration for a period of 3s. This implies the host vehicle does not decelerate enough, which results in a collision. Hence, it can be concluded that the virtual collision is caused by the low-level controllers, which are outside the scope of this thesis. Since already maximum braking is applied, increasing λ_{pred} will not solve this issue.

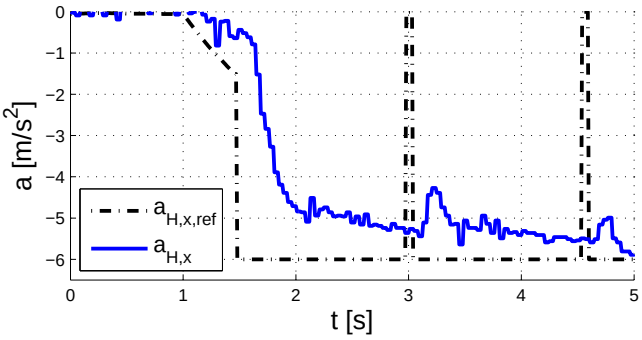

Fig 5.3: The host low-level controller not able to achieve the reference acceleration in Test 13

– **Impact speed**: The virtual collision in Test 13 during the experiments shows an impact speed of approximately 14km/h. In all other tests no collisions occur, so there is no impact speed.
– **Minimum inter-vehicle distance:** A comparison of the minimum inter-vehicle distance is shown in the left bar graph in Fig 5.4. Generally the minimum inter-vehicle distance is higher in the tests. The low-level controller of the lead vehicle is not always able to apply the intended acceleration. Hence less braking is applied by the lead vehicle in the experiments compared to the simulations, which results in

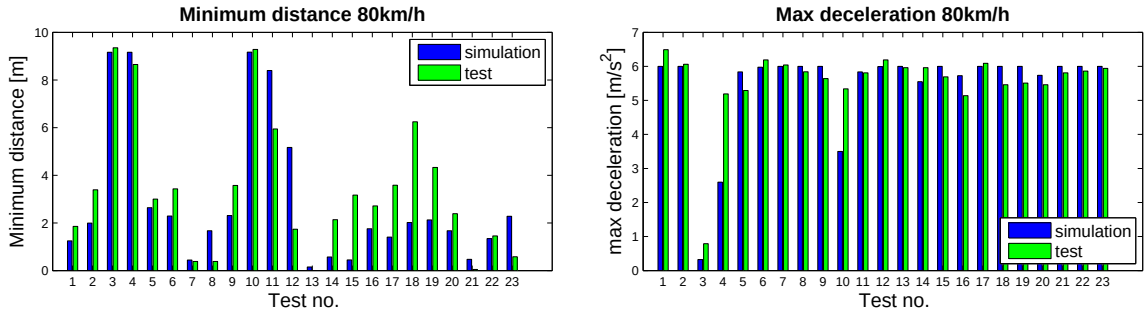

Fig 5.4: Simulation and test results for the prediction-based controller

a higher inter-vehicle distance.

– **Maximum deceleration:** A comparison of the maximum deceleration during the simulations and experiments is shown in the right bar graph in Fig 5.4. The maximum deceleration is similar in the simulations and tests, except for Test 4 and 10. These are tests where the lead vehicle does not brake, in order to evaluate the occurrence of *false positive* interventions. The system is designed to stay in Adaptive Headway Time or Intermediate Braking mode in case the lead vehicle does not brake (Section 4.3). This happens in simulation, but in practice Collision Avoidance becomes active resulting in severe braking. To investigate this, Transition G in Section 4.3 has to be further investigated. Sensor noise on the relative velocity ($\dot{d}_{L,radar}$) measured by the radar is causing the transitions to Collision Avoidance, which indicates the transition condition might be set too soft. However, making the transition condition stricter will lead to more collisions in the test cases. Here, a trade-off between safety and comfort has to be made.

As mentioned in Section 2.1, the experiments are performed with passenger cars instead of trucks. A comparison of the key performance indicators between passenger cars and trucks for the prediction-based controller is shown in Appendix E.1.

Remark. The results in Fig 5.4 are for a passenger car and not for a heavy-duty vehicle. Only adaptation in the longitudinal model is changing the time constant τ_b to 0.1s instead of 0.4s. The actuator time delay remains the same. Simulations for a heavy-duty vehicle show similar behaviour, but this is not validated by experiments.

5.2 Uncertainty analysis

Upto this point, the parameters describing the longitudinal vehicle model are assumed to be known accurately. However, the control methods designed in this thesis are aimed to be applied to heavy-duty vehicles. The variety in operating conditions for heavy-duty vehicles is much wider compared to passenger cars introducing system parameter uncertainties, as will be demonstrated in this section. Section 3.2.1 proved an accurate match between the model and measurements for a deceleration of 1m/s^2. However, if the system behaviour is accurately modelled for larger decelerations and under different circumstances is questionable. Some possible system uncertainties for heavy-duty vehicles are:

- Unmodelled tyre dynamics: for the linearised longitudinal vehicle model, tyre dynamics are neglected.
- The tyre to road friction coefficient is assumed to be constant and accurately known. However, in practice the tyre to road friction coefficient will vary.
- Variable air drag: head-winds influence the vehicle behaviour much more than for passenger cars. Moreover, the air drag is reduced by the leading and following vehicles, which is especially the case in a vehicle platoon.
- Braking system: As mentioned by for instance [34], the performance of heavy-duty vehicle braking systems is limited by pneumatic lag. Moreover, the truck braking system is highly complex; there are several types of brakes that can operate in parallel. For more information with respect to heavy-duty vehicle braking systems can be found in [41].
- The loading conditions can vary significantly, which influences the vehicle dynamic behaviour.

Parameter	Value
$\epsilon_{b,k}$	0.15
$\epsilon_{b,\tau}$	$0.1s$

Table 5.2: Uncertainty parameters

– Different types of semi-trailers might be connected to the same tractor.

Besides the uncertainties mentioned above, integrated braking and steering has the highest potential to avoid collisions according to literature (Section 1.3). However, as shown in Section 3.1.3, lateral forces (slip angles) influence the longitudinal forces in the magic formula. Although this report will not consider integrated braking and steering, this is an additional uncertainty when integrated braking and steering will be applied in the future. As discussed in Section 3.2.1, the nominal vehicle behaviour is modelled by a time constant and time delay:

$$\dot{a}_{H,x}(t) = \frac{1}{\tau_b \pm \epsilon_{b,\tau}} \left((1 \pm \epsilon_{b,k}) a_{H,x,ref}(t - \theta_b) - a_{H,x}(t) \right). \tag{5.2}$$

Whereas previously all parameters are assumed to be certain, now parameter uncertainty is introduced determined by uncertainty parameters $\epsilon_{b,k}$ and $\epsilon_{b,\tau}$. The considered values for the uncertainty parameters are shown in Table 5.2. The value for $\epsilon_{b,k}$ is chosen based on experiments and the value for $\epsilon_{b,\tau}$ is arbitrary chosen to evaluate the robustness of the controller to an uncertain time constant. The influence of the uncertainties on the key performance indicators in the test cases with the prediction-based controller is investigated:

– **Number of collisions**: The number of collisions for changing uncertainty parameters is shown in Table 5.3. The collisions occur especially when in (5.2) the $-\epsilon_{b,k}$ contribution appears, which implies the host vehicle has less braking capacity compared to the lead vehicle. The most collisions occur with a combination of $-\epsilon_{b,k}$ and $+\epsilon_{b,\tau}$.

	$-\epsilon_{b,\tau}$	$+\epsilon_{b,\tau}$
$-\epsilon_{b,k}$	12	14
$+\epsilon_{b,k}$	1	0

Table 5.3: Number of collisions for different uncertainty parameters with the prediction-based controller

– **Impact speed**: The bar graph showing the impact speed for the different uncertainty parameter values is shown in Fig 5.5. First remark is that in Test 1 collisions occur for three out of four parameter combinations. In this test case the lead vehicle starts full braking at the moment communication fails with a *failure* duration of 0.1s. Hence, only Adaptive Headway Time is activated because of the *fault-tolerant* time (Section 4.3 Transition C) and not the collision avoidance controller. This issue is caused by the transition conditions, which might be further tuned. Generally, in case $-\epsilon_{b,k}$ and $+\epsilon_{b,\tau}$ appear in (5.2), the most collisions with the most severe impact occur. Variations in this are due to the nominal controller which behaves differently for changing system parameters. The impact speed remains always below 20km/h.

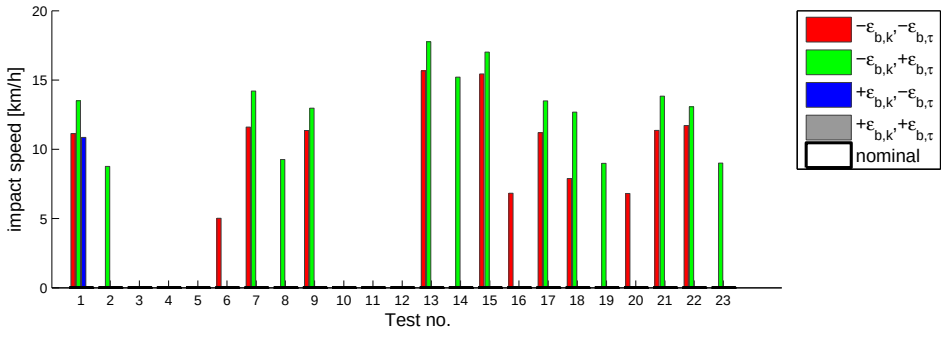

Fig 5.5: Impact speeds for the prediction-based controller applied to the uncertain system

– **Minimum inter-vehicle distance:** Fig 5.6 shows a comparison of the minimum inter-vehicle distance. The inter-vehicle distance is larger in case the host vehicle has more braking capacity ($+\epsilon_{b,k}$). Uncertainty parameter $\epsilon_{b,\tau}$ has only minor influence.

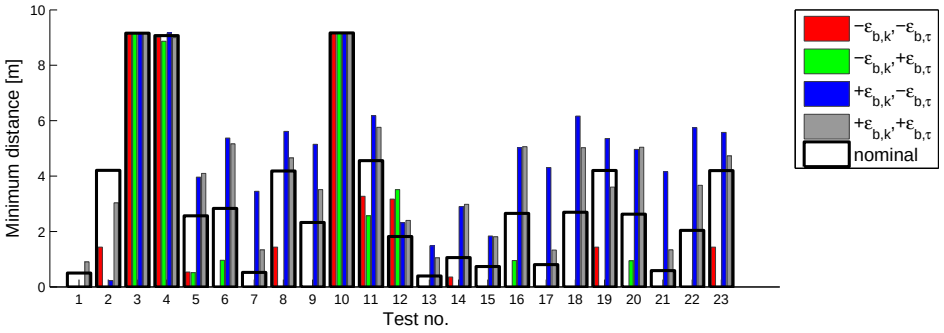

Fig 5.6: Minimum inter-vehicle distance for the prediction-based controller applied to the uncertain system

– **Maximum deceleration:** A comparison of the maximum deceleration for the different uncertainty parameter values is shown in Fig 5.7. Generally, the maximum decelerations are similar. In a few cases with $-\epsilon_{b,k}$, the maximum deceleration is lower since the host vehicle has less braking capacity.

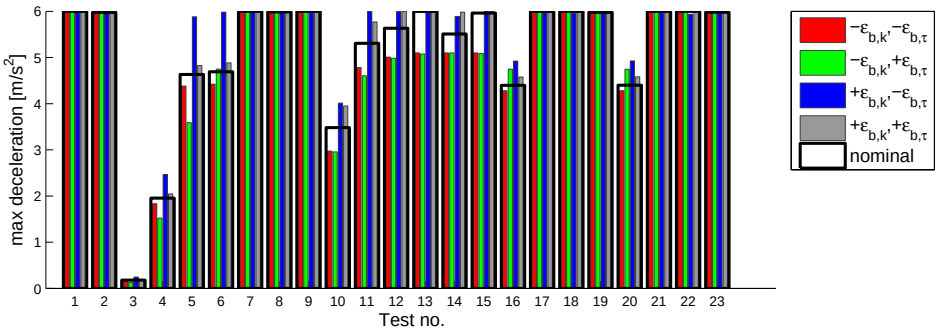

Fig 5.7: Maximum deceleration for the prediction-based controller applied to the uncertain system

It is concluded that parameter uncertainties might cause collisions. However, the impact speeds will be limited to 20km/h. One possibility to compensate for the system uncertainties is to increase the compensation factor (λ_{pred}) of the prediction-based controller in (5.1). Alternatively a robust control method can be applied, which will be discussed in the next section.

5.3 Sliding mode controller

As mentioned in the previous section, system uncertainties might influence the system behaviour significantly. This requests robust control methods that are able to control systems with uncertain parameters. A possible robust control method is Sliding Mode Control (SMC). Apart from the robustness features against possible disturbances and parameter uncertainties of the vehicle model, SMC has a low complexity compared to other robust control methods (H_∞, robust frequency approach, etc.). SMC is able to apply high gains without making the system unstable when designed correctly. One of the main disadvantages of these high gains is that it might lead to energy loss and excessive actuator wear. But since activation of Collision Avoidance should be limited to a minimum and the duration for which it will be active is short, this is not an issue for this specific application. This section proposes a SMC approach for emergency braking in collision avoidance. As for the prediction-based controller, first the controller design is discussed and an example of the controller behaviour in case the vehicle approaches a standing object is shown. Finally, the results in the communication *failure* scenario will be presented.

5.3.1 Controller design

In [23] and [28] a SMC for longitudinal and lateral collision avoidance is designed. These papers use velocity control for longitudinal collision avoidance: the control objective is to control the host velocity to a reference velocity. This reference velocity could be the lead vehicle velocity. In this section an alternative approach is proposed: control the host vehicle acceleration to a desired acceleration. The desired acceleration is calculated based on the threat (BTN), which incorporates the required acceleration to avoid an accident (Definition 4.2.1). The detailed calculation of the required acceleration proposed in Section 4.2.2 is not applicable, since the system parameters are assumed not to be accurately known. Alternatively, the required acceleration is calculated with a limited jerk profile, as shown in Appendix D.

To discuss the controller design, the use case of the host vehicle approaching a standing object at an initial distance x_{stop} will be considered, illustrated in Fig 5.8. The initial host vehicle front bumper position in the global coordinate frame is chosen to be the origin ($x_H(t_0) = 0$). The vehicle velocity profile to stop the vehicle before the object with a constant deceleration is shown in Fig 5.9. When due to system uncertainties or disturbances the system is not able to achieve the required acceleration to avoid a collision, the required acceleration will increase, illustrated by the red arrow. However, the maximum achievable deceleration is limited by the system saturation limits; if this limit is exceeded a collision is unavoidable. Hence the trajectory should be on the required acceleration surface. In case the trajectory leaves the surface it should be directed back towards it, which is illustrated by the green arrow.

Based on the previous discussion, the vehicle acceleration should be on the required acceleration surface. The difference between required acceleration and actual acceleration is defined as sliding variable s_x:

$$s_x(t) = a_{H,x}(t) - a_{H,x,req}(t), \tag{5.3}$$

where $a_{H,x}$ is the host acceleration and $a_{H,x,req}$ the required acceleration to avoid a collision obtained from the BTN. The surface $s_x = 0$ is the surface where the actual acceleration matches the required acceleration. In the controller analysis, for simplicity a constant acceleration model (neglecting actuator dynamics, vehicle dynamics, etc.) will be used for calculation of the required acceleration. The required acceleration to stop before a constant desired stopping distance x_{stop}, using a constant acceleration model can be calculated by:

$$a_{H,x,req}(t) = \frac{v_{H,x}^2(t)}{2(x_H(t) - x_{stop})}, \quad x_H(t_0) = 0, \tag{5.4}$$

where $v_{H,x}$ is the host velocity. A discontinuous control law u_x is defined, as shown in Fig 5.10, to maintain the system trajectories on the surface $s_x = 0$ once the trajectories reached the surface. Control effort u_x^+ is applied if the trajectory is above the surface ($s_x > 0$); u_x^- if the trajectory is below the surface ($s_x < 0$):

$$u_x(t) = \begin{cases} u_x^- & \text{if } s_x(t) < 0, \\ 0 & \text{if } s_x(t) = 0, \\ u_x^+ & \text{if } s_x(t) > 0. \end{cases} \tag{5.5}$$

The control law should fulfil two requirements. First it should ensure the surface can be reached. Second, it should maintain the trajectories to the surface once they reached the surface. Only than the surface is called a sliding surface. First the latter requirement will be elaborated. On the surface (s_x=0), the sliding variable time derivative $\dot{s}_x$ should be zero as well in order to remain on the surface for the future

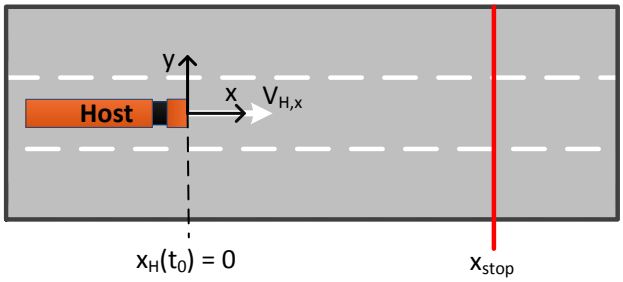

Fig 5.8: Illustration of the host vehicle and a fixed desired stopping distance

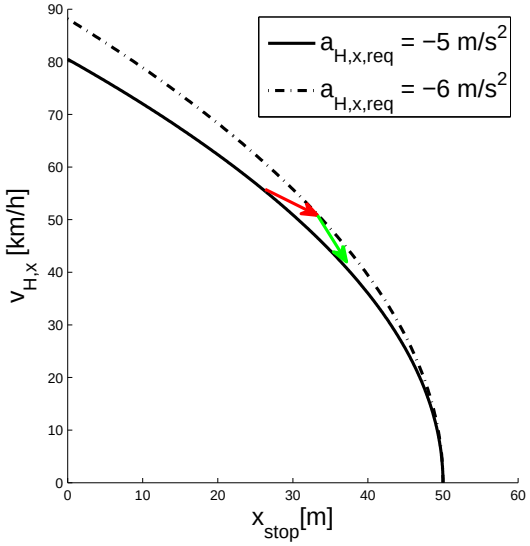

Fig 5.9: Vehicle velocity as function of stopping distance assuming a fixed required acceleration.

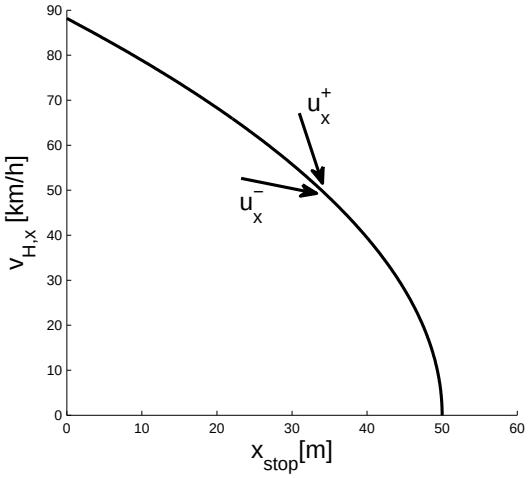

Fig 5.10: Control actions on both sides of the surface to maintain the trajectories on the surface

by applying a proper control strategy. The following holds for first time derivative of the sliding variable:

$$\dot{s}_x(t) = \dot{a}_{H,x}(t) - \frac{v_{H,x}(t)}{x_H(t) - x_{stop}} \left(a_{H,x}(t) - \frac{v_{H,x}^2(t)}{2(x_H(t) - x_{stop})} \right), \tag{5.6a}$$

$$\dot{s}_x(t) = \dot{a}_{H,x}(t) - \frac{v_{H,x}(t)}{x_H(t) - x_{stop}} s_x(t), \tag{5.6b}$$

$$\text{if } s_x(t) = 0 \Rightarrow \quad \dot{s}_x(t) = \dot{a}_{H,x}(t). \tag{5.6c}$$

From (5.6c) it can be concluded that the behaviour on the surface, also referred as sliding behaviour, is completely determined by the jerk ($\dot{a}_{H,x}$). Assume the jerk can be controlled directly

$$u_x(t) = \dot{a}_{H,x}(t), \tag{5.7}$$

and evaluate the Lyapunov candidate

$$V_x(t) = \frac{1}{2} s_x(t)^2. \tag{5.8}$$

The time derivative of this Lyapunov candidate is:

$$\dot{V}_x(t) = s_x(t)\dot{s}_x(t). \tag{5.9}$$

Substitution of equations (5.5) and (5.7) into (5.9) results in the following derivative of the Lyapunov candidate

$$\dot{V}_x(t) = \begin{cases} s_x(t)u_x^- & \text{if } s_x(t) < 0 \\ 0 & \text{if } s_x(t) = 0 \\ s_x(t)u_x^+ & \text{if } s_x(t) > 0. \end{cases} \tag{5.10}$$

When choosing a positive scalar for u_x^- and a negative scalar for u_x^+, this Lyapunov candidate is negative semi-definite. Only on the sliding surface the Lyapunov derivative is zero, which proves that the trajectories will remain on the sliding surface once they reach the surface. Next, the reaching phase will be discussed. In the reaching phase s_x is not zero, hence (5.6b) should be considered. By using (5.7), the Lyapunov candidate derivative is negative semi-definite, if and only if the condition

$$|u_x(t)| \geq \left| \frac{v_{H,x}(t)}{x_H(t) - x_{stop}} s_x(t) \right| \tag{5.11}$$

holds. In case the Lyapunov candidate is not negative semi-definite, reaching the sliding surface cannot be guaranteed. Physically, this corresponds to for instance the case that the inter-vehicle distance

$(x_H(t) - x_{stop})$ is very small, because the right hand side in (5.11) will become large. Hence the required acceleration cannot be reached and a collision is unavoidable. However, the Safety Mode Selection should activate Emergency Braking in time to guarantee reaching of the required acceleration (sliding surface). In that case the controller will direct the trajectories to the surface.

According to (5.7), the jerk is controlled directly. In reality the jerk is not controlled but behaves according to (5.2), where the reference acceleration $a_{H,x,ref}$ is the input. The time delay is chosen to be zero and the actuator time constant is assumed to be unknown. Following the ideas of integral SMC, $\dot{a}_{H,x}$ is assumed to be controlled directly to suppress oscillating behaviour due to unmodelled actuator dynamics. Hence the control input $a_{H,x,ref}$ is defined as:

$$a_{H,x,ref}(t) = \int_{t_0}^{t} u_x(\xi) d\xi \tag{5.12}$$

where u_x is given by (5.5). This control law filters the control signal to prevent oscillations, but it also results in additional phase lag. Another issue due to the integral action is drift. However, since the collision avoidance controller will be active for a limited duration, this is not a problem. The control actions on both sides of the surface (Fig 5.10) can be chosen differently. If the trajectory is above the surface ($s_x > 0$), the required deceleration is not achieved; hence a collision can occur. Therefore, control action u_x^- might be chosen 'softer' and u_x^+ more 'severe'.

Boundary layer

The control law (5.5) applies a infinite high gain in the vicinity of the sliding surface, which results in fast switching behaviour. This switching behaviour leads inherently to chattering: small oscillating behaviour around the sliding surface instead of ideal sliding. These oscillations can be due to time delays and unmodelled dynamics. Because the actuator dynamics are neglected in the design, chattering will occur. A comparison on chattering suppression techniques can be found in [35]; possible chattering suppression methods mentioned are:

- Observer-based chattering suppression.
- State-dependent gain method.
- Equivalent-control-dependent gain method.

In this section the simplest method is chosen: the state-dependent gain method. More specifically, a boundary layer is defined around the sliding surface, proposed in for instance [31]. Inside the boundary layer, the discontinuous control law is replaced by a continuous function to avoid discontinuity in the control signals. The larger the boundary layer width, the smoother the control signal. The boundary layer design will suppress chattering, however the control law will not guarantee that the system trajectories will converge to the sliding surface, but to a region around the sliding surface. The size of this region is determined by the width of the boundary layer: the larger the width of the boundary layer, the larger the region around the sliding surface where the trajectories might end up. Hence, a trade-off between smoothness and accuracy has to be made. Following the boundary layer approach, the control law in (5.5) is replaced by:

$$u_x = \begin{cases} u_x^+ & \text{if } K_x s_x \geq 1 \\ K_x s_x u_x^+ & \text{if } 0 \leq K_x s_x < 1 \\ -K_x s_x u_x^- & \text{if } -1 < K_x s_x < 0 \\ u_x^- & \text{if } K_x s_x \leq -1. \end{cases} \tag{5.13}$$

The larger boundary layer gain K_x is chosen, the closer the controller behaviour is to the original sign function. However, in case K_x is chosen relatively small, the closed loop dynamics within the boundary layer should be considered separately. Using (5.3), (5.12) and (5.13), the required acceleration in the boundary layer can be written as:

$$a_{H,x,ref} = -K_x \left| u_x^{+/-} \right| \int_{t_0}^{t} a_{H,x}(\xi) - a_{H,x,req}(\xi) d\xi. \tag{5.14}$$

This control law applied to System (5.2) results in the closed loop dynamics of the system within the boundary layer. The control gain $-K_x \left| u_x^{+/-} \right|$ determines the closed loop dynamics. Different values for

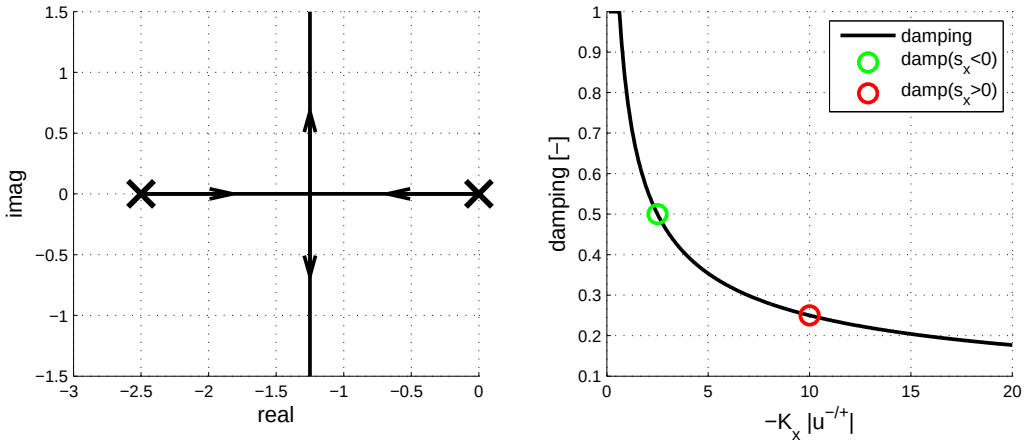

Fig 5.11: The root-locus plot for the nominal system is shown at the left. At the right the nominal system damping as function of gain $-K_x \left| u_x^{+/-} \right|$ is shown.

u_x^- and u_x^+ imply the behaviour on both sides of the surface is different. Assuming the nominal system parameters, the root-locus plot of the closed loop system is shown in left plot of Fig 5.11. The right plot shows the damping of the system as function of the control gain. The damping for the controller parameters given in Table 5.4 is illustrated by the circles. The green circle shows that for $(S_x < 0)$ the damping within the boundary layer is 0.5. The red circle shows that the damping for $(S_x > 0)$ within the boundary layer is 0.25. The damping is higher in case the trajectories are below the surface $(S_x < 0)$ since the value for u^- is smaller compared to u^+. However, the chosen control parameters should ensure stable closed loop system behaviour within the boundary layer.

Predictor

In the previous paragraphs the actuator time delay is neglected. However, this delay is approximately 0.2s, which is non-negligible when driving at a time gap of 0.3s to the preceding vehicle. Therefore a state predictor is designed as in [57], estimating the vehicle trajectory $\mathcal{H}$ for a period equal to the actuator time delay (θ_b) in the future. The definition of $\mathcal{H}$ is given in (4.7).

$$\mathcal{H}(t_0 + \theta_b) = e^{-\underline{A}_x \theta_b} \mathcal{H}_0 + \int_{t_0}^{t_0+\theta_b} e^{-\underline{A}_x (t_0+\theta_b-\xi)} \underline{B}_x u_x(\xi - \theta_b) d\xi,$$
$$\underline{A}_x = \begin{bmatrix} 0 & 1 & 0 \\ 0 & 0 & 1 \\ 0 & 0 & 0 \end{bmatrix}, \quad \underline{B}_x = \begin{bmatrix} 0 \\ 0 \\ 1 \end{bmatrix} \tag{5.15}$$

Example 5.3.1. An example of the behaviour of the host vehicle state predictor is shown in Fig 5.12. The left plot shows the input u_x; the right plot the actual host acceleration $a_{H,x}$ and predicted host vehicle acceleration $\hat{a}_{H,x}$. The predicted values respond faster since input u_x is used to predict the future host vehicle state. Ideally the predicted values should be shifted the actuator time delay $(0.2s)$ to the left compared to the actual values. However, since the actuator dynamics are not taken into account, the amplitude differs slightly. □

Remark. Note that actuator dynamics are not taken into account in the predictor. In case the system parameters are known accurately, taking actuator dynamics into account would increase the accuracy of the predictor. However, since the time constant is assumed to be uncertain, the control variable u_x is directly chosen as an input for the predictor.

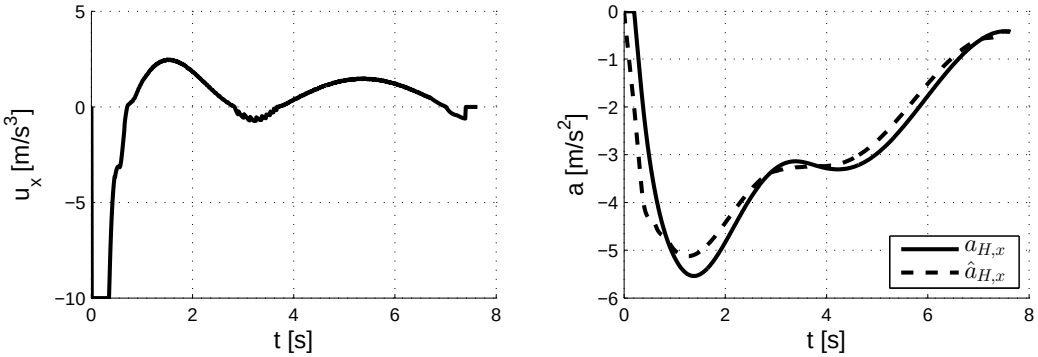

Fig 5.12: Example of the host state predictor behaviour in an emergency braking scenario

Implementation

The control scheme of the implemented SMC is illustrated in Fig 5.13. The scheme will be discussed from left to right. The controller parameter values can be found in Table 5.4. The maximum deceleration value is determined by the saturation of the low-level controller. The other values are tuned in simulation to achieve the desired behaviour. The sensors give input to predict the host state (5.15) and predict a worse case target trajectory, which is discussed in Section 4.1. With this information the required acceleration is calculated according to a limited jerk profile, explained in Appendix D. The jerk limit is given by $j_{x,lim}$. To reduce the threat (BTN) faster, a small bias tuned by the compensation factor λ_{SMC} is added to the required acceleration. Moreover, this bias compensates for inaccuracies in the host state predictor. After that the boundary layer is defined by a saturated function $K_x s_x(t)$. The saturated function is multiplied by u_x^+ or u_x^-, which is used in the host state predictor. The reference jerk is integrated, resulting in the reference longitudinal acceleration applied to the system. The desired acceleration is given as initial condition to the integrator to speed up the response when Collision Avoidance is activated. In literature, usually this term is given as feedforward control signal to the system. However, this complicates the design of the anti-windup integrator. The anti-windup integrator is needed since the output of the integrator is saturated by the minimum possible host acceleration $a_{H,x,min}$ and zero. Positive acceleration in Collision Avoidance is assumed to be undesired. The controller can be described by:

$$
\begin{aligned}
a_{x,ca}(t) &= \int_{t_0}^{t} u_x(t)dt + a_{x,ca,0}, \quad a_{x,ca,0} = a_{H,x,req}(t_0) + \lambda_{SMC}\ a_{H,x,min}, \\
a_{H,x,ref}(t) &= \begin{cases} 0 & \text{if } a_{x,ca}(t) > 0, \\ a_{x,ca}(t) & \text{if } a_{H,x,min} < a_{x,ca}(t) < 0, \quad t \in [t_0, \infty], \\ a_{H,x,min} & \text{if } a_{x,ca}(t) < a_{H,x,min}, \end{cases}
\end{aligned}
\tag{5.16}
$$

where t_0 is the time that Emergency Braking is activated.

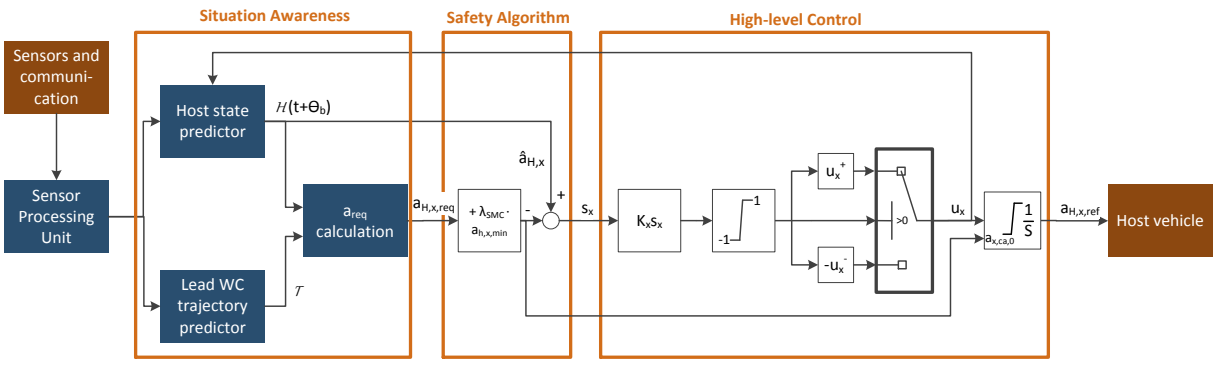

Fig 5.13: Control scheme of the longitudinal SMC

Variable	Description	Value
$a_{H,x,min}$	Maximum deceleration	$-6m/s^2$
$j_{x,lim}$	Jerk limit for required acceleration calculation	$5m/s^3$
K_x	Boundary layer gain	1
u_x^-	Control effort to reduce s_x	$-2.5m/s^3$
u_x^+	Control effort to increase s_x	$10m/s^3$
λ_{SMC}	Compensation factor	0.125

Table 5.4: Chosen parameter values for the longitudinal SMC

Example 5.3.2. In Fig 5.14 the simulation results are shown of the host vehicle approaching a standing object driving initially 80km/h. The top left plot shows the reference acceleration; the top right plot the required and actual acceleration. Heavy braking is applied when Collision Avoidance is activated, which is reduced when the required acceleration (related to the BTN) is reduced. The difference between the required and actual acceleration with a negative bias for safety, is the sliding variable shown in the bottom left plot. A positive value for s_x implies the trajectory is above the sliding surface, hence more braking effort is required. Negative values imply the trajectory is below the sliding surface, hence the braking effort can be reduced. It is evident to say that the situation where the trajectory is above the sliding surface is more critical than if it is below the surface. The sliding variable is positive at the beginning of the simulation and converges towards the sliding surface $s_x = 0$ afterwards. The trajectories do not start to slide immediately because of the boundary layer defined by (5.13) and the smaller control effort u_x^- compared to u_x^+. Due to this asymmetric control law, the sliding variable is clearly more negative than positive. As mentioned, negative values for s_x are less critical. The bottom right plot shows the distance to the standing object. The vehicle comes to a standstill before the inter-vehicle distance $d_{L,radar}$ reaches the red line illustrating the safety margin d_{margin}, implying a collision is avoided.

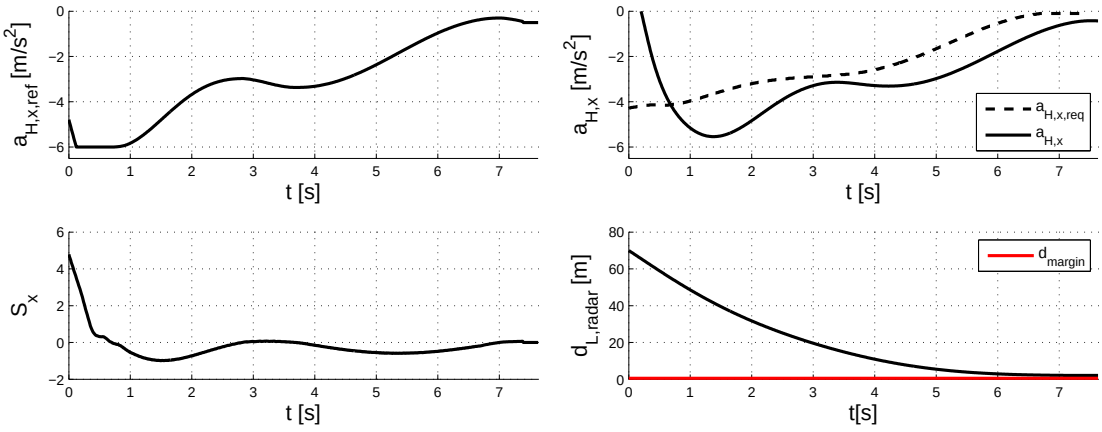

Fig 5.14: Simulation of a vehicle with the SMC approaching a standing object

5.3.2 Simulation results

Similar to the prediction-based controller, the SMC is evaluated in all defined test cases in Appendix E.2 using the key performance indicators stated in Section 2.1. The evaluation is done by simulations with uncertain system parameters. The results will be discussed in this section.

- **Number of collisions**: For the nominal system no collisions occur. The collisions for the uncertain system are shown in Table 5.5. From this table it can be concluded that it is most critical when $-\epsilon_{b,k}$ appears: the host vehicle has less braking capacity.
- **Impact speed**: Fig 5.15 shows the impact speed for the SMC applied to the uncertain system. The same conclusions as drawn for the prediction-based controller in Section 5.2 hold.

	$-\epsilon_{b,\tau}$	$+\epsilon_{b,\tau}$
$-\epsilon_{b,k}$	12	14
$+\epsilon_{b,k}$	1	0

Table 5.5: Number of collisions with varying uncertainty parameters using the SMC

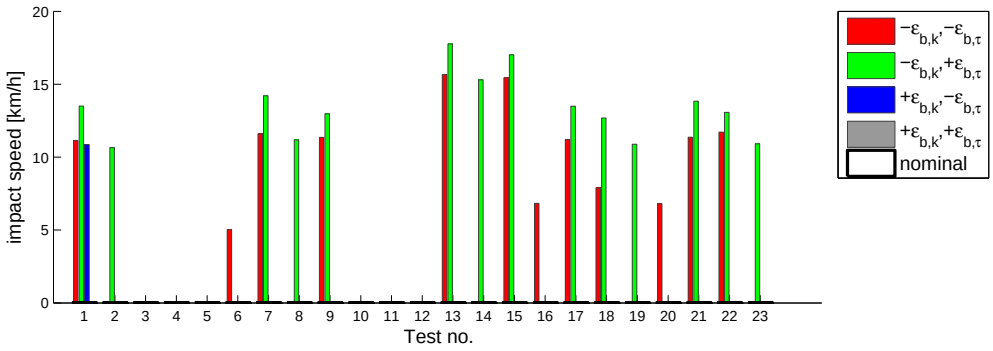

Fig 5.15: Impact speeds for the SMC applied to the uncertain system

– **Minimum inter-vehicle distance:** Fig 5.16 shows a comparison of the minimum inter-vehicle distance. The inter-vehicle distance is the largest in case the host vehicle has more braking capacity $+\epsilon_{b,k}$ and a low time constant $-\epsilon_{b,\tau}$.

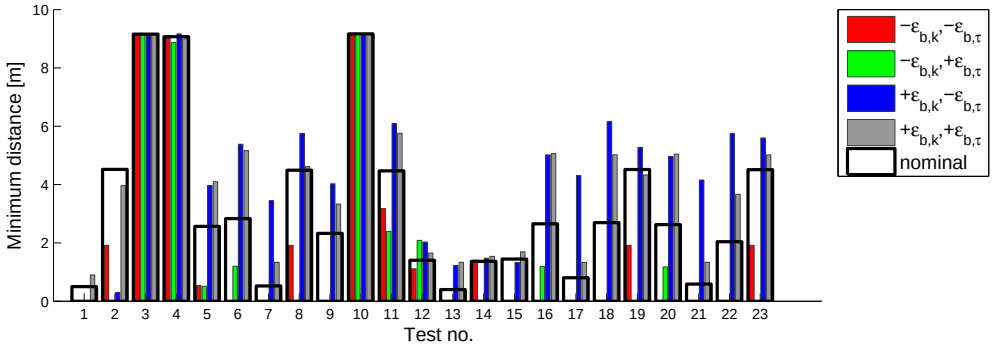

Fig 5.16: Minimum inter-vehicle distance for the SMC applied to the uncertain system

– **Maximum deceleration:** Generally, the maximum decelerations in Fig 5.17 are similar for all uncertainty parameters. For $-\epsilon_{b,k}$ sometimes the maximum deceleration is lower since the host vehicle has less braking capacity.

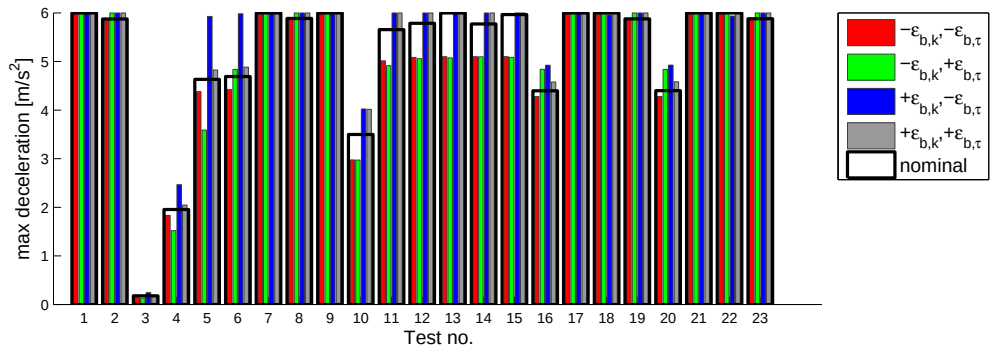

Fig 5.17: Maximum deceleration for the SMC controller applied to the uncertain system

Based on the previous evaluation of the key performance indicators, it can be concluded that the SMC approach is not able to avoid collisions in the defined test cases with uncertain system parameters, where for the nominal system it does prevent collisions in all test cases. Especially in case the host vehicle has less braking capacity compared to the lead vehicle collisions occur. To ensure safety in that case, the time gap should be increased or the order should be changed.

5.4 Controller comparison

In this section the behaviour of the prediction-based controller and SMC are compared. As for the individual controllers, first the controller behaviour approaching a standstill object is compared in an example. An example of the controller sensitivity to system parameter uncertainties is given as well. Finally, the controller behaviour in the communication *failure* scenario is compared by simulations.

Example 5.4.1. The same simulation as for evaluating the prediction-based controller and SMC individually is used for the standstill object example in this comparison: the host vehicle approaches a standing object, driving at a constant velocity of 80km/h when Collision Avoidance is activated. Initially the distance to the standing object is 70m; the vehicle has to be brought to a standstill within 70m. The results are shown in Fig 5.18. The top left plot shows the applied reference acceleration and the top right plot the actual acceleration. The bottom left plot shows the host vehicle velocity; the stopping distance is illustrated by the red line. Both controllers bring the vehicle to a standstill before the stopping line, however the SMC is more conservative leaving a larger standstill distance. The BTN, which is directly related to the required acceleration to avoid a collision, is shown at the bottom right. Note that the travelled distance is on the horizontal axis instead of time. When comparing the acceleration behaviour in the top plots, clearly the prediction-based controller shows smoother behaviour. The SMC brakes more at the start and reduces the braking effort faster afterwards. This is expected behaviour, since the SMC is aimed to be applied to an uncertain system. Therefore it applies more braking at the start to bring the system faster to a safe state. *False positive* interventions should be prevented by the transition conditions in the Safety Mode Selection. If not, more severe braking is applied with the SMC compared to the prediction-based controller in case of *false positives*, which might be hazardous for traffic approaching from behind.

Remark. Note that the BTN for the prediction-based controller is calculated using the method discussed in Section 4.2. The SMC uses a limited jerk profile to calculate the BTN which is shown in Appendix D.

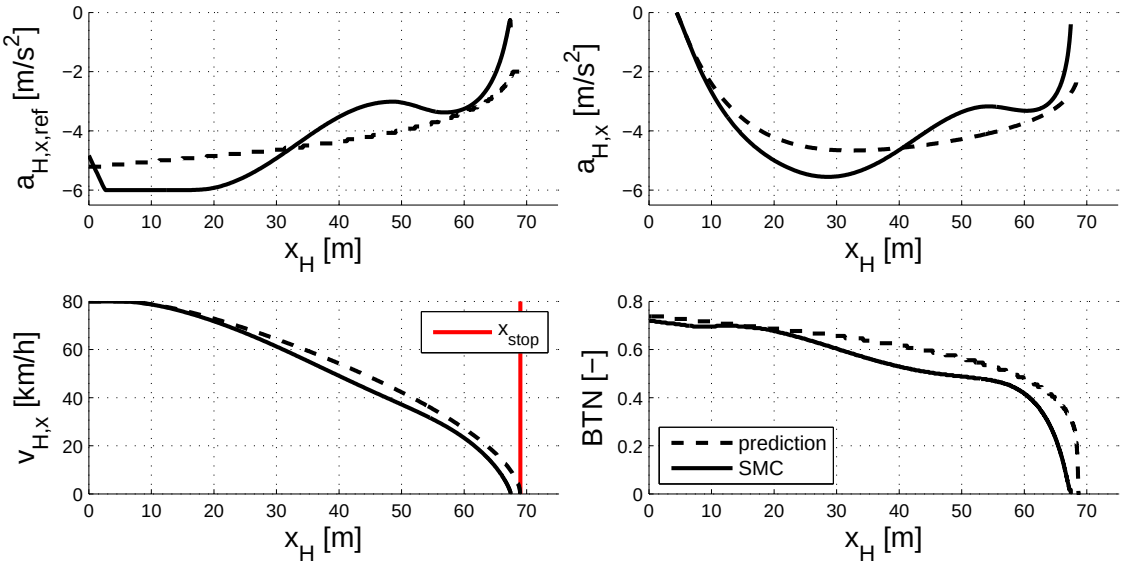

Fig 5.18: Simulation results for the prediction-based controller and SMC applied to the certain system

Example 5.4.2. This example shows the same tests case as Example 5.4.1 for uncertain system parameters. Simulations proved $-\epsilon_{b,k}$ and $+\epsilon_{b,\tau}$ to be the most critical parameter combination for System (5.2), since with these uncertainty parameters the most collisions occur. The simulation results for the prediction-based controller and SMC in this critical case are shown in Fig 5.19. The prediction-based controller starts braking with a braking effort related to the BTN. Because of system uncertainties, this braking effort is not enough to come to a standstill before the object. Hence the BTN increases; consequently more braking is applied. At the end of the braking event the vehicle runs into its deceleration saturation, hence it is not able to stop before reaching the object illustrated by the red line in the bottom left plot. The SMC is able to stop the vehicle before the object. Based on this example it can be concluded that the SMC is less vulnerable for system uncertainties.

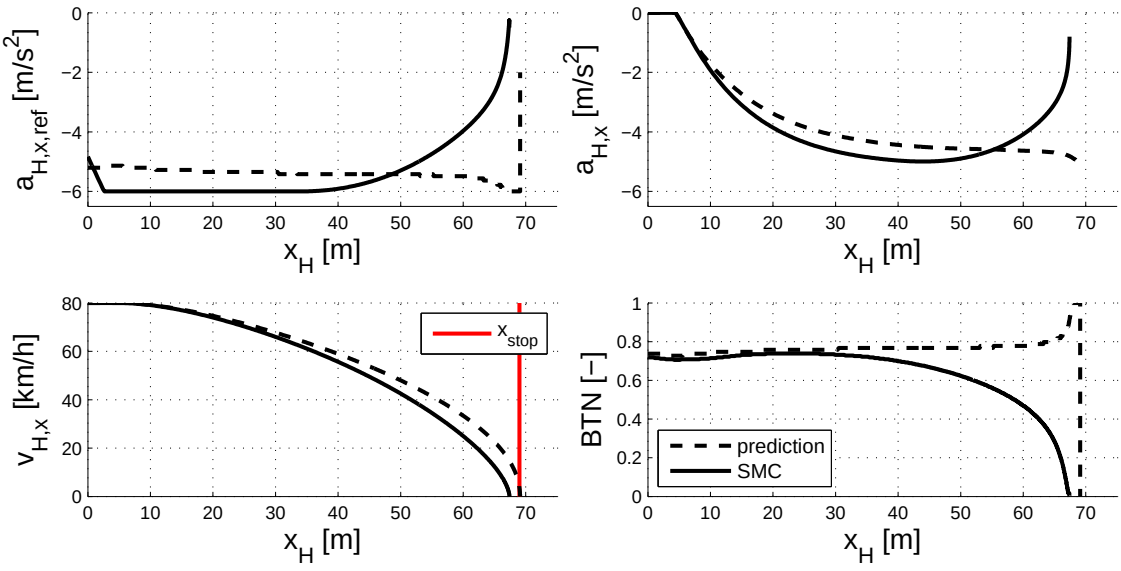

Fig 5.19: Simulation results for the prediction-based controller and SMC applied to a system with $-\epsilon_{b,k}$ and $+\epsilon_{b,\tau}$

Next, a comparison of the prediction-based controller and SMC is presented in the communication *failure* scenario discussed in Section 1.2. The exact description of all tests can be found in Appendix E.2. The comparison is based on the key performance indicators stated in Section 2.1.

- **Number of collisions**: The prediction-based controller and SMC show collisions in exactly the same test cases for the same uncertainty parameters. Especially in case the host vehicle has less braking capacity, none of the controllers will prevent collisions in the critical test cases. The only solution to be safe in that situation is to either make sure the vehicle with less braking capacity is the following vehicle, or increase the following distance.
- **Impact speed**: Fig 5.20 shows a comparison of the impact speed for both controllers. The impact speed is very similar. Since the collisions occur in the test cases where the preceding vehicle applies maximum braking, the host has to apply maximum braking as well. Hence, the timing of Collision Avoidance activation is of major importance and not the controller itself, because both controllers will apply maximum braking.
- **Minimum inter-vehicle distance:** The bar graphs in Fig 5.21 shows a comparison of the minimum inter-vehicle distance during the simulation for the prediction-based controller and SMC. As for the impact speed, the minimum inter-vehicle distances are similar for both controllers.
- **Maximum deceleration:** The comparison of the maximum deceleration in Fig 5.22 shows hardly any difference between the controllers.

To evaluate why the controllers have such a similar behaviour, the results of Test 14 with the nominal system parameters is shown in Fig 5.23. In this test, the lead vehicle brakes with -2m/s^2 at the moment

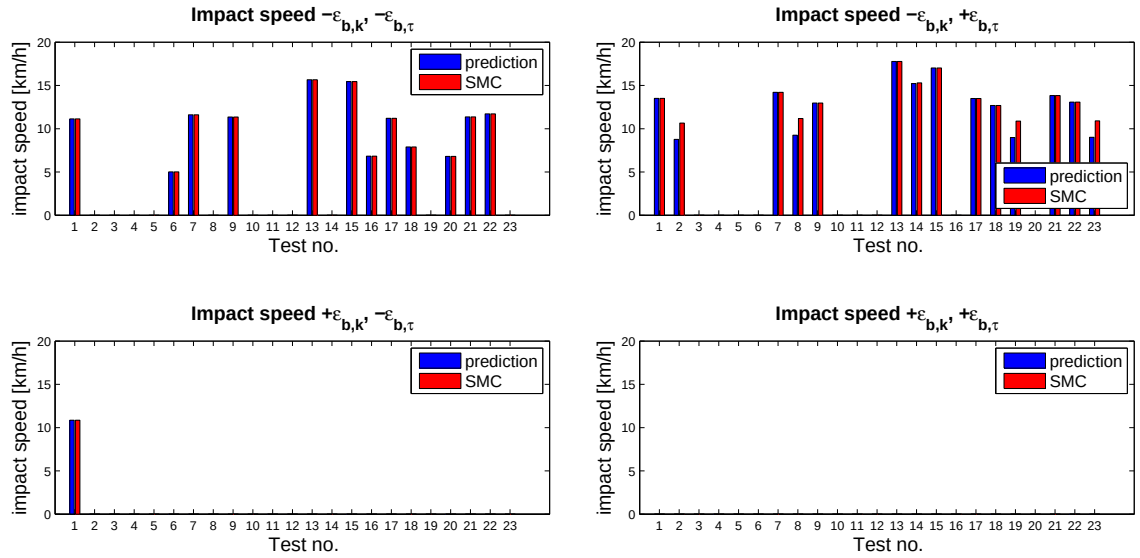

Fig 5.20: Impact speed comparison with varying uncertainty parameters

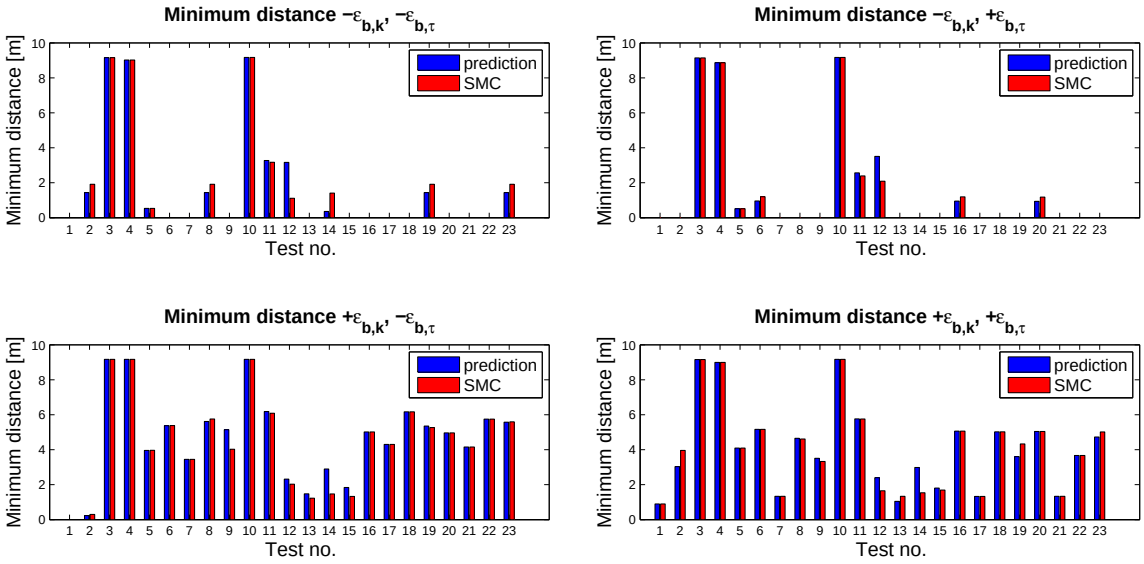

Fig 5.21: Minimum inter-vehicle distance comparison with varying uncertainty parameters

communication fails. Here the largest differences occur; in a test where the lead vehicle applies full braking, the controllers will just apply full braking to the host vehicle as well. The top left plot shows the inter-vehicle distance, the left bottom plot the host and lead vehicle speed and the top right plot the host reference and actual acceleration. On the right bottom the BTN is shown. Both controllers show very similar behaviour: applying full braking when Collision Avoidance is activated and then slowly reduce the braking effort. The SMC applies longer full braking and reduces the braking effort faster afterwards compared to the prediction-based controller.

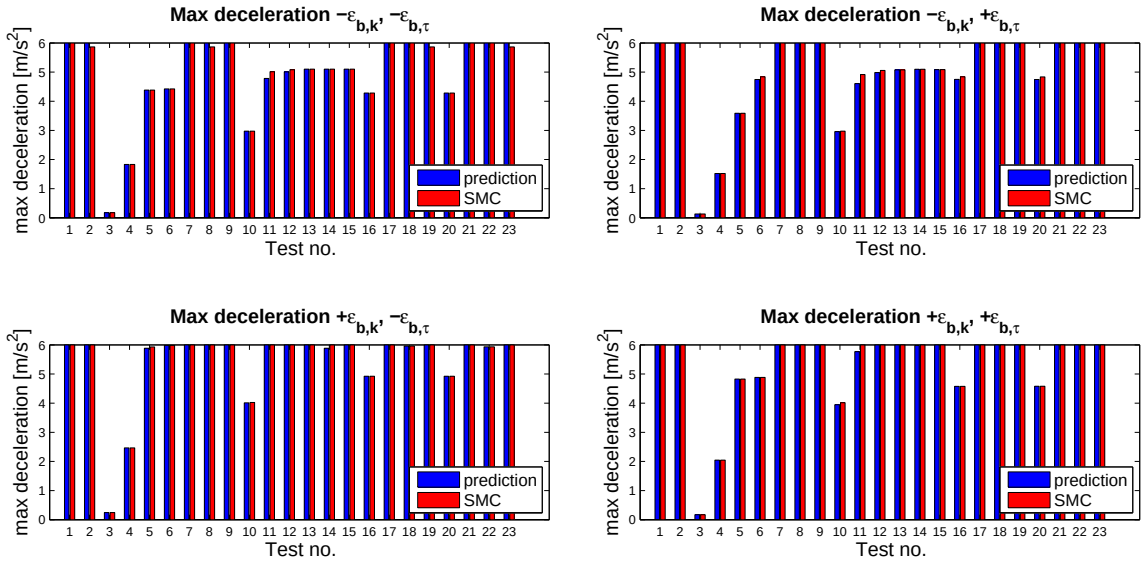

Fig 5.22: Maximum deceleration comparison with varying uncertainty parameters

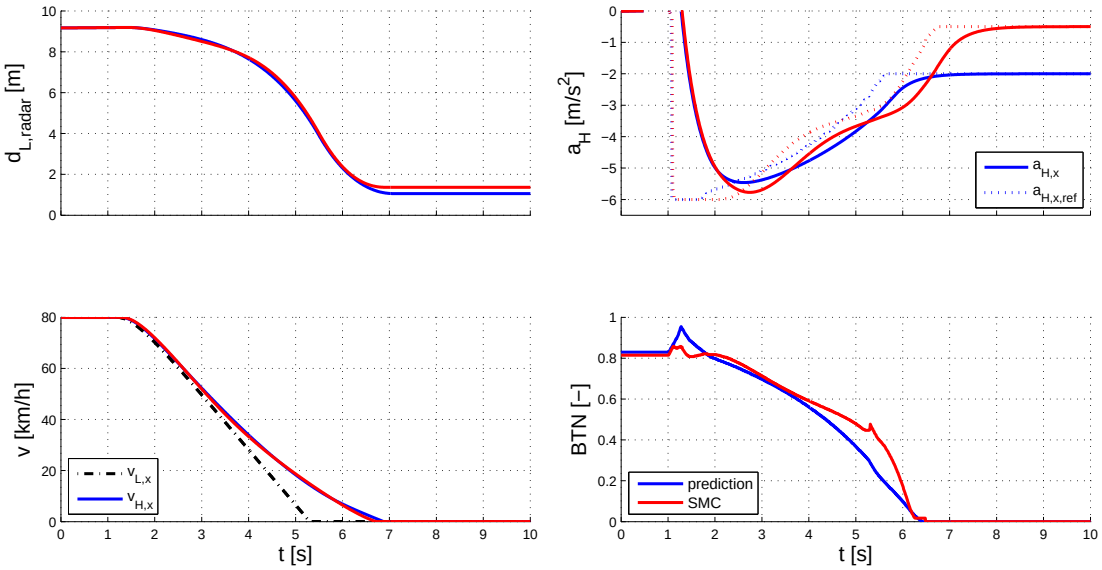

Fig 5.23: Simulation results for the nominal system of Test 14: the lead vehicle brakes with -2m/s^2 from the moment communication fails for 10s

5.5 Conclusion

In this chapter two controller types for longitudinal collision avoidance are designed and evaluated: a prediction-based controller and a SMC. The prediction-based controller delivers smoother behaviour compared to the SMC. There are however possibly several system parameter uncertainties. The varying loading conditions and the complex braking system are two examples of possible factors that may introduce system uncertainties. The SMC has a higher potential in handling system uncertainties, since the prediction-based controller assumes the system behaves like its modelled; the SMC approach does not take system parameters into account. Both the prediction-based controller and SMC are able to avoid

collisions in all defined test cases in the communication *failure* scenario in simulation with the nominal system parameters. For the uncertain system, a collision cannot always be avoided in case the following vehicle has less braking capacity. Although the SMC is potentially more robust to system uncertainties, in simulations the same collisions occur for both controllers. Which controller is selected is upto the designer. The SMC is more robust for a highly uncertain system at the cost of smoothness compared to the prediction-based controller. The prediction-based controller is validated with experiments on the test track with passenger cars. There proves to be a high consistency between the experiment and simulation results. However, sensor noise causes *false positive* interventions. How to prevent these without introducing *false negatives* has to be looked at in the future.

Chapter 6

Lateral collision avoidance control

The previous chapter presented two possible collision avoidance control methods using only braking. This chapter will elaborate on collision avoidance by only steering. First, some adaptations and uncertainties with respect to the lateral vehicle model will be discussed. Second, a discussion on the lateral collision avoidance control objective is given. Then, the controller design and implementation is discussed. Finally, the controller will be evaluated using simulations in the communication *failure* scenario and the controller robustness will be evaluated.

6.1 Vehicle model

In this section, the linear lateral vehicle model presented in Section 3.2.2 will be discussed in more detail. First, the vehicle model will be adapted to the lateral collision avoidance objective. Second, the system parameter uncertainties will be evaluated.

Look ahead distance

The vehicle model in Section 3.2.2 describes the behaviour of the vehicle centre of gravity. However, the centre of gravity is not the point of interest. The front bumper should avoid a collision with an object in front of the vehicle. This section will show how the time derivatives of the position of the front bumper centre are described, since these are needed for the controller design in this chapter. The linearised lateral velocity of the vehicle centre of gravity is given by

$$\dot{y}_{CG}(t) = v_y(t) + v_x\Phi(t), \tag{6.1}$$

where Φ the heading angle, v_y the lateral velocity in the vehicle coordinate frame and v_x is the constant longitudinal velocity. Note that small heading angles are assumed for linearisation. The linearised lateral velocity of the front bumper at a distance l_{fb} in front of the centre of gravity is given by:

$$\dot{y}(t) = v_y(t) + v_x\Phi(t) + l_{fb}\dot{\Phi}(t). \tag{6.2}$$

The point l_{fb} is in literature often referred as lookahead distance and could in principle be chosen at an arbitrary distance in front of the centre of gravity. In (6.2) the lookahead distance is the only vehicle dependent parameter. For the second order time derivative of the lateral position holds:

$$\ddot{y}(t) = \dot{v}_y(t) + v_x\dot{\Phi}(t) + l_{fb}\ddot{\Phi}(t), \tag{6.3}$$

where $\dot{v}_y$ and $\ddot{\Phi}$ are functions, which depend on the system states defined in (3.17). Using these equations, (6.3) can be rewritten to:

$$\ddot{y}(t) = f_1\left(v_y(t), \dot{\Phi}(t), \dot{\phi}(t), \phi(t)\right) + (b_1 + l_{fb}b_2)\delta(t), \tag{6.4}$$

where b_1 and b_2 are the first and second element of the $\underline{B}$ matrix in (3.20) respectively. Function f_1 is some unknown bounded function of the vehicle states. Using the same methodology the third order time derivative of y, which is needed for the controller design in this chapter, can be written as:

$$\dddot{y}(t) = f_2\left(v_y(t), \dot{\Phi}(t), \dot{\phi}(t), \phi(t), \delta(t)\right) + (b_1 + l_{fb}b_2)\ddot{\delta}(t), \tag{6.5}$$

where f_2 is an unknown bounded function of the vehicle states and the steering angle. As will be shown in the remainder of this chapter, exact knowledge of the functions f_1 and f_2 is not needed, as long as they are bounded.

System uncertainties

In Section 5.2 arguments are given that the longitudinal vehicle model parameters are uncertain. Equivalently, this holds for the lateral model which will be shown in this section. The following influences might cause the lateral vehicle model parameters to be uncertain:

- The cornering stiffness can change due to the load transfer, longitudinal tyre slip, tyre pressure etc.
- Side winds can influence the lateral vehicle behaviour seriously.
- The vehicle mass can change due to varying loading conditions.
- The vehicle inertia can change due to the loading conditions.
- A variable vehicle configuration: different types of trailers might be connected to the tractor.
- A varying longitudinal vehicle velocity.

In [16] the uncertain cornering stiffness and the effect of side winds are mentioned as main uncertainties for the lateral vehicle model. However, this thesis will limit itself to an uncertain cornering stiffness. The other uncertainties, especially the effect of side winds, are expected to influence the system behaviour significantly as well. Extension of the uncertainty analysis can be made in the future. The cornering stiffnesses are calculated by (3.21), with the normalized cornering stiffness f_{tyre} being the only variable. A different normalized cornering stiffness for each axle will result in an oversteered or understeered vehicle. An oversteered vehicle is unstable above a critical velocity, which might result in jackknifing. The chosen controller requires the underlying system to be stable, hence only a neutrally steered vehicle is considered. This implies f_{tyre} being equal for all axles. Since the centre of gravity height of the tractor and semi-trailer are assumed to be equal and no braking is considered, this is a valid assumption. Especially when combined braking and steering is considered, the normalized corning stiffness per axle is expected to change. This is not considered in this report. The range for f_{tyre} that will be evaluated is:

$$f_{tyre} \in [0.25 f_{tyre_{nom}}, 2.0 f_{tyre_{nom}}], \tag{6.6}$$

where $f_{tyre_{nom}}$ is the nominal value for the normalized cornering stiffness. The considered range is from 25% to 200% of the nominal value. This range is similar to the range considered for the cornering stiffness in [16]. Referring to the previous section, f_1 and f_2 remain unknown bounded functions. The bounds on these functions are dependent on the system uncertainties. Variables b_1 and b_2 are dependent on the uncertain cornering stiffness as well. Hence the following holds

$$b_1 + l_{fb}b_2 \in [b^-, b^+], \tag{6.7}$$

where the bounds b^- and b^+ on the input scalar are determined by the system uncertainties. As discussed in this section, only an uncertain normalized cornering stiffness is considered. The limits on the input scalar corresponding to the considered values for the normalized cornering stiffness (6.6) are shown in Table 6.1.

limit	value	unit
b^-	20.8	$\frac{\text{m}}{\text{s}^2\text{rad}}$
b^+	167	

Table 6.1: Bounds on the input scalar belonging to (6.6)

6.2 Lateral collision avoidance objective

The primary goal of collision avoidance is to move the vehicle as fast as possible from an unsafe initial condition to a safe region. From there the nominal controller can take over. Hence, asymptotic stability is not of major interest for the collision avoidance controller. Therefore, the terms *practical stability* and *finite time stability* (FTS) are introduced. *Practical stability* was first introduced by LaSalle and Lefschets [45]. While classical *Lyapunov stability* requires values to be bounded for infinite time, the values of the bounds are not prescribed. *Practical stable* systems operate for an infinite time interval within some prescribed bounds. FTS deals with prescribed bounds in finite time intervals. This relates to the goal of collision avoidance: the system should bring the vehicle in a safe region described by certain bounds in finite time. An elaboration on FTS using Linear Matrix Inequality's (LMI's) for solving the problem can be found in Appendix F. However, this method has computational drawbacks: solving large sets of LMI's is even off-line computationally infeasible. Moreover, the FTS approach discussed in Appendix F requires accurate knowledge of the system parameters. The basic definitions of FTS could be applied to alternative approaches as well. However, how to achieve this requires more research which is not available yet in literature. With this in mind, the problem is tackled by a more classical robust control approach using *Lyapunov stability*. Definitions like finite time convergence are also important in robust control, however the starting point is different. Drawback of this approach is that the controller objective becomes path following instead of controlling the vehicle to a safe region. Calculation of the evasive path and the error to the evasive path might not be trivial. However, to come from a *finite time stability* bound definition to a feasible controller design requires more research.

6.3 Controller design

As mentioned in the previous section, a robust control approach is used for lateral collision avoidance. A possible robust control method is sliding mode control (SMC). The reasons to apply SMC for lateral collision avoidance are similar to those presented for the longitudinal SMC in Section 5.3. SMC offers the possibility for a low complexity controller applying high gains without making the system unstable when designed correctly. Drawbacks due to the high gain method are actuator wear and power loss, which are irrelevant since activation of Collision Avoidance should be limited to a minimum and the intended duration for which it will be active is short. In this chapter a lateral SMC for evasive manoeuvring in collision avoidance is proposed, assuming only the lateral vehicle position (y) can be measured. Some more background on SMC and the reasoning behind using error coordinates instead of absolute coordinates can be found in Appendix G. The ideas presented by Guldner et al. [26] are followed. Guldner et al. propose two SMC methods for lateral vehicle control: SMC only using lateral position and a cascaded SMC using yaw-rate and lateral position. This chapter will apply the first one. For the interested reader, more information with respect to the cascaded controller can be found in [4] and [57]. In this section the SMC design will be discussed is more detail. First, the controller lay-out will be shown. Second, the applied control law will be stated, than the sliding surface design. Next, the stability of the proposed strategy is evaluated. Finally, the boundary layer design, observer design and controller implementation will be discussed.

Controller layout

The proposed control scheme, without details of the SMC is shown in Fig 6.1. The scheme will be discussed from left to right. Based on sensor data, the host state variables and worse case target trajectory (Section 4.1.2) are determined. The host state estimator includes the state predictor discussed in the previous chapter (5.15) and the calculation of the lateral vehicle position at the look ahead point (6.2). The path generator calculates an evasive path in case there is a valid path available. Calculation of the trapezoidal lane change path is discussed in Section 4.2.3 and Appendix C. The lateral error between the reference path y_{ref} and the actual host position y, defined as

$$y_e(t) = y_{ref}(t) - y(t) \tag{6.8}$$

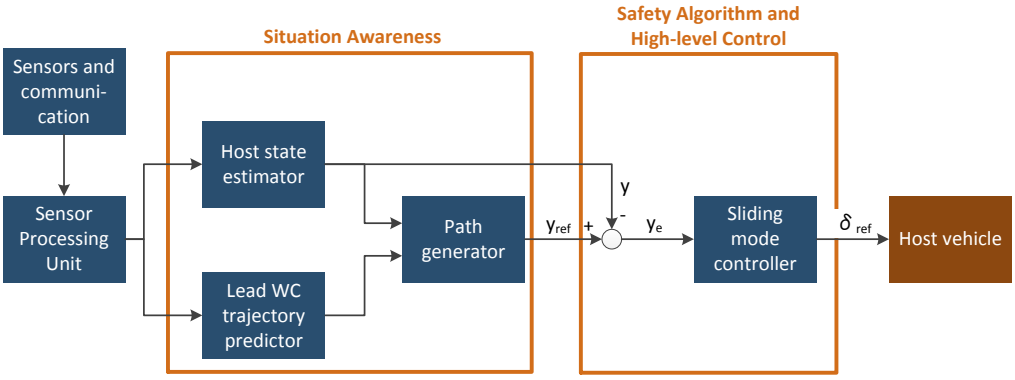

Fig 6.1: Control scheme of the lateral control

is input for the controller. The controller will calculate a reference steering angle based on that. Actuator and sensor time delays are neglected.

Control law

Next, the applied SMC control law will be discussed in more detail. A very effective approach to suppress oscillations due to the unmodelled actuator dynamics is integral SMC: not the real input variable is controlled but its derivative. The lateral control input is defined as:

$$\delta_{ref}(t) = \int_{t_0}^{t} u_y(\xi) d\xi. \tag{6.9}$$

Control effort u_y is the derivative of the reference steering angle: the reference steering rate. Disadvantages of this control law definition are phase lag and drift due to the integral action. However, since the collision avoidance controller is expected to be active for a limited duration, the drift is expected to be negligible. In SMC, the control action can be divided into two phases: the reaching phase and the sliding phase. In the reaching phase, the objective is to reach the sliding surface in finite time. The dynamics in the sliding phase are completely determined by the sliding surface. Therefore, the sliding surface design is the main challenge for the design of the SMC, which will be discussed in the next section. The control law that should guarantee reaching the sliding surface in finite time and sliding on the surface thereafter yields:

$$u_y(t) = -u_{y,lim} \text{sign}\left(s_y(t)\right), \tag{6.10}$$

where $u_{y,lim}$ is the steering rate limit determined by the steering actuator constraints, chosen to be the value in Table 6.2. In case $s_y = 0$, the vehicle is exactly on the sliding surface. The control input to remain on the surface once the system reached the surface is referred as the equivalent controller. In for instance [4] and [57], this analytical control input is given as feedforward steering angle to the system. To obtain an analytical control input, the state variables need to be predicted and by inversion of the function f_2 in (6.5) the equivalent control input can be obtained. For a certain bicycle model of a rigid vehicle, state variables on the reference path can be predicted accurately. However, for an articulated vehicle and uncertain system parameters, prediction of the state variables on the reference path is not trivial because the articulation angle and its derivative need to be estimated. Hence, no feedforward term is given to the system; the system is only controlled by the feedback SMC.

Sliding surface

This section will elaborate on the design of the sliding surface. As it will be shown in the following, it is convenient to have a sliding surface one order lower than the order where the control variable is present. The third order time derivative of the lateral position (6.5) is the lowest order where the steering rate (control input) is present. Hence, the following sliding variable is defined, which includes upto the second

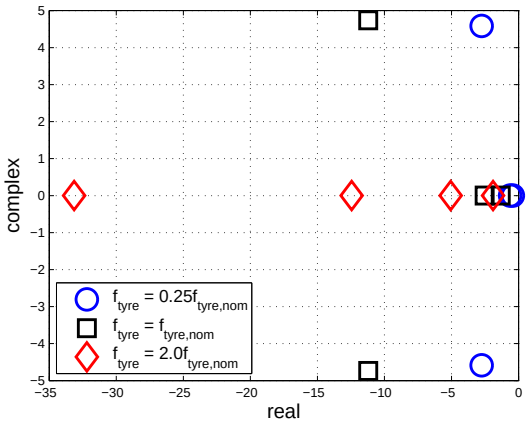

Fig 6.2: System poles for a varying normalized cornering stiffness

order time derivative of the lateral position:

$$s_y(t) = \ddot{y}_e(t) + k_1\dot{y}_e(t) + k_0 y_e(t), \tag{6.11}$$

where the surface $s_y = 0$ is the sliding surface. The gains k_0 and k_1 defining the sliding surface (6.11) have to be determined. Requirement for the surface is that it should be followable by the system, such that ideal sliding can occur.

The error to the reference path should converge to zero on the sliding surface. This is guaranteed in case the poles of the surface $s_y = 0$ in (6.11) are negative. In case the surface poles are chosen to be complex, the trajectories will on the sliding surface converge to a lateral error of zero with overshoot. Since there is only little margin for overshoot when performing an evasive manoeuvre, the surface poles are chosen to be real. In order to bring the lateral error to zero as fast as possible on the sliding surface, the value of the surface poles should be chosen small. However, the surface should be followable by the system. To guarantee this, the equivalent control input on the sliding surface could be calculated. However, as mentioned previously, finding an analytical expression for the equivalent control input is hard since an uncertain tractor semi-trailer model is considered. Hence, the sliding surface poles are chosen larger (slower) compared to the system poles. If the surface is really followable by the system will be evaluated later. Fig 6.2 shows the system poles for a varying normalized cornering stiffness. For a high cornering stiffness, the system has no complex poles. For a lower cornering stiffness there is a complex pole pair, that moves towards the real axis for a decreasing cornering stiffness. With a normalized cornering stiffness of 25% of the nominal value, the eigenfrequency of this pole pair is approximately 5rad/s. To ensure a stable sliding motion, the surface poles are chosen to be a factor two slower. To determine the gains k_0 and k_1 based on the surface pole choice, the location of the surface poles is characterized with variable λ_y as in [16]. Surface gains k_0 and k_1 are related to the surface poles as:

$$s_y(t) = \ddot{y}_e(t) + 2\lambda_y\dot{y}_e(t) + \lambda_y^2 y_e(t), \quad k_0 = \lambda_y^2, \qquad k_1 = 2\lambda_y, \tag{6.12}$$

Since the sliding surface poles are chosen to be a factor two slower compared to the system dynamics, λ_y=2.5rad/s. The control law in (6.10) and sliding surface (6.12) define together the SMC design.

Stability analysis

Next step is to prove the stability of the proposed SMC design. Therefore,

$$V_y(t) = \frac{1}{2}s_y^2(t) \tag{6.13}$$

is considered as Lyapunov candidate. The time derivative of this Lyapunov candidate is

$$\dot{V}_y(t) = s_y(t)\dot{s}_y(t), \tag{6.14}$$

Variable	Description	Value
l_{fb}	Look ahead distance	1.5m
$j_{y,lim}$	Jerk limit for path generator	5m/s^3
$a_{y,lim}$	Acceleration limit for path generator	2.5m/s^2
$u_{y,lim}$	Maximum steering rate	26.5^o/s
λ_y	Eigenvalues of the sliding surface	2.5rad/s

Table 6.2: Parameters for the SMC: ideal SMC parameters

where the time derivative of the sliding variable is given by

$$\dot{s}_y(t) = \dddot{y}_e(t) + k_1\ddot{y}_e(t) + k_0\dot{y}_e(t). \tag{6.15}$$

Equation (6.15) can equivalent to (6.4) and (6.5) be written as a combination of the control input and some unknown bounded function f_3:

$$\dot{s}_y(t) = f_3\left(v_y(t), \dot{\Phi}(t), \dot{\phi}(t), \phi(t), \delta(t), y_{ref}(t)\right) + (b_1 + l_{fb}b_2)u_y(t). \tag{6.16}$$

Note that since the sliding variable consists of error coordinates rather than absolute coordinates, the function f_3 is also a function of the reference path y_{ref}. Because the function f_3 is bounded and using (6.7), equation (6.16) can equivalently be written as a differential inclusion:

$$\dot{s}_y(t) \in [-C, C] + [b^-, b^+]u_y(t), \tag{6.17}$$

where C is the limit on the function f_3, which should be valid for the operating range of the vehicle. Substitution of (6.17) into (6.14) yields

$$\dot{V}_y(t) \in s_y(t)\left([-C, C] + [b^-, b^+]u_y(t)\right). \tag{6.18}$$

Control law (6.10) can be substituted into (6.18) resulting in

$$\dot{V}_y(t) \in s_y(t)\left([-C, C] - [b^-, b^+]u_{y,lim}\text{sign}(s_y(t))\right). \tag{6.19}$$

In case $u_{y,lim}$ is selected such that the condition

$$b^- u_{y,lim} > C \tag{6.20}$$

holds, the following holds for the Lyapunov candidate time derivative

$$\dot{V}_y(t) < -\alpha \quad \forall t \geq t_0 : s_y(t) \neq 0, \tag{6.21}$$

for some positive scalar α, resulting in a negative semi-definite Lyapunov candidate time derivative. In that case, the maximum convergence time to the surface is given by

$$t_{reach}(t) = \frac{s_y(t)}{\alpha} \quad \forall t \geq t_0 : s_y(t) \neq 0. \tag{6.22}$$

Hence, in case Condition (6.20) holds, the control strategy ensures reaching the sliding surface in finite time and sliding on the surface afterwards.

This paragraph will prove Condition (6.20) is satisfied. Parameter C is the bound on the unknown function f_3. The SMC with the controller parameters stated in Table 6.2, applied to the linear vehicle model with the parameters stated Appendix A.1 is used for this validation. The values for the controller stated in Table 6.2 are determined as follows. The path generator parameters $a_{y,lim}$ and $j_{y,lim}$ are discussed in Section 4.2.3, the look ahead distance l_{fb} is determined by the vehicle geometry, $u_{y,lim}$ is determined by the actuator constraints and the surface pole location λ_y is discussed in the previous section. Actuator dynamics are neglected for the stability analysis. Two important variables influencing the function f_3 are the uncertain cornering stiffness f_{tyre} and the jerk limit $j_{y,lim}$ on the reference path y_{ref}. Simulations are performed with the controller performing the trapezoidal lane change (Section 4.2.3). Fig 6.3 shows the dependency of f_3 on the normalized cornering stiffness; Fig 6.4 the dependency on the jerk limit of the reference path. The amplitude of f_3 increases for an increasing normalized cornering stiffness. However, the function remains for all normalized cornering stifnesses in the uncertainty range (6.6) below the stability limit $b^- u_{y,lim}$. Fig 6.4 shows that the amplitude of f_3 decreases in case the jerk limit on the reference path is decreased. This implies that in case condition (6.20) is violated, decreasing the jerk limit on the reference path might help in limiting the amplitude of function f_3, at the cost of an increased evasive time. However, according to the analysis in this paragraph the system should be stable for the chosen parameters.

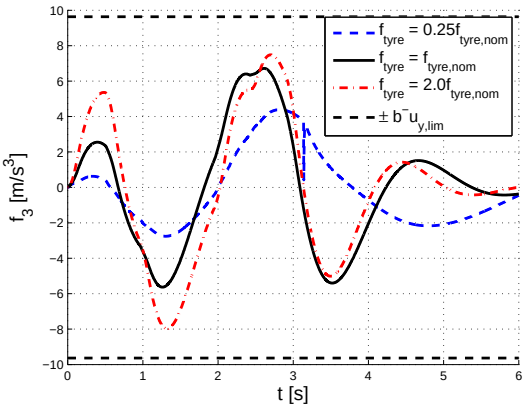

Fig 6.3: Behaviour of function f_3 in an evasive manoeuvre with an uncertain normalized cornering stiffness

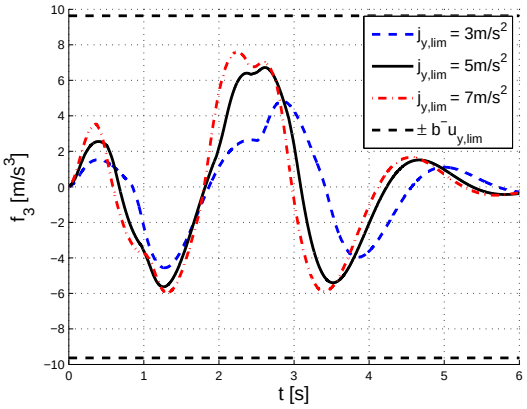

Fig 6.4: Behaviour of function f_3 in an evasive manoeuvre for different jerk limits $j_{y,lim}$ on the reference path

Boundary layer

As discussed for the longitudinal SMC controller, the lateral SMC will suffer from chattering due to the high gain control law (6.10). Equivalent to the longitudinal SMC in Section 5.3.1, the state-dependent gain method is proposed as chattering suppression method for the lateral SMC. The sign function in the control law (6.10) is replaced by:

$$u_y(t) = \begin{cases} -u_{y,lim}\text{sign}(s_y(t)) & \text{if } |K_y s_y(t)| \geq 1 \\ -u_{y,lim} K_y s_y(t) & \text{if } |K_y s_y(t)| < 1, \end{cases} \tag{6.23}$$

where K_y is the gain determining the dynamics within the boundary layer. A larger K_y brings the control law closer to the original sign function. The applied value for K_y shown in Table 6.3 is determined based on simulations.

Observer

For the sliding variable (6.11), the lateral position error, its first and second order time derivative are used. However, it is assumed that only y_e can be measured by the sensors. Hence the higher order time derivatives need to be estimated, but numerical differentiation leads to noise. Therefore an observer for estimation of the higher order derivatives of y_e is designed, as in [26].

$$\begin{aligned} &\dot{\underline{\hat{z}}}(t) = \underline{A}_{obs}\underline{\hat{z}}(t) + \underline{B}_{obs}u_y(t) + \underline{L}\bar{y}_e(t), \quad \underline{\hat{z}}(t) = [\hat{y}_e(t),\ \dot{\hat{y}}_e(t),\ \ddot{\hat{y}}_e(t)]^T, \\ &\dot{\underline{\hat{z}}}(t) = \begin{bmatrix} 0 & 1 & 0 \\ 0 & 0 & 1 \\ 0 & 0 & 0 \end{bmatrix} \underline{\hat{z}}(t) + \begin{bmatrix} 0 \\ 0 \\ b_1 + l_{fb}b_2 \end{bmatrix} u_y(t) + \begin{bmatrix} l_1 \\ l_2 \\ l_3 \end{bmatrix} \bar{y}_e(t), \end{aligned} \tag{6.24}$$

where the hats denote the estimated values and $\bar{y}_e = y_e - \hat{y}_e$ the error between the estimated and actual value of the lateral position error. The observer gain matrix L should be tuned to have sufficient filtering, but the observer dynamics should be faster compared to the vehicle dynamics to limit the phase lag and ensure the estimation errors will be small. The observation error decays according to:

$$\dot{\underline{\bar{z}}}(t) = \begin{bmatrix} -l_1 & 1 & 0 \\ -l_2 & 0 & 1 \\ -l_3 & 0 & 0 \end{bmatrix} \underline{\bar{z}}(t) + \begin{bmatrix} 0 \\ 0 \\ b_1 + l_{fb}b_2 \end{bmatrix} u_y(t), \quad \bar{z} = z - \hat{z}. \tag{6.25}$$

The poles of the first matrix should be sufficiently fast compared to the vehicle dynamics. The gains are chosen such that the observer poles are placed on the real axis with a natural frequency of 33rad/s, which is faster than the system poles. The resulting observer gains are shown in Table 6.3. Choosing the

Variable	Description	Value
K_y	Boundary layer gain	20
l_1	Observer gain 1	1e2
l_2	Observer gain 2	3.3e3
l_3	Observer gain 3	3.7e4

Table 6.3: Parameters for the SMC: boundary layer gain and observer gains

observer dynamics slower will limit the controller performance. Increasing the observer gains will limit the controller robustness to sensor noise, since the noise will be amplified in the observer.

Example 6.3.1. An example of the observer behaviour is shown in Fig 6.5. The parameters used for this simulation are shown in Table 6.2 and Table 6.3. The solid back line represents the actual values and the dotted blue line the estimated values. For the lateral position shown in the left plot, the estimated value is accurate. For the velocity shown in the middle plot, the estimated and the measured value start to deviate. For the acceleration shown in the right plot, the estimated and actual value deviate significantly. The estimation errors can be reduced by increasing the observer gains. However, this would lead to more noise amplification in the observer. □

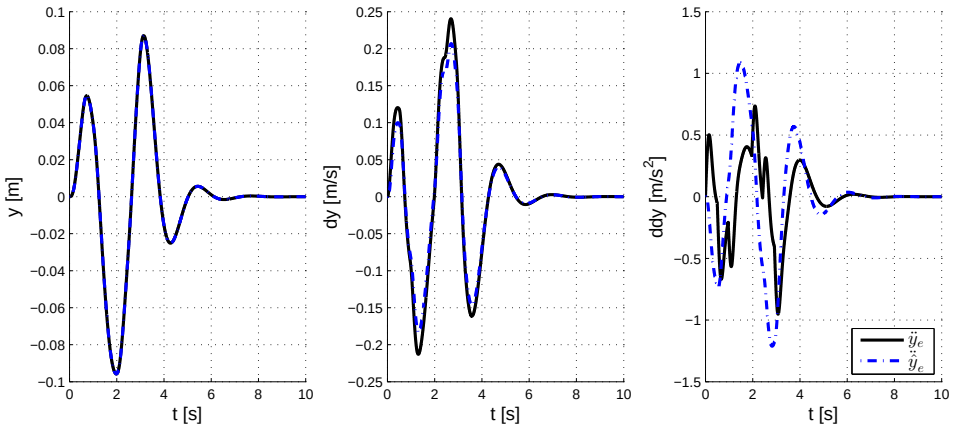

Fig 6.5: Example of the observer behaviour during a lane change

Implementation

Fig 6.6 shows the implementation of the SMC, which is the content of the SMC block in Fig 6.1. The measured position error is input for the observer. The observer estimates the position error and its time derivatives (6.24). With these estimates the sliding variable (6.11) is calculated. The boundary layer gain followed by a saturation multiplied by the steering rate limit gives the reference steering rate (6.23). The reference steering rate is after integration given as reference steering angle to the low-level controllers in the vehicle. The design parameters and the chosen values are shown in Table 6.2 and Table 6.3, which are discussed previously.

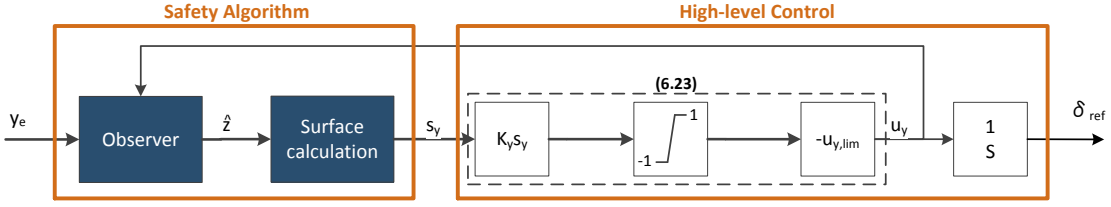

Fig 6.6: Control scheme of the lateral SMC

6.4 Simulation results

In this section, first an example of the system behaviour during an evasive manoeuvre will be shown. Next, the controller performance in the communication *failure* scenario will be evaluated with simulations. Finally, the controller robustness will be discussed.

Example 6.4.1. Fig 6.7 shows the behaviour of the nominal system during a lane change. The top left plot shows the reference and actual value for the lateral position; the top right plot the lateral acceleration. The lateral acceleration has the shape of the trapezoidal reference path defined in Section 4.2.3. The bottom left plot illustrates the sliding variable. The sliding variable remains well within the boundary layer, which implies the path is tracked accurately. The bottom right plot shows the reference steering angle applied to the system to perform the evasive manoeuvre. The Situation Awareness and Safety Mode Selection have to ensure that the reference path is collision free. The controller objective is to track the path determined by the Situation Awareness algorithm, which is achieved according to this example. □

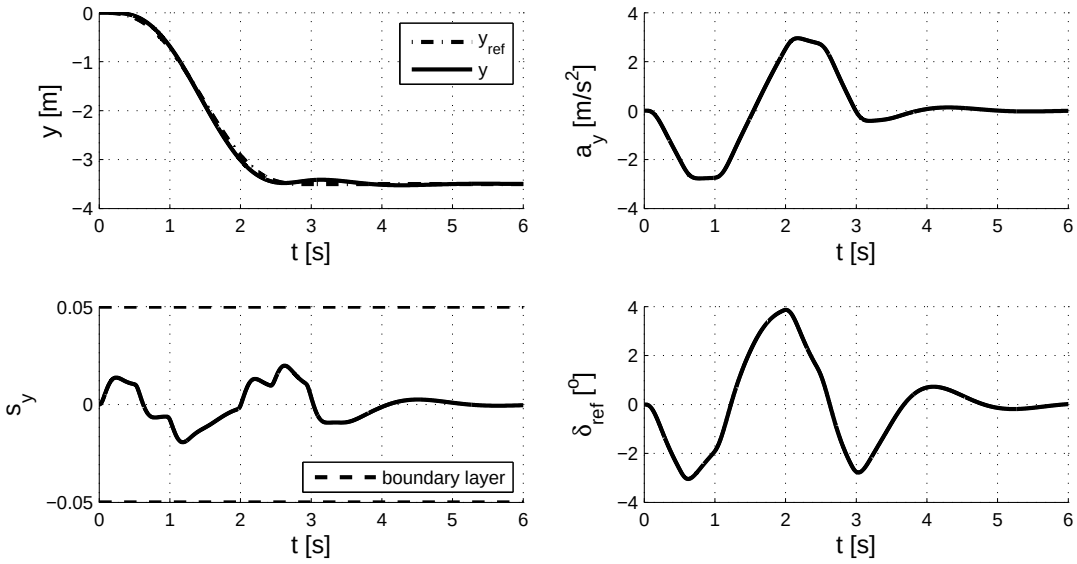

Fig 6.7: Simulation results of a lane change with the nominal system parameters

6.4.1 Communication failure scenario

As shown in Table 1.1, collisions are not always avoided by the nominal controller in case of a communication *failure*. The lateral collision avoidance controller is evaluated by simulations for all in Appendix E.2 defined test cases. The controller performance in the test cases is evaluated based on the key performance indicators defined in Section 2.1. During the simulations, Evasive Manoeuvre is always activated in case Collision Avoidance mode is entered by the Safety Mode Selection, discussed in Section 4.3. Normally first Emergency Braking would be activated, but since the previous chapter proved the longitudinal collision avoidance controller to be sufficient to avoid collisions, Emergency Braking is turned off for evaluation of the lateral controller. A scenario could be approaching traffic from behind, such that severe braking is not safe and an evasive manoeuvre is required. An illustration of this scenario is shown in Fig 6.8. For simulations, the non-linear model presented in Section 3.1 is used, without steering actuator time delay.

– **Number of collisions**: No collision occurs in any test case in simulation.
– **Impact speed**: There is only impact if a collision occurs, so the impact speed is zero in all test cases.

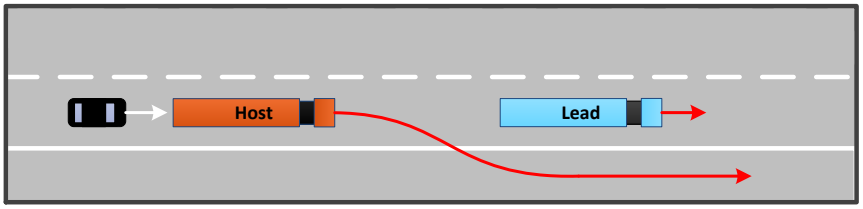

Fig 6.8: Safety use case for evasive manoeuvring

– **Maximum lateral acceleration:** The maximum lateral acceleration in the test cases is illustrated by the bar graph in Fig 6.9. Since the reference path is always the same, the maximum lateral acceleration is equal in case an evasive manoeuvre is performed. The value of the maximum lateral acceleration is 3m/s^2. The planned trapezoidal trajectory has a maximum lateral acceleration of 2.5m/s^2. The difference between the reference and the actual maximum lateral acceleration is due to overshoot. However, 3m/s^2 is still within the defined roll-over limit of the vehicle. Only in Test 3 and 18 Evasive Manoeuvre not activated (maximum lateral acceleration is zero), since the *failure* duration is within the *fault-tolerant* time (Section 4.3). The system will return to the nominal controller without activating Collision Avoidance since the Adaptive Headway Time algorithm is sufficient to ensure safety. In Test 4 and 10 the preceding vehicle does not brake, however the system activates Evasive Manoeuvre to ensure a rear-end collision with the preceding vehicle can be avoided. These *false positive* interventions might be prevented by stricter transition conditions for the intervention activation.

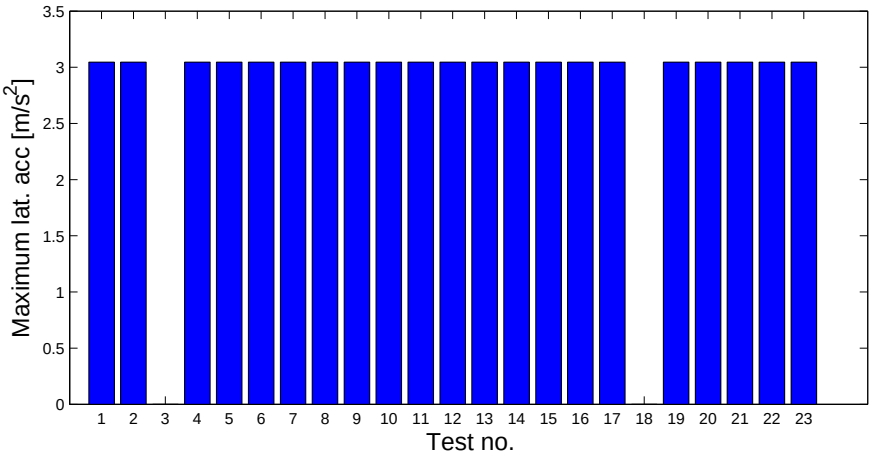

Fig 6.9: Maximum lateral acceleration in the test cases

– **Minimum inter-vehicle distance:** The minimum inter-vehicle distance in the test cases is shown in Fig 6.10. In Test 3 and 18 a higher inter-vehicle distance is shown, because in these test cases Evasive Manoeuvre is not activated. In all other cases the minimum distance is small. In the tests where the lead vehicle applies full braking, the inter-vehicle distance shows distances down to 0.12m. Hence, there is only minor margin to change to stricter transition conditions to avoid *false positive* interventions.
– **Maximum deceleration:** The minimum deceleration for the 23 test cases is shown in Fig 6.11. In Test 5 and 18 the braking effort is larger than the 3.5m/s^2 defined in Intermediate Braking, however the emergency braking controller is deactivated in these simulations. In these cases, the nominal controller is applying severe braking since the lead vehicle brakes. In all other cases the maximum deceleration is within 0.5m/s^2.

In the 23 test cases collisions can always be avoided by the lateral collision avoidance algorithm presented in this chapter. If an evasive manoeuvre is feasible depends on the environmental conditions: traffic, barriers etc. However, *false positive* interventions cannot be avoided by only steering whereas braking could. Evasive manoeuvring therefore is not able to reduce the safety distance and thereby increase the system availability compared to emergency braking. Section 4.3 already concluded that the safety distance for emergency braking and evasive manoeuvring by only steering is similar. The safety distance could

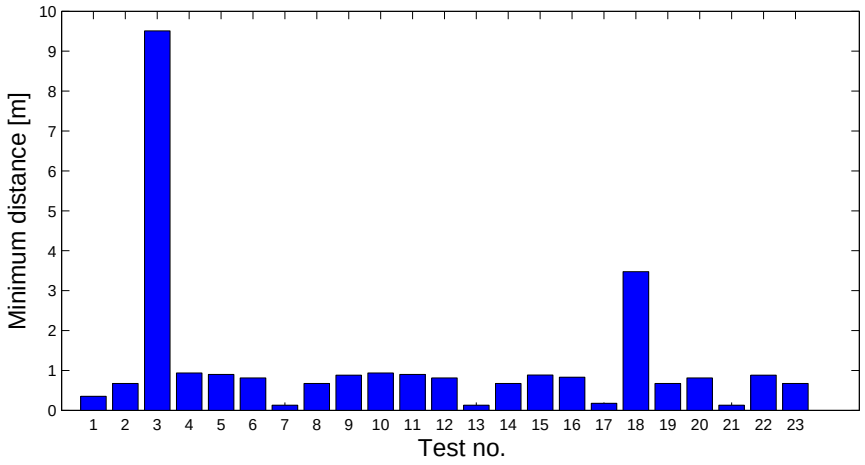

Fig 6.10: Minimum inter-vehicle distance in the test cases

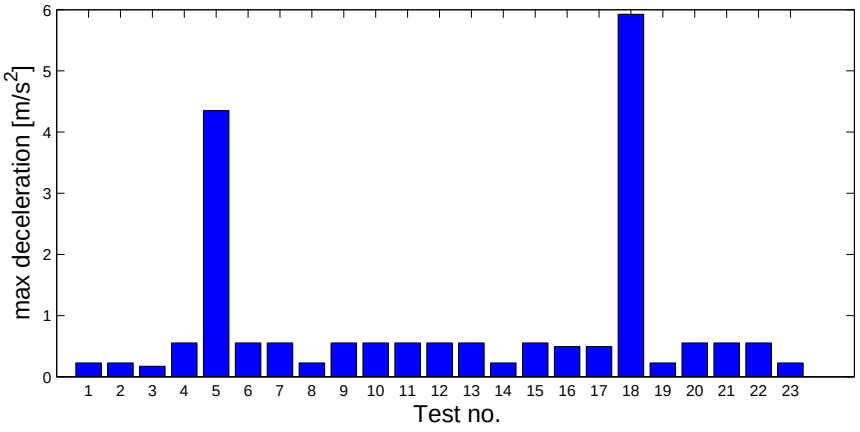

Fig 6.11: Maximum deceleration in the test cases

significantly be decreased in case an evasive manoeuvre combining braking and steering is considered. However, the coupled longitudinal and lateral dynamics should be taken into account in the controller design, whereas the current controller design is based on a decoupled system.

6.4.2 Robustness analysis

This section will evaluate the robustness of the controller by simulations based on the requirements defined in Section 2.1. In Appendix H the simulation results are described in more detail. The following conclusions can be drawn from the results:

- The controller performs well for the system parameter uncertainties discussed in Section 6.1; an uncertain normalized cornering stiffness is considered in the range of (6.7).
- The controller performs well for initial position errors upto 30cm.
- The controller with the observer gains shown in Table 6.3 performs well for sensor noise with a standard deviation upto 0.03rad/s with a sample time of 1ms. The robustness of the controller with respect to noise is tunable by the observer. However, increasing the smoothing factor of the observer will introduce additional phase lag limiting the controller performance.
- During the controller design, time delays are neglected. However, steering actuator delay is limiting the controller performance dramatically. Upto an actuator time delay of 5ms the system performs well; for 10ms severe chattering occurs. Possibly a state predictor as proposed in [57] and introduced for the longitudinal SMC in the previous chapter can be added to compensate for actuator and measurement time delay. Alternatively, to compensate for measurement time delay [53] applies

a Kalman filter to estimate the lateral position from a lateral accelerometer and yaw rate sensor, which generally have less delay compared to a direct position measurement.

The values for initial errors, sensor noise and time delays are based on the capabilities of the current controller determined by simulations. The controller robustness to uncertainties other than the normalized corning stiffness should be investigated further, especially the effect of side winds is expected to influence the system behaviour significantly. The most limiting factors for the controller performance are sensor noise and time delays. The current sensor equipment of the vehicles is not able to deliver the required accuracy. Therefore, new sensors are needed. The values determined in this section can be used for the sensor requirements definition.

6.5 Sequential lateral and longitudinal controller activation

In this section, a final safety use case in the communication *failure* scenario is considered, where the lateral and longitudinal SMC are activated sequentially. An illustration of the specific use case is shown in Fig 6.12. Two trucks are driving in a platoon at the moment that a communication *failure* occurs. The lead vehicle decides to brake; Collision Avoidance mode is activated. Because there is a vehicle approaching from behind the host vehicle, emergency braking is not safe. The system decides to perform an evasive manoeuvre to move to the emergency lane. However, there is a vehicle in the emergency lane, so the system has to be brought to a standstill. The selected steady safe state is standstill in the emergency lane.

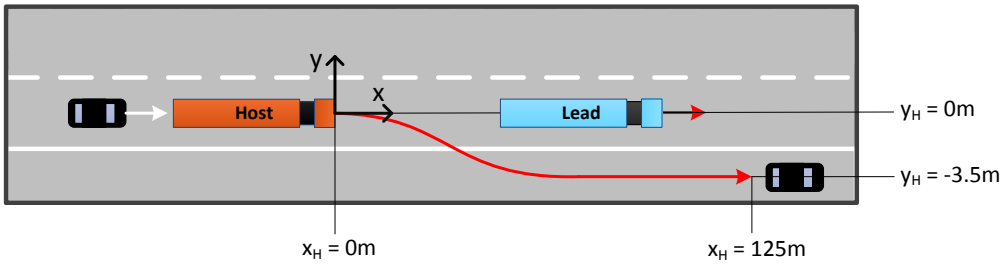

Fig 6.12: Safety use case for evasive manoeuvring followed by an emergency stop

The non-linear vehicle model (Section 3.1) without steering actuator delay is used for the simulation in this section. Fig 6.13 shows the intended sliding surfaces for longitudinal and lateral control in this use case. The surface $S_y = 0$ represents the surface where all error terms in (6.11) are zero. The surface $S_x = 0$ represents the surface where the vehicle brakes with the required acceleration from the moment

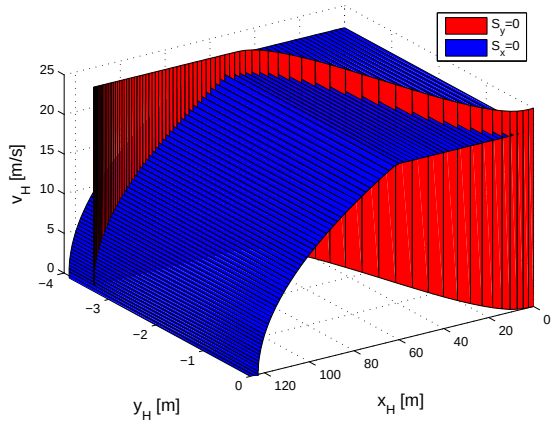

Fig 6.13: Sliding surfaces for the final safety use case

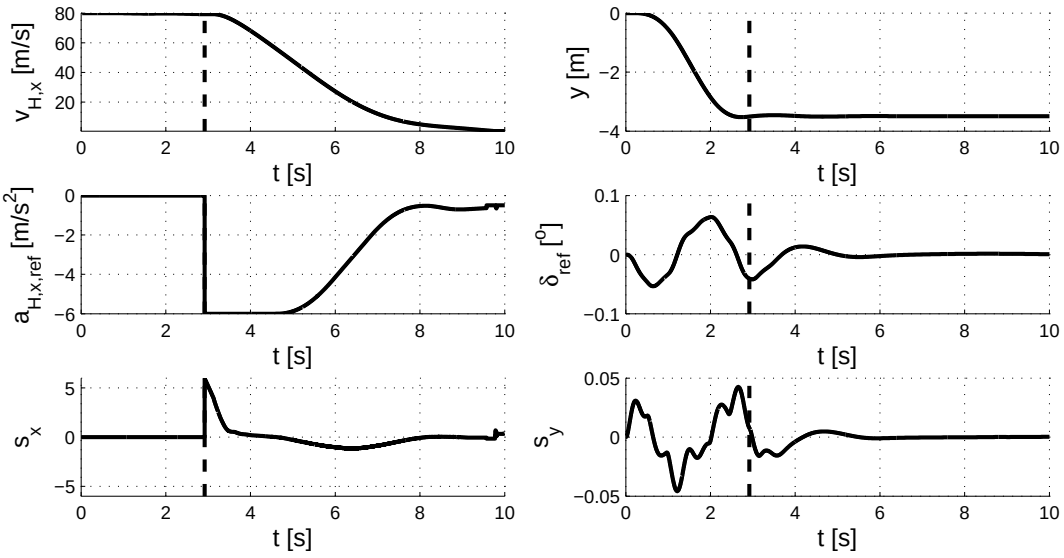

Fig 6.14: Results for performing an evasive manoeuvre followed by a braking action in the emergency lane

the evasive manoeuvre is completed (lateral position of the generated reference path is constant). In the first part, ($x_H \in [0, 60]$) the lateral position of sliding surface $S_y = 0$ is varying while the velocity of sliding surface $S_x = 0$ is constant. This is the part where the evasive manoeuvre takes place. As soon the lateral reference position is constant, the velocity of the sliding surface $S_x = 0$ is reduced to bring the vehicle to a standstill ($x_H \in [60, 125]$) . Longitudinal and lateral SMC are active in parallel, but since the manoeuvre is performed sequentially, the controllers designed for the decoupled models can be used. The plan is to remain on both sliding surfaces once a surface is reached, implying sliding takes place on the intersection of both surfaces. The results are shown in Fig 6.14. The top left plot shows the vehicle speed and the top right plot the lateral vehicle position. The dotted vertical line illustrates the time instant where the system switches from Evasive Manoeuvre to Emergency Braking. The middle left plot shows the reference acceleration. The vehicle starts full braking when Emergency Braking is activated and then slowly reduces the braking effort till standstill. The middle right plot shows the reference steering angle applied to the system. Clearly, the steering angle has not settled before Emergency Braking is activated. However, the system stability seems not to be influenced by this overlap phase. The bottom left plot shows the longitudinal sliding variable. It is positive when Emergency Braking is activated, and then converges quickly towards the sliding surface. Due to the asymmetric control law and boundary layer, it remains below the sliding surface such that the braking effort is reduced slowly to standstill. The bottom right plot shows the lateral sliding variable. The values remain within the boundary layer, hence sufficient tracking is achieved. Based on these results it can be concluded that sequential activation of the controllers is working properly in simulation with a non-linear vehicle model without steering actuator delay. It is possible to perform an evasive manoeuvre followed by an emergency stop by applying the in this thesis developed sliding mode controllers.

6.6 Conclusion

In this chapter a SMC for evasive manoeuvring is presented. The controller objective is to follow a reference path with the centre of the front bumper. A linear model for lateral vehicle dynamics is used with some uncertain parameters, decoupled from the longitudinal dynamics. The cornering stiffness is considered as main uncertainty. It is assumed that the steering rate can be controlled directly. This approach is effective to suppress chattering due to actuator dynamics. The controller is robust to model uncertainties due to normalized cornering stiffness values between 25% and 200% of the nominal value.

Moreover, the controller is robust to initial errors upto 30cm and lateral position measurement noise with a standard deviation upto 0.03m with a sample time of 1ms. Upto an actuator time delay of 5ms, the controller showed accurate tracking behaviour. With an actuator time delay of 10ms, severe chattering occurs. Hence limiting the time delays in the hardware design and sensor selection is of major interest. Moreover, time delay compensation in the controller should be investigated further. The controller is in simulation validated in all 23 defined test cases for the communication *failure* scenario. It will prevent collisions in all test cases, but it also intervenes in cases where the lead vehicle does not brake. To avoid these *false positive* interventions, it is not possible to activate the controller later, since in that case collisions will occur in the worse case scenario. Hence, an evasive manoeuvre does not increase the safety distance and thereby the system availability is also not increased compared to emergency braking. In case combined braking and steering is applied during the evasive manoeuvre, the system availability is expected to increase, which implies shorter following distances are realizable. Further, a final use case is evaluated which shows the potential of sequential activation of the proposed lateral and longitudinal collision avoidance SMC approaches in simulation.

Chapter 7

Conclusions and recommendations

7.1 Conclusions

Heavy-duty vehicle platooning has the potential to decrease fuel consumption with 5-20%. Since fuel consumption accounts for 30% of the total expenses of transportation companies, heavy-duty vehicle platooning is expected to gain major interest by the industry and market. Other motivators for vehicle platooning are labour cost reduction, road capacity optimization, improvement of the road safety, emission reduction and asset utilization optimization. The time gap between the vehicles is aimed to be 0.3s to maximally exploit the fuel saving potential. Consequently the driver view is blocked and lateral automation is required. While driving fully automatically the driver reaction time can be 1.5 upto 10s. Hence the driver cannot serve as backup for the CAD system, implying the system should have a reliable backup itself: the *fail-safety* mode. On the other hand, the system should keep its functionality, or part of its functionality, as long as possible in case *threats* occur to increase the system availability.

This thesis concentrates on a specific safety scenario: a communication *failure* in combination with a possible braking action of the lead vehicle for trucks. Communication of the actual longitudinal acceleration enables the vehicles to drive safely at a time gap of 0.3s. Therefore, a communication *failure* is a potential *threat* to the system. This master's thesis proposes control methods to bring the vehicle to a safe state in case of a communication *failure* applying longitudinal and/or lateral control. Controller requirements are defined: the controller should prevent *false positive* interventions, *false negative* interventions and it should aim for a high system availability. To achieve this, a system architecture is defined which splits the safety mechanism into three parts:

1. Detection mechanism (Situation Awareness).
2. Decisions (Safety Mode Selection).
3. Actions (Safety Algorithm).

To evaluate the proposed algorithms, a non-linear vehicle model is developed. The controller design is based on linearised, decoupled models for longitudinal and lateral dynamics, derived from the non-linear model. Two actions in *fail-safety* are considered: emergency braking and evasive manoeuvring. A set of 23 test cases is defined based on several braking values, communication *failure* durations and timing of braking with respect to the communication *failure*. This set is used to evaluate the occurrence of *false positives*, the occurrence of *false negatives*, safety and comfort. For evaluation of these properties, the following key performance indicators are defined:

- Number of collisions: the number of collisions in the test cases.
- Impact speed: in case a collision occurs, the accident severity can be rated by the impact speed.
- Minimum inter-vehicle distance: A large distance might indicate the algorithm is too conservative; a short distance might indicate too risky behaviour.
- Maximum deceleration: Less deceleration is assumed to be more comfortable.
- Maximum lateral acceleration: Lateral acceleration is only relevant for evasive manoeuvring. More lateral acceleration is considered as uncomfortable and dangerous, since heavy-duty vehicles are sensible for lateral instability.

This thesis focussed on the detection mechanism and actions (Step 1 and 3 of the safety mechanism) in *fail-safety*. To determine the preferable action, the *threat* should be assessed accurately. Therefore, safety measures are defined to assess the *threat* on a rear-end collision with the preceding vehicle by emergency braking or an evasive manoeuvre. Worse case behaviour of the preceding vehicle is assumed: the preceding vehicle will apply full braking from the moment communication fails. For emergency braking, the *threat* is rated by the BTN: the required deceleration to avoid a collision over the maximum achievable deceleration of the vehicle. The *threat* for evasive manoeuvring is rated by the TTS: the time till the last point to steer to avoid a collision is reached. In case a collision is potentially unavoidable, an impact speed in the worse case scenario is calculated to rate the severity of a possible collision. Dependent on the accuracy of the used models, these safety measures are accurate measures, based on which decisions can be made and actions be performed. The safety measures potentially can be applied to any safety scenario.

For collision avoidance by emergency braking, two types of controllers are developed. The first controller assumes that the vehicle braking behaviour is known accurately (a prediction-based controller). The second controller is a SMC, which is robust to system uncertainties and disturbances. In simulation, both controllers are able to avoid collisions for the nominal system in all defined test cases. Although the SMC is potentially more robust to system parameter uncertainties, the same number of collisions occur for both controllers in case of uncertain system parameters. Collisions occur mainly when the preceding vehicle has more braking capacity compared to the host vehicle. Only possibility to guarantee safety in this situation is to increase the time gap between the vehicles or change order. The prediction-based controller offers smoother braking behaviour at the cost of robustness to system uncertainties compared to the SMC. The prediction-based controller is validated on the test track with passenger cars. The results show a high consistency with the simulations. However, due to sensor noise *false positive* interventions occur. How to prevent *false positives* in practice without endangering rear-end collisions should be investigated in the future.

The lateral collision avoidance objective can be translated to bringing the system within a finite time interval from an unsafe region to a safe region. An approach describing this objective is *finite time stability*. *Finite time stability* prescribes bounds on the state trajectories for a finite time interval. How to come from this bound definition to a robust controller design for a complex model of an articulated vehicle requires more research. Therefore, this thesis proposes a robust SMC approach based on classical *Lyapunov stability* for lateral manoeuvring, applying only steering input and assuming only the lateral vehicle position can be measured. Drawback of this approach is that the controller objective becomes following an evasive path instead of control towards a safe region. Calculating the error to the evasive path might not be trivial during an evasive manoeuvre. An evasive path to bring the vehicle to a safe region is calculated by the Situation Awareness. In this thesis the evasive path is limited to a trapezoidal lateral acceleration profile for a lane change trajectory. The robustness of the lateral controller is evaluated for:

- System parameter uncertainties: The SMC is evaluated for a varying normalized cornering stiffness, which is assumed to be one of the most significant uncertainties.
- Initial errors: The controller performs well upto an initial position error of 30cm.
- Sensor noise: Sensor noise on the lateral position with a standard deviation of 0.03m (with a sample time of 1ms) is possible for the controller. The robustness of the controller to sensor noise can be increased by an observer, where a trade-off between noise suppression and controller performance has to be made. Increasing the smoothing factor of the observer will inherently lead to additional phase lag and thereby limit the controller performance.
- Time delay: The controller performs well for a steering actuator delay of 5ms, however for 10ms severe chattering occurs.

Simulations prove the lateral controller for evasive manoeuvring to be able to avoid collisions in all defined test cases, however *false positives* occur. Since *false positives* applying steering are very much undesired, this implies the system availability cannot be increased by evasive manoeuvring applying only steering compared to emergency braking. However, combined braking and steering in evasive manoeuvring has the potential to increase the system availability significantly. This possibly requires extension of the vehicle model and redesign of the controller in the future. However, the proposed SMC methods for longitudinal and lateral control are potentially able to control an evasive manoeuvre with combined braking and steering. As a first step, a final use case shows the potential of the proposed SMC strategies by activating the longitudinal and lateral controller in a sequential way

7.2 Recommendations

The main recommendations for future work are:

1. Considering time delays: Time delays limit the controller performance in an evasive manoeuvre significantly. Limiting the measurement delay in the sensors, limiting the actuator delay and time delay compensation in the software should be considered.
2. Sensor choices: This thesis focussed on the control in *fail-safety*. How the signals are obtained is not considered. Accurate sensors with limited time delay and limited noise are required. The sensors should be able to measure the vehicle position in a global coordinate frame in order to calculate the error to the evasive path.
3. The transition to emergency braking should be tuned or redesigned. In simulations the expected behaviour is achieved, but in practice *false positive* interventions occur due to sensor inaccuracies. This is also dependent on the sensor choice.
4. Investigate combined braking and steering: Since combined braking and steering has a high potential to increase the system availability, the influence of combined braking and steering on the vehicle dynamic behaviour should be investigated. Also differential braking might be considered.
5. The proposed *fail-safety* methods should be extended to other safety scenarios.
6. Evaluation of the system robustness against parameter uncertainties should be extended in the future with for instance the effect of side winds.

This thesis presented promising methods for longitudinal and lateral collision avoidance. With the previous mentioned points, the methods can be further optimized. However, SMC will always be vulnerable to time delays. Moreover, for lateral control, obtaining the error to a reference path during an evasive manoeuvre might not be trivial. In that case more fundamental research should be performed, focussing on how to come from a *finite time stability* bound definition to a feasible controller design.

Bibliography

[1] ISO 26262 road vehicles - functional safety. 2009.

[2] ISO 15622 intelligent transport systems - adaptive cruise control systems. 2010.

[3] C. Ackermann, R. Isermann, S. Min, and C. Kim. Collision avoidance with automatic braking and swerving. In *World Congress*, volume 19, pages 10694–10699, 2014.

[4] J. Ackermann, J. Guldner, W. Sienel, and V. Steinhauser, R. Utkin. Linear and nonlinear controller design for robust automatic steering. *IEEE Transactions on Control Systems Technology*, 3(1):132–143, 1995.

[5] A.A. Alam, A. Gattami, and K.H. Johansson. An experimental study on the fuel reduction potential of heavy duty vehicle platooning. In *13th International Conference on Intelligent Transportation Systems*, pages 306–311. IEEE, 2010.

[6] A.A. Alam, A. Gattami, K.H. Johansson, and C.J. Tomlin. Guaranteeing safety for heavy duty vehicle platooning: Safe set computations and experimental evaluations. *Control Engineering Practice*, 24:33–41, 2014.

[7] F. Amato, R. Ambrosino, M. Ariola, C. Cosentino, and G.D. Tommasi. *Finite-time stability and control*. Springer, 2014.

[8] F. Amato, M. Ariola, and C. Cosentino. Finite-time control of linear time-varying systems via output feedback. In *Proceedings of the American Control Conference*, volume 7, pages 4722–4726, 2005.

[9] F. Amato, M. Ariola, C. Cosentino, C.T. Abdallah, and P. Dorato. Necessary and sufficient conditions for finite-time stability of linear systems. In *Proceedings of the American Control Conference*, volume 5, pages 4452–4456. IEEE, 2003.

[10] B. van Arem, C.J.G. van Driel, and R. Visser. The impact of cooperative adaptive cruise control on traffic-flow characteristics. *IEEE Transactions on Intelligent Transportation Systems*, 7(4):429–436, 2006.

[11] H. Bae and Y. Kang. Decision making methods based on nonlinear model predictive control for emergency collision avoidance in complex situations. In *14th International Conference on Control, Automation and Systems*, pages 1424–1427. IEEE, 2014.

[12] J. Bernussou, P.L.D. Peres, and J.C. Geromel. A linear programming oriented procedure for quadratic stabilization of uncertain systems. *Systems & Control Letters*, 13(1):65–72, 1989.

[13] L. Biagiotti and C. Melchiorri. *Trajectory planning for automatic machines and robots*. Springer Science & Business Media, 2008.

[14] Ö. Bilen. Path control algorithms for autonomous steering and braking of heavy vehicles. Master's thesis, Chalmers University of Technology, 2010.

[15] C. Bonnet and H. Fritz. Fuel consumption reduction in a platoon: Experimental results with two electronically coupled trucks at close spacing. Technical report, SAE, 2000.

[16] W. Chee and M. Tomizuka. Vehicle lane change maneuver in automated highway systems. *California Partners for Advanced Transit and Highways*, 1994.

[17] C. Chen, G. Wagner, M. Pace, and T. Rogness. Prediction of heavy truck stopping distance and vehicle behavior using real-time hil and sil simulation. Technical report, SAE, 2008.

[18] E. Coelingh, A. Eidehall, and M. Bengtsson. Collision warning with full auto brake and pedestrian detection-a practical example of automatic emergency braking. In *13th International Conference on Intelligent Transportation Systems*, pages 155–160. IEEE, 2010.

[19] D.J. Cole, A.J. Pick, and A.M.C. Odhams. Predictive and linear quadratic methods for potential application to modelling driver steering control. *Vehicle System Dynamics*, 44(3):259–284, 2006.

[20] A. Davila. Report on fuel consumption. *Deliverable 4.3, SARTRE*, 2013.

[21] A. Eidehall. Multi-target threat assessment for automotive applications. In *14th International Conference on Intelligent Transportation Systems*, pages 433–438. IEEE, 2011.

[22] A. Eidehall and D. Madas. Real time path planning for threat assessment and collision avoidance by steering. In *16th International Conference on Intelligent Transportation Systems*, pages 916–921. IEEE, 2013.

[23] A. Ferrara and C. Vecchio. Second order sliding mode control of vehicles with distributed collision avoidance capabilities. *Mechatronics*, 19(4):471–477, 2009.

[24] S.K. Gehrig and F.J. Stein. Collision avoidance for vehicle-following systems. *IEEE Transactions on Intelligent Transportation Systems*, 8(2):233–244, 2007.

[25] J.C. Gerdes and E.J. Rossetter. A unified approach to driver assistance systems based on artificial potential fields. *Journal of Dynamic Systems, Measurement, and Control*, 123(3):431–438, 2001.

[26] J. Guldner, V. Utkin, and J. Ackermann. A sliding mode control approach to automatic car steering. In *Proceedings of the American Control Conference*, volume 2, pages 1969–1973. IEEE, 1994.

[27] M. Hassanzadeh, M. Lidberg, M. Keshavarz, and L. Bjelkeflo. Path and speed control of a heavy vehicle for collision avoidance manoeuvres. In *Intelligent Vehicles Symposium*, pages 129–134. IEEE, 2012.

[28] P. Hung, J.K. Hedrick, and M. Tomizuka. Combined lateral and longitudinal control of vehicles for ivhs. In *Proceedings of the American Control Conference*, volume 2, 1994.

[29] J. Jansson. *Collision Avoidance Theory: With application to automotive collision mitigation*. PhD thesis, Linköping University, 2005.

[30] T. A. Johansen. Toward dependable embedded model predictive control. *Systems Journal*, PP(99):1–12, 2014.

[31] H.K. Khalil and J.W. Grizzle. *Nonlinear systems*, volume 3. Prentice hall New Jersey, 1996.

[32] P.P. Khargonekar, K.M. Nagpal, and K.R. Poolla. H_∞ control with transients. *SIAM Journal on Control and Optimization*, 29(6):1373–1393, 1991.

[33] R.J. Kiefer and L.S. Angell. A comparison of the effects of an analog versus digital speedometer on driver performance in a task environment similar to driving. *Vision in Vehicles*, 4:283–290, 1993.

[34] F.W. Kienhöfer, J.I. Miller, and D. Cebon. Design concept for an alternative heavy vehicle abs system. *Vehicle System Dynamics*, 46(S1):571–583, 2008.

[35] H. Lee and V. Utkin. Chattering suppression methods in sliding mode control systems. *Annual Reviews in Control*, 31(2):179–188, 2007.

[36] M. Luijten. Lateral dynamic behaviour of articulated commercial vehicles. Master's thesis, Eindhoven University of Technology, 2010.

[37] J. Mårtensson, M. Nybacka, J. Jerrelind, and L. Drugge. Evaluation of safety distance in vehicle platoons by combined braking and steering. In *11th International Symposium on Advanced Vehicle Control*. Japan Society of Mechanical Engineers, 2012.

[38] A. Nozad. Heavy vehicle path stability control for collision avoidance applications. Master's thesis, Chalmers University of Technology, 2011.

[39] E. van Nunen, J. Ploeg, A. Morales Medina, and H. Nijmeijer. Fault tolerancy in cooperative adaptive cruise control. In *16th International Conference on Intelligent Transportation Systems*, pages 1184–1189. IEEE, 2013.

[40] H. Pacejka. *Tire and vehicle dynamics*. Butterworth-Heinemann, third edition, 2012.

[41] L. Palkovics and A. Fries. Intelligent electronic systems in commercial vehicles for enhanced traffic

safety. *Vehicle System Dynamics*, 35(4-5):227–289, 2001.

[42] J. Ploeg. *Analysis and design of controllers for cooperative and automated driving*. PhD thesis, Technische Universiteit Eindhoven, 2014.

[43] P.A.J. Ruijs, S.T.H. Jansen, and Ruiter A.A.W. AOS referentie testen. Technical report, TNO, 2009.

[44] P.A.J. Ruijs, S.T.H. Jansen, and Ruiter A.A.W. Testbaan expirimenten voor aos functies. Technical report, TNO, 2009.

[45] J. La Salle and S. Lefschetz. *Stability by Liapunov's direct methods*. Elsevier, 1961.

[46] D.J.M. Sampson and D. Cebon. Achievable roll stability of heavy road vehicles. *Proceedings of the Institution of Mechanical Engineers, Part D: Journal of Automobile Engineering*, 217(4):269–287, 2003.

[47] F. Emre Sancar, B. Fidan, J.P. Huissoon, and S.L. Waslander. Mpc based collaborative adaptive cruise control with rear end collision avoidance. In *Intelligent Vehicles Symposium Proceedings*, pages 516–521. IEEE, 2014.

[48] B. Schiller, V. Morellas, and M. Donath. Collision avoidance for highway vehicles using the virtual bumper controller. In *Intelligent Vehicles Symposium Proceedings*, pages 28–30. IEEE, 1998.

[49] J. Shah, M. Best, A. Benmimoun, and M.L. Ayat. Autonomous rear-end collision avoidance using an electric power steering system. *Proceedings of the Institution of Mechanical Engineers, Part D: Journal of Automobile Engineering*, 229(12):0954407014567517, 2015.

[50] N. Shibata, S. Sugiyama, and T. Wada. Collision avoidance control with steering using velocity potential field. In *Intelligent Vehicles Symposium Proceedings*, pages 438–443. IEEE, 2014.

[51] T. Shim, G. Adireddy, and H. Yuan. Autonomous vehicle collision avoidance system using path planning and model-predictive-control-based active front steering and wheel torque control. *Proceedings of the Institution of Mechanical Engineers, Part D: Journal of automobile engineering*, 226(6):767–778, 2012.

[52] G.A. Sparks and C. Berthelot. The cost/benefit analysis of a rollover warning device for large trucks. 1989.

[53] M. Tomizuka, S. Patwardhan, and W.B. Zhang. Experimental study of lane change manoeuvre for ahs applications. In *Proceedings of the American Control Conference*, volume 1, pages 139–143. IEEE, 1995.

[54] Volvo Trucks. European accident research and safety report 2013. "`http://www.volvotrucks.com/trucks/lithuanian-market/lt-lt/NEWSMEDIA/Publications/Safety/Documents/European%20Accident%20Research%20and%20safety%20report%202013.pdf`". Accessed February 6, 2015.

[55] V. Turri, A. Carvalho, H.E. Tseng, K.H. Johansson, and F. Borrelli. Linear model predictive control for lane keeping and obstacle avoidance on low curvature roads. In *International Conference on Intelligent Transportation Systems*, pages 378–383. IEEE, 2013.

[56] D. Tzempetzis. Towards a safety concept for cooperative automated driving. Technical report, SAI, Eindhoven University of Technology, 2015.

[57] V. Utkin, J. Guldner, and J. Shi. *Sliding mode control in electro-mechanical systems*, volume 34. CRC press, 2009.

[58] R. Zheng, K. Nakano, S. Yamabe, M. Aki, H. Nakamura, and Y. Suda. Study on emergency-avoidance braking for the automatic platooning of trucks. *IEEE Transactions on Intelligent Transportation Systems*, 15(4):1748–1757, 2014.

[59] C. Zong, T. Zhu, C. Wang, and H. Liu. Multi-objective stability control algorithm of heavy tractor semi-trailer based on differential braking. *Chinese Journal of Mechanical Engineering*, 25(1):88–97, 2012.

Appendix A

Derivation vehicle model

A.1 Parameters

Parameter	Value	Unit
C_f	4.3×10^5	$[N/rad]$
C_r	7.0×10^5	$[N/rad]$
C_t	1.1×10^6	$[N/rad]$
f_{tyre}	5.73	$[1/rad]$
h_{cog}	1.4	$[m]$
h_{cog_t}	1.4	$[m]$
J_{zz}	2.7×10^4	$[kg\ m^2]$
$J_{zz,t}$	5.3×10^5	$[kg\ m^2]$
$J_{wh,fl/r}$	20	$[kg\ m^2]$
$J_{wh,rl/r}$	40	$[kg\ m^2]$
$J_{wh,tl/r}$	20	$[kg\ m^2]$
L	3.8	$[m]$
L_t	8.13	$[m]$
l_f	1.1	$[m]$
$l_{f,t}$	4.98	$[m]$
l_h	2.02	$[m]$
l_r	2.7	$[m]$
m	7449	$[kg]$
m_t	32551	$[kg]$
$r_{eff,fl/r}$	0.507	$[m]$
$r_{eff,rl/r}$	0.522	$[m]$
$r_{eff,tl/r}$	0.522	$[m]$
s_f	2.03	$[m]$
s_r	1.82	$[m]$
s_t	1.82	$[m]$
θ_b	0.2	$[s]$
θ_s	0.0	$[s]$
μ	1	$[-]$
σ_x	0.4	$[m]$
σ_y	0.6	$[m]$
τ_b	0.4	$[s]$
τ_s	0.05	$[s]$

A.2 Equations of motion

In this appendix, the derivation of the vehicle model will be discussed in detail. For readability of the equations are the time dependencies not shown in the equations. The equations of motion are derived using Lagrange:

$$\frac{d}{dt}\frac{\partial T}{\partial \dot{q}_i} - \frac{\partial T}{\partial q_i} + \frac{\partial V}{\partial q_i} = Q_i \qquad i = 1, 2, ..., n, \tag{A.1}$$

where T is the kinetic energy, V the potential energy, Q_i the generalised forces, q_i the generalised coordinates and n the number of states. The free body diagram of the tractor semi-trailer combination is illustrated in Fig 3.2. The system consists out of two masses. Hence the unconstrained system in the 2 dimensional space has 6 degrees of freedom:

$$\underline{\hat{q}}_g = [x \quad y \quad \Phi \quad x_t \quad y_t \quad \Phi_t]^T. \tag{A.2}$$

The hitch point is described by a revolute joint, with constraints 2 degrees of freedom. Hence the system motion in the 2 dimensional space can be described by the following 4 generalized coordinates:

$$\underline{q}_g = [x \quad y \quad \Phi \quad \Phi_t]^T. \tag{A.3}$$

For coordinates x_t and y_t the following relations apply due to the revolute joint:

$$\begin{aligned} x_t &= x - l_h\, cos(\Phi) - l_{f,t}\, cos(\Phi_t) \\ y_t &= y - l_h\, sin(\Phi) - l_{f,t}\, sin(\Phi_t). \end{aligned} \tag{A.4}$$

Applying the small angle assumption for Φ and Φ_t, and neglecting the constants in the equations, the relations can be rewritten as:

$$\begin{aligned} x_t &\approx x \\ y_t &\approx y - l_h\Phi - a_t\Phi_t. \end{aligned} \tag{A.5}$$

The kinetic energy can be expressed as:

$$T = \frac{1}{2}m(\dot{x}^2 + \dot{y}^2) + \frac{1}{2}m_t(\dot{x}_t^2 + \dot{y}_t^2) + \frac{1}{2}I\dot{\Phi}^2 + \frac{1}{2}I_t\dot{\Phi}_t^2. \tag{A.6}$$

The kinetic energy equation linearised around $\Phi = 0$ and $\Phi_t = 0$, expressed only as function of the generalized coordinates reads:

$$T = \frac{1}{2}(m+m_t)\dot{x}^2 + \frac{1}{2}(m+m_t)\dot{y}^2 + \frac{1}{2}(J_{zz}+m_t l_h^2)\dot{\Phi}^2 + \frac{1}{2}(J_{zz,t}+m_t l_{f,t}^2)\dot{\Phi}_t^2 - m_t l_h \dot{y}\dot{\Phi} - m_t l_{f,t}\dot{y}\dot{\Phi}_t + m_t h l_{f,t}\dot{\Phi}\dot{\Phi}_t. \tag{A.7}$$

For the potential energy holds:

$$V = \underline{0}. \tag{A.8}$$

With the relations for kinetic and potential energy, the following yields for the Lagrange terms:

$$\begin{aligned} \frac{d}{dt}\frac{\partial T}{\partial \dot{x}} &= (m + m_t)\ddot{x} \\ \frac{d}{dt}\frac{\partial T}{\partial \dot{y}} &= (m + m_t)\ddot{y} - m_t l_h \ddot{\Phi} - m_t l_{f,t}\ddot{\Phi}_t \\ \frac{d}{dt}\frac{\partial T}{\partial \dot{\Phi}} &= (J_{zz} + m_t l_h^2)\ddot{\Phi} - m_t l_h \ddot{y} + m_t l_h l_{f,t}\ddot{\Phi}_t \\ \frac{d}{dt}\frac{\partial T}{\partial \dot{\Phi}_t} &= (J_{zz,t} + m_t l_{f,t}^2)\ddot{\Phi}_t - m_t l_{f,t}\ddot{y} + m_t h l_{f,t}\ddot{\Phi} \\ \frac{\partial T}{\partial q_{g,i}} &= \underline{0} \\ \frac{\partial V}{\partial q_{g,i}} &= \underline{0}. \end{aligned} \tag{A.9}$$

The generalized forces are derived from the virtual work using $\dot{x} \approx \dot{x}_t$.

$$\begin{aligned}\Delta W =&\Big((F_{x,fl}+F_{x,fr})\,cos(\delta)+(F_{x,rl}+F_{x,rr})+(F_{x,tl}+F_{x,tr})\,cos(\phi)-\\&(F_{y,fl}+F_{y,fr})\,sin(\delta)-(F_{y,tl}+F_{y,tr})\,sin(\phi)\Big)\Delta x+\\&\Big((F_{y,fl}+F_{y,fr})\,cos(\delta)+(F_{x,fl}+F_{x,fr})\,sin(\delta)\Big)\Delta\big(y+l_f\,sin(\Phi)\big)+\\&(F_{y,rl}+F_{y,rr})\Delta\big(y-l_r\,sin(\Phi)\big)+\\&(F_{x,tl}+F_{x,tr})\,sin(\phi)\Delta\big(y-l_h\,sin(\Phi)\big)+\\&(F_{y,tl}+F_{y,tr})\,cos(\phi)\Delta\big(y-l_h\,sin(\Phi)-L_t\,sin(\Phi_t)\big)+\\&\Big((F_{x,fr}-F_{x,fl})\,cos(\delta)-(F_{y,fr}+F_{y,fl})\,sin(\delta)\Big)\frac{s_f}{2}\Delta(\Phi)+(F_{x,rr}-F_{x,rl})\frac{s_r}{2}\Delta(\Phi)+\\&(F_{x,tr}-F_{x,tl})\frac{s_t}{2}\Delta(\Phi_t)\end{aligned}\tag{A.10}$$

Linearising the virtual work around $\delta = 0$, $\Phi = 0$ and $\Phi_t = 0$ results in:

$$\begin{aligned}\Delta W \approx&\big(F_{x,fl}+F_{x,fr}+F_{x,rl}+F_{x,rr}+F_{x,tl}+F_{x,tr}-\\&(F_{y,fl}+F_{y,fr})\delta-(F_{y,tl}+F_{y,tr})\phi\big)\Delta x+\\&\Big((F_{y,fl}+F_{y,fr})+(F_{x,fl}+F_{x,fr})\delta\Big)\Delta\big(y+l_f\Phi\big)+\\&(F_{y,fl}+F_{y,rr})\Delta\big(y-l_r\Phi\big)+\\&(F_{x,tl}+F_{x,tr})\phi\Delta\big(y-l_h\Phi\big)+\\&(F_{y,tl}+F_{y,tr})\Delta\big(y-l_h\Phi-L_t\Phi_t\big)+\\&\Big((F_{x,fr}-F_{x,fl})-(F_{y,fr}+F_{y,fl})\delta\Big)\frac{s_f}{2}\Delta(\Phi)+(F_{x,rr}-F_{x,rl})\frac{s_r}{2}\Delta(\Phi)+\\&(F_{x,tr}-F_{x,tl})\frac{s_t}{2}\Delta(\Phi_t)\end{aligned}\tag{A.11}$$

This yields for the generalized forces:

$$\begin{aligned}Q_x &= F_{x,fl}+F_{x,fr}+F_{x,rl}+F_{x,rr}+F_{x,tl}+F_{x,tr}-(F_{y,fl}+F_{y,fr})\delta-(F_{y,tl}+F_{y,tr})\phi\\Q_y &= (F_{y,fl}+F_{y,fr})+(F_{x,fl}+F_{x,fr})\delta+(F_{y,rl}+F_{y,rr})+(F_{x,tl}+F_{x,tr})(\phi)+(F_{y,tl}+F_{y,tr})\\Q_\Phi &= l_f\big((F_{y,fl}+F_{y,fr})+(F_{x,fl}+F_{x,fr})\delta\big)-l_r(F_{y,rl}+F_{y,rr})-l_h\big((F_{x,tl}+F_{x,tr})(\phi)+\\&\quad F_{y,tl}+F_{y,tr}\big)+\Big((F_{x,fr}-F_{x,fl})-(F_{y,fr}+F_{y,fl})\delta\Big)\frac{s_f}{2}+(F_{x,rr}-F_{x,rl})\frac{s_r}{2}\\Q_{\Phi_t} &= -L_t(F_{y,tl}+F_{y,tr})+(F_{x,tr}-F_{x,tl})\frac{s_t}{2}\end{aligned}\tag{A.12}$$

Up to this point global coordinates are used. The relative angle between the two bodies will be defined as the articulation angle.

$$\phi = \Phi_t - \Phi \tag{A.13}$$

The velocities in global coordinates can be expressed in local coordinate frame velocities v_x and v_y as follows:

$$\begin{aligned}\dot{x} &= v_x\,cos(\Phi)-v_y\,sin(\Phi)\\\dot{y} &= v_x\,sin(\Phi)+v_y\,cos(\Phi)\\\dot{\Phi} &= \dot{\Phi}\\\dot{\Phi}_t &= \dot{\Phi}+\dot{\phi}.\end{aligned}\tag{A.14}$$

and the accelerations:

$$\begin{aligned}\ddot{x} &= \dot{v}_x\,cos(\Phi)-\dot{v}_y\,sin(\Phi)+(-v_x\,sin(\Phi)-v_y\,cos(\Phi))\dot{\Phi}\\\ddot{y} &= \dot{v}_x\,sin(\Phi)+\dot{v}_y\,cos(\Phi)+(v_x\,cos(\Phi)-v_y\,sin(\Phi))\dot{\Phi}\\\ddot{\Phi} &= \ddot{\Phi}\\\ddot{\Phi}_t &= \ddot{\Phi}+\ddot{\phi}.\end{aligned}\tag{A.15}$$

By linearising the accelerations in local coordinates around $\Phi = 0$, the following expressions for the accelerations hold:

$$\begin{aligned} \ddot{x} &= \dot{v}_x - v_y\dot{\Phi} \\ \ddot{y} &= \dot{v}_y + v_x\dot{\Phi} \\ \ddot{\Phi} &= \ddot{\Phi} \\ \ddot{\Phi}_t &= \ddot{\Phi} + \ddot{\phi}. \end{aligned} \tag{A.16}$$

Hence a set of generalized coordinates can be expressed in the local coordinate frame:

$$\dot{\underline{q}} = [v_x,\ v_y,\ \dot{\Phi},\ \dot{\phi}]^T. \tag{A.17}$$

The equations can be written in the form:

$$\underline{M}\ddot{\underline{q}} + \underline{H}(\dot{\underline{q}}) = \underline{Q}, \tag{A.18}$$

with a mass matrix

$$\underline{M} = \begin{bmatrix} m+m_t & 0 & 0 & 0 \\ 0 & m+m_t & -m_t(l_h+l_{f,t}) & -m_t l_{f,t} \\ 0 & -m_t l_h & J_{zz}+m_t h(l_h+l_{f,t}) & m_t l_h l_{f,t} \\ 0 & -m_t l_{f,t} & J_{zz,t}+m_t l_{f,t}(l_h+l_{f,t}) & J_{zz,t}+m_t l_{f,t}^2 \end{bmatrix} \tag{A.19}$$

and matrix $\underline{H}(\underline{q})$, containing the Coriolis terms, defined as:

$$\underline{H}(\dot{\underline{q}}) = \begin{bmatrix} -(m+m_t)v_y\dot{\Phi} \\ (m+m_t)v_x\dot{\Phi} \\ -m_t l_h v_x\dot{\Phi} \\ -m_t l_{f,t} v_x\dot{\Phi} \end{bmatrix} \tag{A.20}$$

A.3 Linearisation of the lateral slip angles

The slip angle α_i is defined as:

$$\alpha_i = atan\left(\frac{v_{y,i}}{v_{x,i}}\right), \tag{A.21}$$

where v_x is the longitudinal velocity and v_y the lateral velocity at the tyre contact point. To find the velocities, first the position vectors in the fixed reference frame need to be determined. Note that the slip angles and steering angles are assumed to be equal left and right. Hence the slip angles have to be found per axle.

$$\begin{aligned} \underline{r}_f &= \begin{bmatrix} x + l_f\, cos(\Phi) \\ y + l_f\, sin(\Phi) \end{bmatrix} \\ \underline{r}_r &= \begin{bmatrix} x - l_r\, cos(\Phi) \\ y - l_r\, sin(\Phi) \end{bmatrix} \\ \underline{r}_t &= \begin{bmatrix} x - l_h\, cos(\Phi) - L_t\, cos(\Phi_t) \\ y - l_h\, sin(\Phi) - L_t\, sin(\Phi_t) \end{bmatrix}. \end{aligned} \tag{A.22}$$

Linearising the position vectors around $\Phi = 0$ and $\Phi_t = 0$ results in:

$$\begin{aligned} \underline{r}_f &= \begin{bmatrix} x + l_f \\ y + l_f\Phi \end{bmatrix} \\ \underline{r}_r &= \begin{bmatrix} x - l_r \\ y - l_r\Phi \end{bmatrix} \\ \underline{r}_t &= \begin{bmatrix} x - l_h - L_t \\ y - l_h\Phi - L_t\Phi_t \end{bmatrix}. \end{aligned} \tag{A.23}$$

Then by differentiating, the velocity vectors are obtained:

$$\begin{aligned}
\dot{\underline{r}}_f &= \begin{bmatrix} \dot{x} \\ \dot{y} + l_f\dot{\Phi} \end{bmatrix} \\
\dot{\underline{r}}_r &= \begin{bmatrix} \dot{x} \\ \dot{y} - l_r\dot{\Phi} \end{bmatrix} \\
\dot{\underline{r}}_t &= \begin{bmatrix} \dot{x} \\ \dot{y} - (l_h + L_t)\dot{\Phi} + L_t\dot{\phi} \end{bmatrix}.
\end{aligned} \tag{A.24}$$

For small heading angles Φ, $\dot{x} \approx v_x$ and $\dot{y} \approx v_y$. This implies:

$$\begin{aligned}
\alpha_f &= \delta - atan\left(\frac{v_y + l_f\dot{\Phi}}{v_x}\right) \\
\alpha_r &= -atan\left(\frac{v_y - l_r\dot{\Phi}}{v_x}\right) \\
\alpha_t &= \phi - atan\left(\frac{v_y - (l_h + L_t)\dot{\Phi} + L_t\dot{\phi}}{v_x}\right).
\end{aligned} \tag{A.25}$$

Linearising these equations for slip angles around $\alpha_i = 0$ yields:

$$\begin{aligned}
\alpha_f &= \delta - \left(\frac{v_y + l_f\dot{\Phi}}{v_x}\right) \\
\alpha_r &= -\left(\frac{v_y - l_r\dot{\Phi}}{v_x}\right) \\
\alpha_t &= \phi - \left(\frac{v_y - (l_h + L_t)\dot{\Phi} + L_t\dot{\phi}}{v_x}\right).
\end{aligned} \tag{A.26}$$

Appendix B

Activity diagrams for BTN and impact speed calculation

[BTN, v_{imp}] = ThreatAssessment(HT,TT)

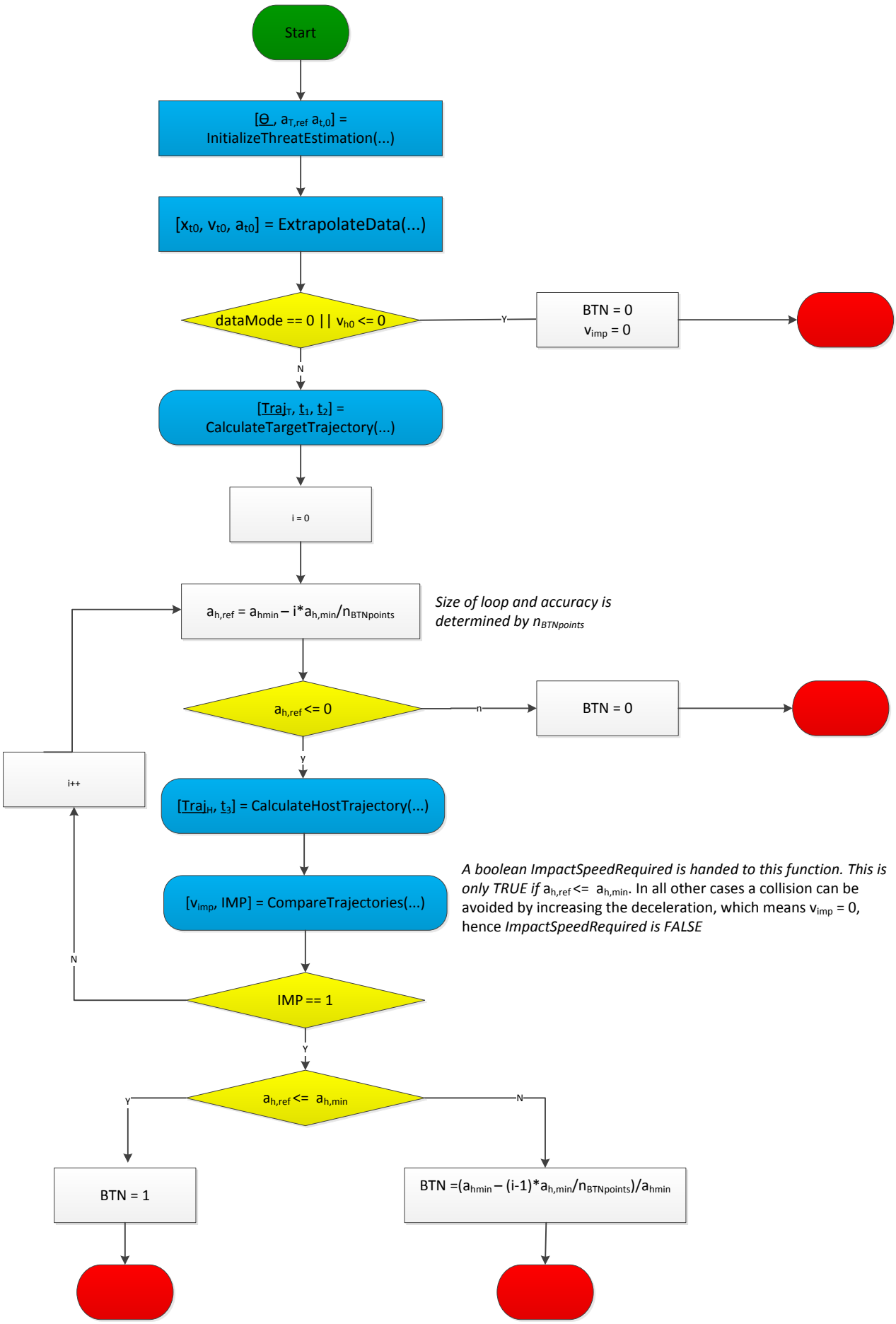

$[\underline{Traj_T}, \underline{t_1}, \underline{t_2}] = CalculateTargetTrajectory(x_{t,0}, v_{t,0}, a_{t,0}, a_{t,min})$

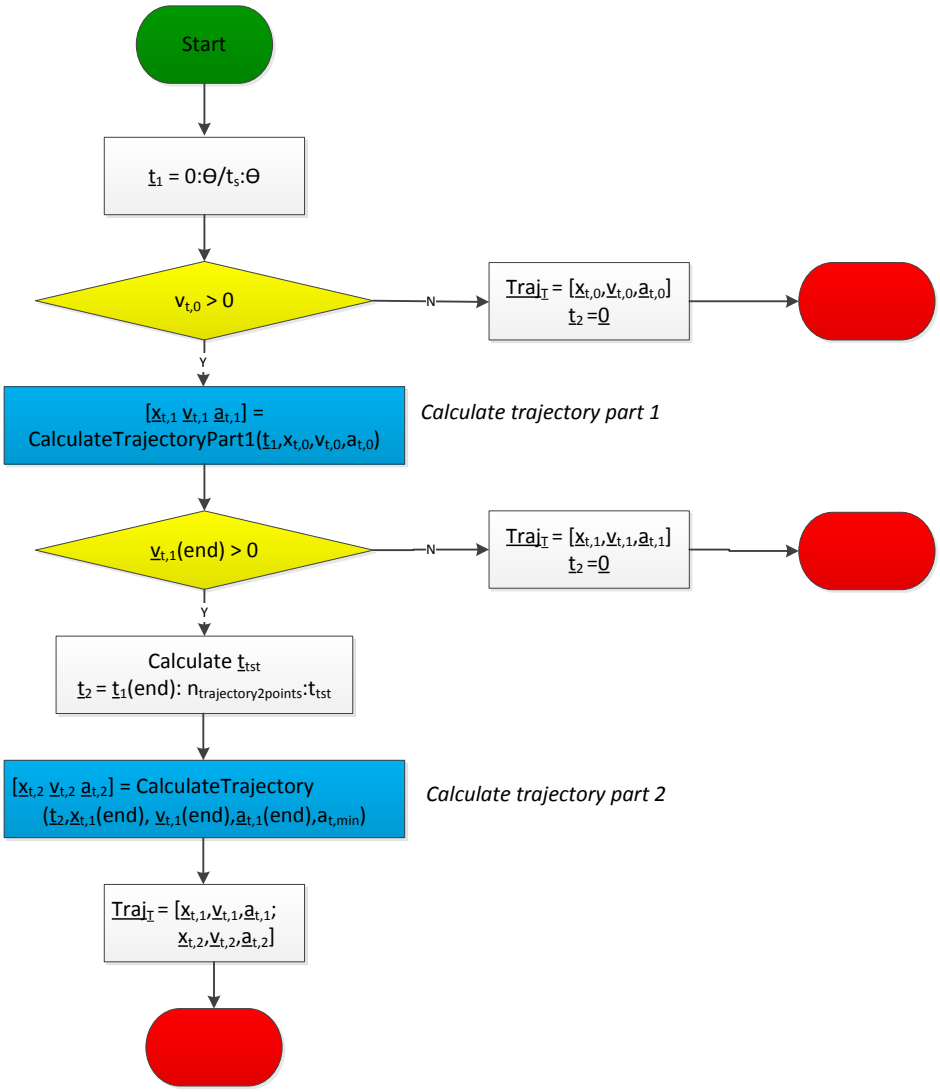

$[\underline{Traj}_H, \underline{t}_3] = CalculateHostTrajectory(\underline{t}_1, \underline{t}_2, x_{h,0}, v_{h,0}, a_{h,0}, a_{h,ref})$

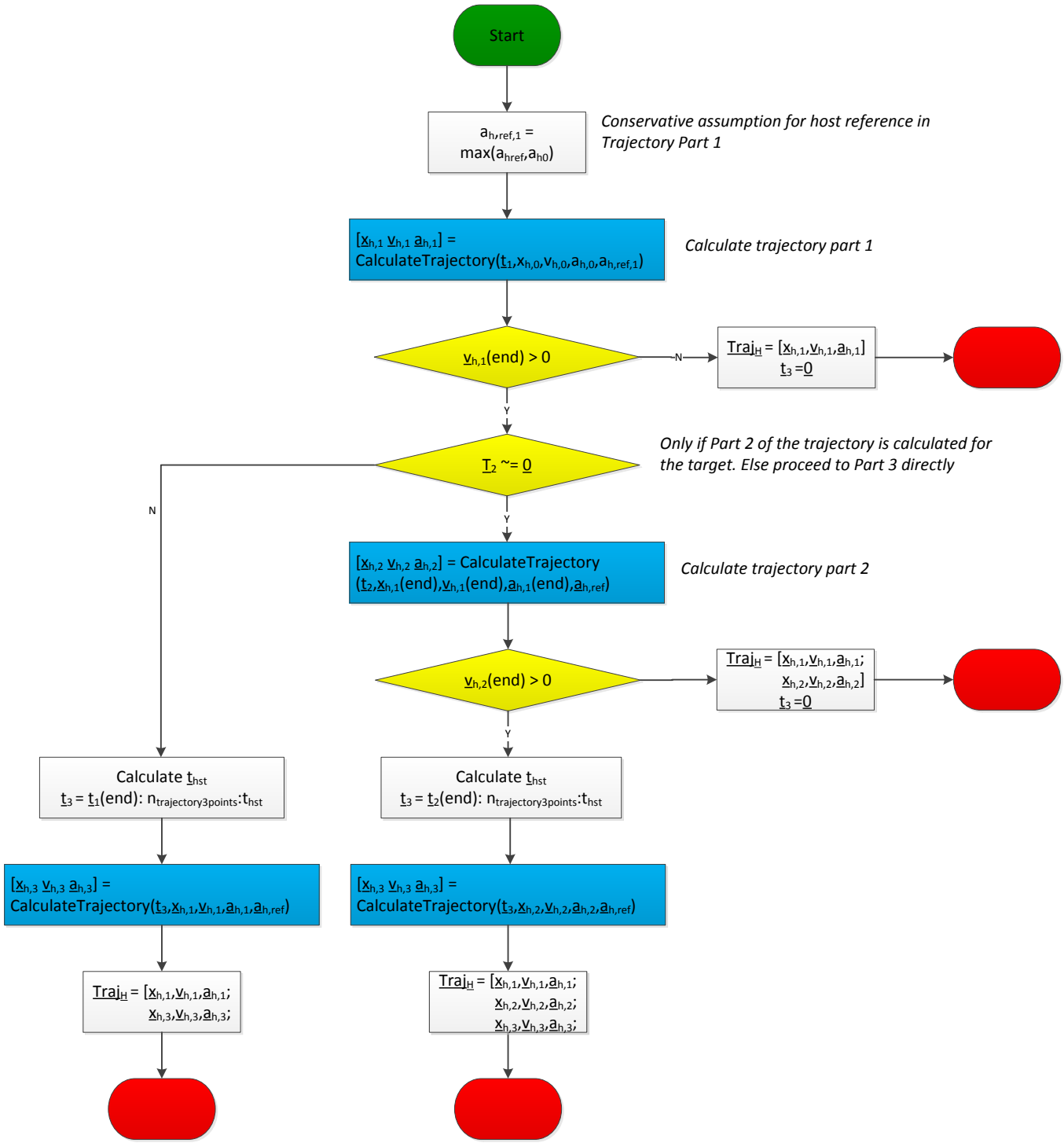

[v_{imp}, IMP] = CompareTrajectories($\underline{t_1}$,$\underline{t_2}$,$\underline{t_3}$,$\underline{Traj_H}$, $\underline{Traj_T}$,ImpSpeedRequired)

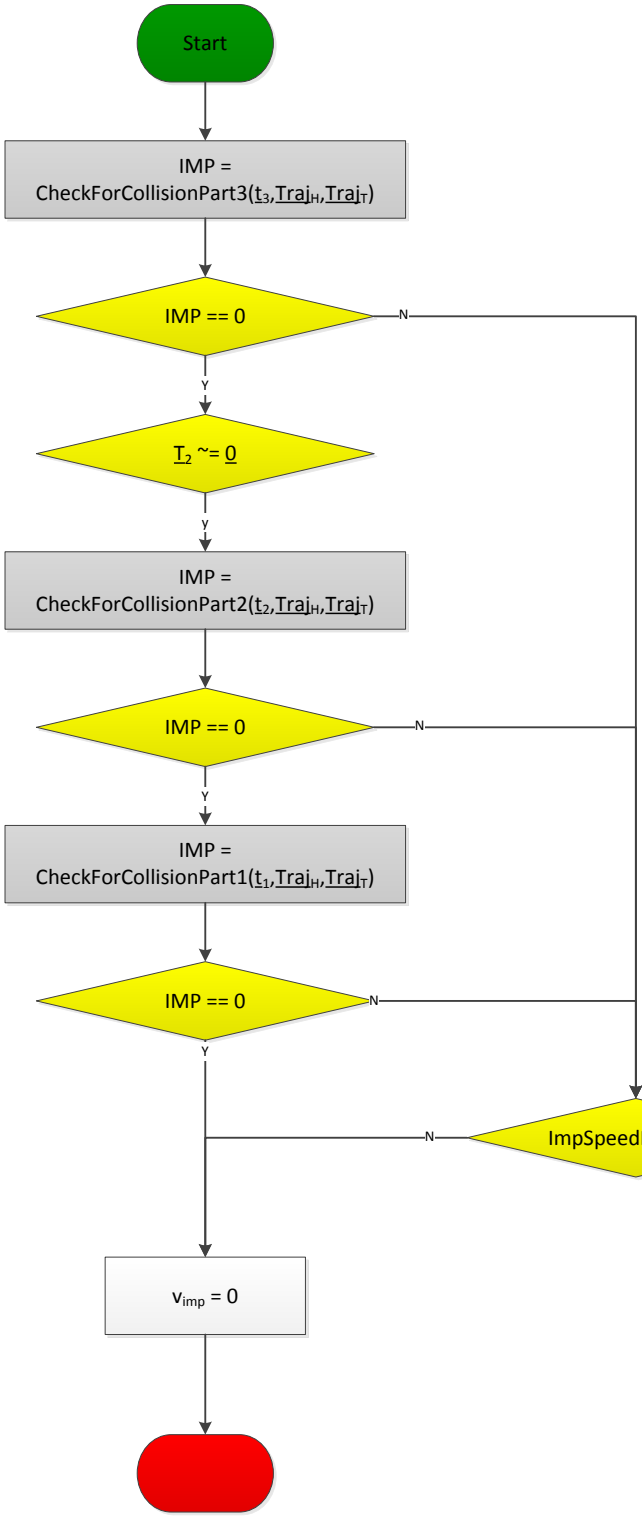

A boolean ImpactSpeedRequired is handed to this function. This is only TRUE if $a_{h,ref} <= a_{h,min}$. In all other cases a collision can be avoided by increasing the deceleration, which means $v_{imp} = 0$, hence *ImpactSpeedRequired is FALSE*

Appendix C

Path generation

For lateral path generation, a trapezoidal profile is used with limited lateral acceleration in jerk under the following assumptions:

1. The time at the start of the path is assumed to be zero and the time when the lane change is completed T.
2. The minimum and maximum jerk limit are equal.
3. The minimum and maximum acceleration limit are equal.
4. The initial and final velocities are zero $\dot{y}(0) = 0$ and $\dot{y}(T) = 0$.
5. The initial and final accelerations are zero $\ddot{y}(0) = 0$ and $\ddot{y}(T) = 0$.
6. The manoeuvre duration is long enough to reach the lateral acceleration limit, which implies

$$\Delta y \geq 2\frac{a_{lim}^3}{j_{lim}^2} \tag{C.1}$$

holds. Here, Δy is the travelled distance during the full lane change. The case for non-zero initial and final velocities, non-symmetric constraints and the case that the acceleration limit is not reached are derived in [13]. For each of the segments defined in Fig C.1, the position y, velocity $\dot{y}$, acceleration $\ddot{y}$ and $\dddot{y}$ on the trajectory can be calculated. In these equations $y(T) > y(0)$. The transition times are defined as follows:

$$\begin{aligned} T_j &= \frac{a_{lim}}{j_{lim}} \\ T_a = T_d &= \frac{T_j}{2} + \sqrt{\left(\frac{T_j}{2}\right)^2 + \frac{\Delta y}{a_{lim}}} \\ T &= T_a + T_d \\ v_{lim} &= (T_a - T_j)a_{lim} \end{aligned} \tag{C.2}$$

The individual segments can be described by the following function:

$a)$ $t \in [0, T_j]$

$$\begin{cases} y(t) & = j_{lim}\dfrac{t^3}{6} \\ \dot{y}(t) & = j_{lim}\dfrac{t^2}{2} \\ \ddot{y}(t) & = j_{lim}t \\ \dddot{y}(t) & = j_{lim} \end{cases} \tag{C.3}$$

$b)$ $t \in [T_j, T_a - T_j]$

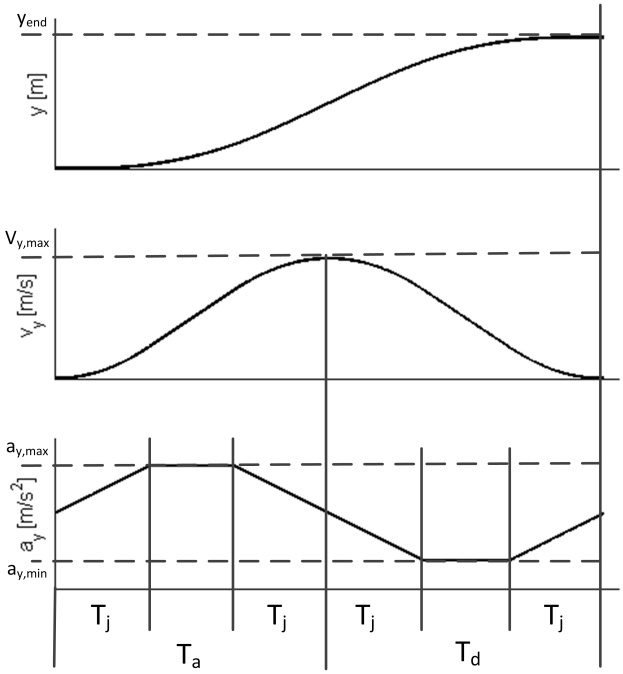

Fig C.1: Trapezoidal path with limits

$$\begin{cases} y(t) &= \frac{a_{lim}}{6}\left(3t^2 - 3T_j t + Tj^2\right) \\ \dot{y}(t) &= a_{lim}\left(t - \frac{T_j}{2}\right) \\ \ddot{y}(t) &= a_{lim} \\ \dddot{y}(t) &= 0 \end{cases} \tag{C.4}$$

c) $t \in [T_a - T_j, T_a + T_j]$

$$\begin{cases} y(t) &= -v_{lim}\left(\frac{T_a}{2} + t\right) + j_{lim}\frac{(T_a - t)^3}{6} \\ \dot{y}(t) &= -j_{lim}\frac{(T_a - t)^2}{2} \\ \ddot{y}(t) &= -j_{lim}(t - T_a) \\ \dddot{y}(t) &= -j_{lim} \end{cases} \tag{C.5}$$

d) $t \in [T - T_d + T_j, T - T_j]$

$$\begin{cases} y(t) &= v_{lim}\left(t - T + \frac{T_d}{2}\right) - \frac{a_{lim}}{6}\left(3(t - T + T_d)^2 - T_j(t - T + T_d) + T_j^2\right) \\ \dot{y}(t) &= v_{lim} - a_{lim}\left(t - T + T_d - \frac{T_j}{2}\right) \\ \ddot{y}(t) &= -a_{lim} \\ \dddot{y}(t) &= 0 \end{cases} \tag{C.6}$$

e) $t \in [T - T_j, T]$

$$\begin{cases} y(t) &= -j_{lim}\frac{(T - t)^3}{6} \\ \dot{y}(t) &= j_{lim}\frac{(T - t)^2}{2} \\ \ddot{y}(t) &= j_{lim}(T - t) \\ \dddot{y}(t) &= j_{lim} \end{cases} \tag{C.7}$$

(C.8)

Appendix D

Calcluation of required acceleration for SMC

This appendix will show how a longitudinal required acceleration is obtained using a limited jerk trajectory. For more information with respect to trajectory planning the reader is referred to [13]. The goal is to bring the actual host vehicle velocity $v_{H,x,0}$ to zero at the stopping point x_{stop} calculated by the method proposed in Section 4.1. The limited jerk time T_j is given by:

$$T_j = \frac{|a_{H,x,req} - a_{H,x,0}|}{j_{x,lim}}, \tag{D.1}$$

where $a_{H,x,req}$ is the required acceleration, $a_{H,x,0}$ the actual acceleration and $j_{x,lim}$ the jerk limit. The standstill distance can be calculated by:

$$t_{H,st} = \begin{cases} \dfrac{-v_{H,x,0} + (a_{H,x,req} - a_{H,x,0}) * T_j/2}{a_{H,x,req}}, & \text{if } t_{H,st} > T_j, \\ \dfrac{-a_{H,x,0} + \sqrt{a_{H,x,0}^2 - 2j_{x,lim}v_{H,x,0}}}{j_{x,lim}\text{sign}(a_{H,x,req} - a_{H,x,0})}, & \text{if } t_{H,st} \leq T_j. \end{cases} \tag{D.2}$$

The stopping distance can be calculated by:

$$x_H(t_{H,st}) = \begin{cases} v_{H,x,0}t_{H,st} + \dfrac{1}{2}a_{H,x,0}t_{H,st}^2 + \dfrac{a_{H,x,req} - a_{H,x,0}}{6}\left(3t_{H,st}^2 - 3T_j t_{H,st} + T_j^2\right), & \text{if } t_{H,st} > T_j, \\ v_{H,x,0}t_{H,st} + \dfrac{1}{2}a_{H,x,0}t_{H,st}^2 - \dfrac{1}{6}j_{x,lim}t_{H,st}^3, & \text{if } t_{H,st} \leq T_j. \end{cases} \tag{D.3}$$

An algorithm has been implemented that determines $a_{H,x,req}$ such that $x_H(t_{st}) = x_{stop}$

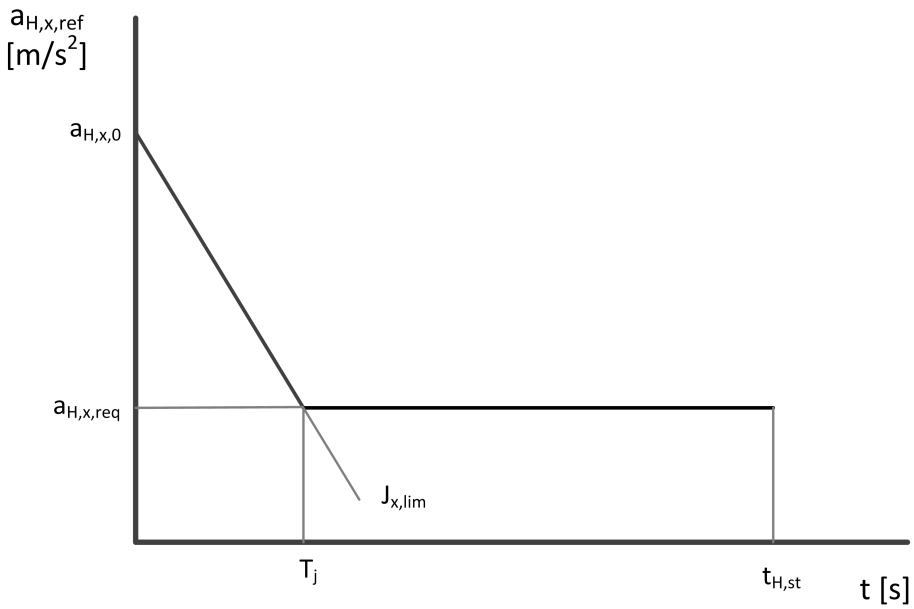

Fig D.1: Find required acceleration on a limited jerk trajectory

Appendix E

Tests for the communication failure use case

E.1 Passenger car and truck comparison prediction-based controller

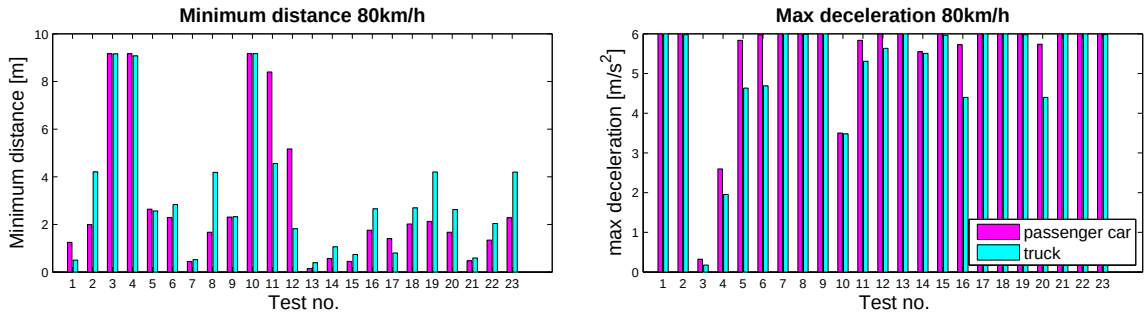

Fig E.1: Comparison between results for a passenger car and truck

E.2 Test cases

Test no.	Test description
1	Communication failure for 0.1 sec and lead vehicle brakes at t=0 sec with $a_{L,x,ref}$ = -6 m/s^2 without any preceding vehicle in front of it.
2	Communication failure for 0.1 sec and lead vehicle brakes at t=0 sec with $a_{L,x,ref}$ = -6 m/s^2,with a preceding vehicle driving with d_{LL} = 10 m and $\dot{d}_{LL}$ = -0.1 m/s.
3	Communication failure for 0.1 sec and lead vehicle does not brake ($a_{L,x,ref}$ = 0 m/s^2) without any preceding vehicle in front of it.
4	Communication failure for 1 sec and lead vehicle does not brake ($a_{L,x,ref}$ = 0 m/s^2) without any preceding vehicle in front of it.
5	Communication failure for 1 sec and lead vehicle brakes at t=0 sec with $a_{L,x,ref}$ = -2 m/s^2 without any preceding vehicle in front of it.
6	Communication failure for 1 sec and lead vehicle brakes at t=0 sec with $a_{L,x,ref}$ = -4 m/s^2 without any preceding vehicle in front of it.
7	Communication failure for 1 sec and lead vehicle brakes at t=0 sec with $a_{L,x,ref}$ = -6 m/s^2 without any preceding vehicle in front of it.
8	Communication failure for 1 sec and lead vehicle brakes at t=0 sec with $a_{L,x,ref}$ = -6 m/s^2 with d_{LL} = 10 m and $\dot{d}_{LL}$ = -0.1 m/s.
9	Communication failure for 1 sec and lead vehicle brakes at t=0.5 sec with $a_{L,x,ref}$ = -6 m/s^2 without any preceding vehicle in front of it.
10	Communication failure for 10 sec and lead vehicle does not brake ($a_{L,x,ref}$ = 0 m/s^2) without any preceding vehicle in front of it.
11	Communication failure for 10 sec and lead vehicle brakes at t=0 sec with $a_{L,x,ref}$ = -2 m/s^2 without any preceding vehicle in front of it.
12	Communication failure for 10 sec and lead vehicle brakes at t=0 sec with $a_{L,x,ref}$ = -4 m/s^2 without any preceding vehicle in front.
13	Communication failure for 10 sec and lead vehicle brakes at t=0 sec with $a_{L,x,ref}$ = -6 m/s^2 without any preceding vehicle in front of it.
14	Communication failure for 10 sec and lead vehicle brakes at t=0 sec with $a_{L,x,ref}$ = -6 m/s^2 with d_{LL} = 10 m and $\dot{d}_{LL}$ = -0.1 m/s.
15	Communication failure for 10 sec and lead vehicle brakes at t=0.5 sec with $a_{L,x,ref}$ = -6 m/s^2 without any preceding vehicle in front of it.
16	Communication failure for 0.4 sec and lead vehicle brakes at t=0 sec with $a_{L,x,ref}$ = -4 m/s^2 without any preceding vehicle in front of it.
17	Communication failure for 0.4 sec and lead vehicle brakes at t=0 sec with $a_{L,x,ref}$ = -6 m/s^2 without any preceding vehicle in front of it.
18	Communication failure for 0.4 sec and lead vehicle brakes at t=0.5 sec with $a_{L,x,ref}$ = -6 m/s^2 without any preceding vehicle in front of it.
19	Communication failure for 0.4 sec and lead vehicle brakes at t=0 sec with $a_{L,x,ref}$ = -6 m/s^2 with d_{LL} = 10 m and $\dot{d}_{LL}$ = -0.1 m/s.
20	Communication failure for 0.7 sec and lead vehicle brakes at t=0 sec with $a_{L,x,ref}$ = -4 m/s^2 without any preceding vehicle in front of it.
21	Communication failure for 0.7 sec and lead vehicle brakes at t=0 sec with $a_{L,x,ref}$ = -6 m/s^2 without any preceding vehicle in front of it.
22	Communication failure for 0.7 sec and lead vehicle brakes at t=0.5 sec with $a_{L,x,ref}$ = -6 m/s^2 without any preceding vehicle in front of it.
23	Communication failure for 0.7 sec and lead vehicle brakes at t=0 sec with $a_{L,x,ref}$ = -6 m/s^2 with d_{LL} = 10 m and $\dot{d}_{LL}$ = -0.1 m/s.

Table E.1: Test cases for the communication failure scenario

Remark. Variable d_{LL} is the distance from the preceding vehicle to its preceding vehicle and $\dot{d}_{LL}$ is the derivative of d_{LL}. These variables are used to calculate a measure for the traffic density. The transition to Collision Avoidance is made faster in case of heavy traffic, e.g. a low d_{LL}. Variable $a_{L,x,ref}$ is reference acceleration of the lead vehicle at the moment it starts to brake.

Appendix F

Finite time stability

In this appendix the principle of finite time stability (FTS) will be discussed. Finite time stability prescribes (time dependent) bounds which the system should not exceed within a certain time window. Hence the FTS stability concept is independent from the Lyapunov Asymptotic Stability (LAS) concept. FTS allows the system to be not LAS, as long as it does not exceed the prescribed bounds. Conversely, LAS does not guarantee FTS, because it does not guarantee that the state trajectories will remain within the prescribed bounds. Although the FTS concept can incorporate time varying and uncertain systems, a time invariant and linear system will be considered in this chapter for simplicity:

$$\begin{aligned} \dot{x}(t) &= Ax(t) + Bu(t), \\ y(t) &= Cx(t), \end{aligned} \tag{F.1}$$

where $x(t)$ is the state vector, $u(t)$ the input and $y(t)$ the output vector. For the analysis and controller design Linear Matrix Inequalities (LMI's) are used. The LMI's are solved using the Matlab Robust Control Toolbox. The Euclidean vector norm is denoted by $|\cdot|$.

Over the years several definitions of FTS are used. In Section F.1 definitions and lemmas are given to arrive at a theorem for FTS of a system. This theorem will be used for the controller design. In Section F.2 design of a state feedback controller will be presented, which finite time stabilizes the system. To find a controller for the continuous system, a set of Differential Linear Matrix Inequalities (DLMI's) should be solved. These cannot be solved by the solver, hence the same theory is derived for discrete time systems in Sections F.3 and F.4. For the discrete time system we end up with a set of LMI's, which can be solved by the solver. Finally in Section F.5 a numerical example is presented.

F.1 System analysis

This section will derive a theorem which proves a system to be FTS. Although the FTS concept can incorporate time varying and uncertain systems, this section will for simplicity consider a linear time invariant system of the form

$$\dot{x}(t) = Ax(t), \quad x(0) = x_0, \quad t \in [0, T]. \tag{F.2}$$

Definition F.1.1. (From [9], Definition 1)
The linear system (F.2) is said to be FTS with respect to (T,δ,$\gamma(t)$) if and only if

$$|x_0| \leq \delta \Rightarrow |x(t)| < \gamma(t) \quad \forall t \in [0, T]. \tag{F.3}$$

□

Remark. Constraint $\gamma(t)$ is a continuous function, which gives the bound $|x(t)|$ should not exceed. Note that Definition F.1.1 is implies that $\delta < \gamma(0)$.

Definition F.1.1 defines FTS in the simplest form. Given some bounds for the Euclidean norm of the initial states, the Euclidean norm of the states in a certain time window should remain within some other bound. Instead of simply calculating the Euclidean norm, a weighting matrix can be added to weight the states differently:

Definition F.1.2. (From [8], Definition 1)
Given three positive scalars (c_1,c_2,T), with $c_1 < c_2$ and a positive definite weighting matrix $\Gamma(t)$, system F.2 is said to be FTS with respect to (c_1,c_2,T,$\Gamma(t)$), if and only if

$$x_0^T \Gamma(0) x_0 \leq c_1 \Rightarrow x^T(t)\Gamma(t)x(t) < c_2, \quad \forall t \in [0,T]. \tag{F.4}$$

□

Remark. Note that if $\Gamma(t) = I$, Definition F.1.1 and Definition F.1.2 are equivalent by choosing $c_1 = \delta^2$ and $c_2 = \gamma^2$.

Because the constraints on one state can be more important than the constraints on another state, the weighting matrix can be very useful. Since Definition F.1.2 adds the functionality of a time dependent weighting matrix $\Gamma(t)$, Definition F.1.2 will be used for further analysis. Before continuing, first the state transition matrix is defined as

$$\Phi(t,0) = \frac{x(t)}{x_0}. \tag{F.5}$$

Remark. Since $x_0 = x(0)$, $\Phi(0,0) = I$.

With the state transition matrix, it is straightforward to derive the following definition for FTS.

Lemma F.1.1. (From [8], Theorem 1 ii)
System (F.2) is said to be FTS wrt (c_1,c_2,T,$\Gamma(t)$), if and only if

$$\Phi^T(t,0)\Gamma(t)\Phi(t,0) < \frac{c_2}{c_1}\Gamma(0) \quad \forall t \in [0,T]. \tag{F.6}$$

□

Another definition for FTS given in [8] is less straightforward.

Lemma F.1.2. (From [8], Theorem 1 iv)
System (F.2) is said to be FTS wrt (c_1,c_2,T,$\Gamma(t)$) if and only if the differential Lyapunov inequality

$$\dot{P}(t) + A^T P(t) + P(t)A < 0 \quad \forall t \in [0,T] \tag{F.7a}$$

$$P(t) > \Gamma(t) \quad \forall t \in [0,T] \tag{F.7b}$$

$$P(0) < \frac{c_2}{c_1}\Gamma(0) \tag{F.7c}$$

admits a piecewise continuously differentiable symmetric solution to $P(\cdot)$ The proof for this Lemma follows. □

Proof. (This proof is derived from [7], p.13)
Let us consider $V(t,x) = x^T(t)P(t)x(t)$. Given a system trajectory $x(\cdot)$, the time derivative of $V(t,x)$ reads by applying the chain rule and $\dot{x} = Ax$

$$\dot{V}(t,x) = x^T(t)\Big(\dot{P} + A^T P(t) + P(t)A\Big)x(t), \tag{F.8}$$

which is negative definite according to F.7a. This implies that $V(t,x)$ is strictly decreasing along the trajectories of the system. With an initial state x_0 such that $x_0^T \frac{c_2}{c_1}\Gamma(0)x_0 \leq 1$, this results in:

$$x^T(t)\Gamma(t)x(t) < x^T(t)P(t)x(t), \quad \forall t \in [0,T] \quad \text{by (F.7b)} \tag{F.9a}$$

$$< x_0^T P(0) x_0, \tag{F.9b}$$

$$< x_0^T \frac{c_2}{c_1}\Gamma(0)x_0 \leq 1, \quad \forall t \in [0,T] \quad \text{by (F.7c)} \tag{F.9c}$$

This implies that system (F.2) is FTS wrt (c_1,c_2,T,$\Gamma(t)$) for all $t \in [0,T]$ □

Lemma F.1.2 can be written in a different form, following the methodology used in [32].

Theorem F.1.1. (From [8] (19))
System (F.2) is said to be FTS wrt (c_1,c_2,T,$\Gamma(t)$) for all $t \in [0,T]$, if and only if the differential Lyapunov inequality:

$$-\dot{Q}(t) + AQ(t) + Q(t)A^T < 0, \quad t \in [0,T] \tag{F.10a}$$

$$Q(t) < \Gamma^{-1}(t) \quad \forall t \in [0,T] \tag{F.10b}$$

$$Q(0) > \frac{c_1}{c_2}\Gamma^{-1}(0) \tag{F.10c}$$

admits a piecewise continuously differentiable symmetric solution to $Q(\cdot)$. The proof follows. □

Proof. Given is the DLMI in Lemma F.1.2. Let $Q(t) = P^{-1}(t)$ and pre and post-multiply (F.7a) by $Q(t)$, taking into account that $\dot{Q}(t) = -P^{-1}(t)\dot{P}(t)P^{-1}(t)$, Theorem F.1.1 is obtained. □

Lemma F.1.1 is useful for system analysis, however it cannot be used for design purposes since it puts constrains on trajectories instead of system state matrices. Therefore Theorem F.1.1, which is equivalent to Lemma F.1.2, will be used for the controller design. The form of Theorem F.1.1 has some advantages in understanding the physical meaning of the inequalities compared to Lemma F.1.2, as will be shown in the following corollary

Corollary F.1.1. The transition matrix $\Phi(t,0)$ solves the matrix-valued differential equation:

$$\frac{\partial}{\partial t}\Phi(t,0) = A\Phi(t,0), \quad \forall t \in [0,T], \quad \Phi(0,0) = I, \tag{F.11}$$

and by choosing

$$W(t) = \Phi(t,0)\frac{c_1}{c_2}\Gamma^{-1}(0)\Phi^T(t,0), \quad \forall t \in [0,T], \tag{F.12}$$

it follows that $W(t)$ is symmetric, positive definite and

$$-\dot{W}(t) + AW(t) + W(t)A^T = 0, \quad \forall t \in [0,T]. \tag{F.13a}$$

$$W(0) = \frac{c_1}{c_2}\Gamma^{-1}(0) \tag{F.13b}$$

Remark. By choosing $\frac{c_1}{c_2}\Gamma^{-1}(0) = x_0x_0^T$, $W(t) = x(t)x^T(t)$.

Note that $W(t)$ in equalities (F.13) is closely related to the inequalities in Theorem F.1.1. How they relate will be shown following the methodology in [7] p.13-14.

Theorem F.1.1 gives a sufficient condition for FTS of System (F.2) wrt (c_1,c_2,T,$\Gamma(t)$). If FTS of this system is proven, there exists a real scalar $\epsilon > 0$ such that the system

$$\dot{x}(t) = \big(A + \frac{\epsilon}{2}I\big)x(t), \tag{F.14}$$

is FTS wrt (c_1,c_2,T,$\Gamma(t)$). Using (F.14) in (F.13), and by taking $W = \frac{1}{\alpha}Q$, where $\alpha > 1$, results in the following equalities:

$$-\dot{Q}(t) + AQ(t) + Q(t)A^T + \epsilon Q(t) = 0, \quad t \in [0,T]. \tag{F.15a}$$

$$\frac{1}{\alpha}Q(0) = \frac{c_1}{c_2}\Gamma^{-1}(0) \tag{F.15b}$$

Taking into account that $\alpha > 1$, that $\epsilon > 0$ and the positive definiteness of $W(t)$ and thereby $Q(t)$, this results in the inequalities of Theorem F.1.1. For $\alpha \to 1$ and $\epsilon \to 0$, the limits of the DLMI's in Theorem F.1.1 are exploited and $Q(t) \to W(t)$ □

F.2 State feedback controller design

This section will provide a sufficient and necessary condition for a state feedback controller that finite time stabilizes the System (F.1). The conditions are based on Theorem F.1.1. For state feedback, the following holds for the system input

$$u(t) = K(t)x(t), \tag{F.16}$$

where $K(t)$ is a row vector where each entry corresponds to a feedback gain for an individual state. Because of (F.16), System (F.1) can be rewritten as

$$\dot{x}(t) = (A + BK(t))x(t) \tag{F.17}$$

As in [12] a new variable matrix $L(t)$ is defined, where $L(t) = K(t)Q(t)$. Hence Theorem F.1.1 can be rewritten for state feedback as:

Theorem F.2.1. System (F.17) with state feedback is FTS wrt (c_1,c_2,T,$\Gamma(t)$), if and only if there exists a piecewise continuously differentiable symmetric matrix-valued function $Q(\cdot)$ and a continuous matrix valued function $L(\cdot)$ that satisfies the DLMI problem with initial and terminal conditions:

$$-\dot{Q}(t) + AQ(t) + Q(t)A^T + L^T(t)B^T + BL(t) < 0, \quad \forall t \in [0, T] \tag{F.18a}$$

$$Q(t) < \Gamma^{-1}(t), \quad \forall t \in [0, T] \tag{F.18b}$$

$$Q(0) > \frac{c_1}{c_2}\Gamma^{-1}(0) \tag{F.18c}$$

With the controller gains equal to:

$$K(t) = L(t)Q^{-1}(t) \tag{F.19}$$

□

F.3 Discrete time system analysis

In the previous sections a theorems for FTS of a linear time invariant system and state feedback controller design are presented. These theorems include continuous time DLMI's. To make them solvable by a LMI solver, the equations have to be discretized. In [7] p.15 the continuous system matrices are used and the optimization matrices are assumed to be piecewise linear. This method is accurate if a low sample time is selected. Consequently the number of LMI's increases drastically, making the set of LMI's unsolvable by the solver. Hence the sample time should be increased, making the piecewise linear optimization matrices assumption inaccurate. Therefore the system is discretized. Following the methodology of the previous sections, theorems for FTS of discrete time systems are given. The method is based on [7] Chapter 5.

A discrete time linear time invariant system will be considered of the form

$$x(k+1) = A_d x(k), \quad x(k_0) = x_0, \tag{F.20}$$

where A_d is the discretized state matrix, which can be obtained using the Matlab Control System Toolbox c2d command. For discrete FTS a lemma similar to Lemma F.1.1 can be stated.

Lemma F.3.1. (From [7] Theorem 5.1 ii)
System (F.20) is said to be FTS wrt (c_1,c_2,N,$\Gamma(\cdot)$), if and only if

$$\Phi(k, k_0)^T \Gamma(k) \Phi(k, k_0) < \frac{c_2}{c_1}\Gamma(k_0) \quad k \in [k_0, k_0 + 1, ..., N]. \tag{F.21}$$

□

Compared to Lemma F.1.1, c_1, c_2 and $\Gamma(\cdot)$ have the same meaning. The time window T is replaced by a number of points N. Variable $\Phi(\cdot, k_0)$ denotes the state transition matrix of System (F.20).

Now a theorem similar to Theorem F.1.1 will be stated.

Theorem F.3.1. (From [7] Theorem 5.1 iv)
System (F.20) is said to be FTS wrt (c_1,c_2,N,$\Gamma(\cdot)$), if and only if there exists a symmetric real valued matrix Q such that

$$A_d Q(k) A_d^T - Q(k+1) < 0, \quad k \in [k_0, k_0+1, ..., N-1], \tag{F.22a}$$

$$Q(k) < \Gamma^{-1}(k), \quad k \in [k_0+1, k_0+2, ..., N], \tag{F.22b}$$

$$Q(k_0) > \frac{c_1}{c_2}\Gamma^{-1}(k_0) \tag{F.22c}$$

The proof follows. □

Proof. (From [7] p.56-58)
Since $\Gamma(\cdot)$ should be a positive definite symmetric matrix function, there always exists a solution to $T^T(\cdot)T(\cdot) = \Gamma(\cdot)$. Moreover a matrix $R = \frac{c_2}{c_1}\Gamma(k_0)$ is defined. From Lemma F.3.1 the following holds for $k \in [k_0, k_0+1, ..., N]$.

$$\begin{aligned}
&\Phi^T(k,k_0)\Gamma(k)\Phi(k,k_0) - R < 0 \\
&\Leftrightarrow \Phi^T(k,k_0)T^T(k)T(k)\Phi(k,k_0) - R < 0 \\
&\Leftrightarrow R^{-1/2}\Phi^T(k,k_0)T^T(k)T(k)\Phi(k,k_0)R^{-1/2} - I < 0 \\
&\Leftrightarrow T(k)\Phi(k,k_0)R^{-1}\Phi^T(k,k_0)T^T(k) - I < 0
\end{aligned} \tag{F.23}$$

Let

$$Q(k) = \Phi(k,k_0)R^{-1}\Phi^T(k,k_0) \tag{F.24}$$

From (F.23) and (F.24) follows directly (F.22b). Noticing that $\Phi(k_0,k_0) = I$, it follows that

$$Q(k_0) = R^{-1} = \frac{c_1}{c_2}\Gamma(k_0)^{-1} \quad k \in [k_0, k_0+1, ..., N]. \tag{F.25}$$

For System (F.20) the following can be written:

$$\Phi(k+1,k_0) = A_d\Phi(k,k_0). \tag{F.26}$$

By applying (F.24) and (F.26), it follows that

$$Q(k+1) = A_d Q(k) A_d^T \tag{F.27}$$

Equalities (F.27) and (F.25) can be replaced by the inequalities (F.22a) and (F.22c) following the methodology applied to the continuous system in Corollary F.1.1. □

For output feedback an alternative notation for Theorem F.3.1 will turn out to be useful. Applying Schur compliments, (F.22a) can equivalently be written as:

$$\begin{bmatrix} -Q(k+1) & A_d P(k) \\ Q(k)A_d^T & -Q(k) \end{bmatrix} < 0. \tag{F.28}$$

By pre- and post multiplying inequality (F.28) by

$$\begin{bmatrix} Q^{-1}(k+1) & 0 \\ 0 & Q^{-1}(k) \end{bmatrix}, \tag{F.29}$$

(F.28) can be written as

$$\begin{bmatrix} -Q^{-1}(k+1) & Q^{-1}(k)A_d \\ A_d^T Q^{-1}(k+1) & -Q^{-1}(k) \end{bmatrix} < 0. \tag{F.30}$$

By applying the Schur compliment again, and taking $P(\cdot) = Q^{-1}(\cdot)$, (F.22a) can equivalently be written as:

$$A_d^T P(k) A_d - P(k+1) < 0, \quad k \in [k_0, k_0+1, ..., N-1]. \tag{F.31}$$

Now a theorem equivalent to Theorem F.3.1 can be stated, with $P(\cdot) = Q^{-1}(\cdot)$.

Theorem F.3.2. (From [7] Theorem 5.1 v)
System (F.20) is said to be FTS wrt (c_1,c_2,N,$\Gamma(\cdot)$), if and only if there exists a symmetric real valued matrix Q such that

$$A_d^T P(k) A_d - P(k+1) < 0, \quad k \in [k_0, k_0+1, ..., N-1], \tag{F.32a}$$
$$P(k) > \Gamma(k), \quad k \in [k_0+1, k_0+2, ..., N], \tag{F.32b}$$
$$P(k_0) < \frac{c_2}{c_1}\Gamma(k_0) \tag{F.32c}$$

By writing the Theorem in this form, the applicability of the theorem can be proven alternatively, as will be shown in the following proof. □

Proof. (This proof is derived from [7], p.58)
Consider a quadratic Lyapunov function $x^T(k)P(k)x(k)$, where $P(\cdot) = Q^{-1}(\cdot)$. For a given state variable trajectory the Lyapunov difference $\Delta V(x,k)$ reads:

$$\begin{aligned} \Delta V(x,k) &= V(x,k+1) - V(x,k) \\ &= x^T(k+1)P(k+1)x(k+1) - x^T(k)P(k)x(k) \\ &= x^T(k)\Big(A_d^T P(k+1)A_d - P(k)\Big)x(k), \end{aligned} \tag{F.33}$$

which is negative definite since (F.32a) holds. This implies that $V(x,k)$ is strictly decreasing along the trajectories of System (F.20). With an initial state x_0 such that $x_0^T \frac{c_2}{c_1}\Gamma(k_0)x_0 \leq 1$, this results for all $k \in [k_0, k_0+1, ..., N]$ in:

$$xT(k)\Gamma(k)x(k) < x^T(k)P(k)x(k) \quad \text{by (F.32b)} \tag{F.34a}$$
$$< x_0^T P(k_0)x_0 \tag{F.34b}$$
$$< x_0^T \frac{c_2}{c_1}\Gamma(k_0)x_0 \leq 1 \quad \text{by (F.32c)} \tag{F.34c}$$

This implies that system (F.20) is FTS wrt (c_1,c_2,N,$\Gamma(k)$) for all $k \in [k_0, k_0+1, ..., N]$ □

F.4 Discrete time feedback controller design

This section will provide a sufficient and necessary condition for a state feedback controller that finite time stabilizes the discrete time System (F.20). The conditions are based on Theorem F.3.1.

For the state feedback case, A_d in System (F.2) is replaced by $A_d + B_d K_d(\cdot)$. $K_d(\cdot)$ is a row vector where each entry corresponds to a feedback gain for an individual state. B_d is the discretized input matrix.

$$x(k+1) = (A_d + B_d K_d(k))x(k) \tag{F.35}$$

As for the continuous system, a matrix $L(\cdot)$ is defined, where $L(\cdot) = K_d(\cdot)Q(\cdot)$. Hence Theorem F.3.1 can be rewritten for state feedback as:

Theorem F.4.1. (From [7] Theorem 5.)
A state feedback controller can finite time stabilize System (F.35) wrt (c_1,c_2,N,$\Gamma(\cdot)$), if and only if there exists a symmetric real valued matrix sequence $Q(\cdot)$ and a matrix sequence $P(\cdot)$, such that

$$\begin{bmatrix} -Q(k+1) & A_d Q(k) + B_d L(k) \\ Q(k)A_d^T + L^T(k)B_d^T & -Q(k) \end{bmatrix} < 0, \quad k \in [k_0, k_0+1, ..., N-1], \tag{F.36a}$$
$$Q(k) < \Gamma^{-1}(k), \quad k \in [k_0+1, k_0+2, ..., N], \tag{F.36b}$$
$$Q(k_0) > \frac{c_1}{c_2}\Gamma^{-1}(k_0) \tag{F.36c}$$

The proof follows. □

Proof. (This proof is derived from [7], p.59)
Note that (F.22a) can be written using Schur compliments:

$$\begin{bmatrix} -Q(k+1) & A_d Q(k) \\ Q(k)A_d^T & -Q(k) \end{bmatrix} \tag{F.37}$$

By replacing A_d by $A_d + B_d K_d(k)$ and $K_d(k)Q(k)$ by $L(k)$, Theorem F.4.1 is obtained. □

F.5 Numerical example

This section will show an example of a FTS approach applied to lateral evasive manoeuvring control of a vehicle. Consider a simple 4 state bicycle vehicle model with an additional state for the steering actuator. The system is written in state space notation

$$\dot{x}(t) = Ax(t) + Bu(t). \tag{F.38}$$

The system state vector $x(t)$ consists out of the lateral velocity $v_y(t)$, yaw rate $\dot{\phi}(t)$, lateral position $y(t)$, heading angle $\phi(t)$ and steering angle $\delta(t)$. The derivation of this model can be found in e.g. [19] Appendix A. The used parameter values are shown in Table F.1.

$$\begin{bmatrix} \dot{v_y} \\ \ddot{\phi} \\ \dot{y} \\ \dot{\phi} \\ \dot{\delta} \end{bmatrix} = \begin{bmatrix} -\frac{C_f+C_r}{v_x m} & -\frac{aC_f-bC_r}{v_x m} - v_x & 0 & 0 & \frac{C_f}{m} \\ -\frac{aC_f-bC_r}{v_x I_{zz}} & -\frac{a^2C_f+b^2C_r}{v_x I_{zz}} & 0 & 0 & \frac{aC_f}{I_{zz}} \\ 1 & 0 & 0 & v_x & 0 \\ 0 & 1 & 0 & 0 & 0 \\ 0 & 0 & 0 & 0 & -\frac{1}{\tau_s} \end{bmatrix} \begin{bmatrix} v_y \\ \dot{\phi} \\ y \\ \phi \\ \delta \end{bmatrix} + \begin{bmatrix} 0 \\ 0 \\ 0 \\ 0 \\ \frac{1}{\tau_s} \end{bmatrix} u, \quad x_0 = \begin{bmatrix} 10^{-6} \\ 10^{-6} \\ 3.5 \\ 10^{-6} \\ 10^{-6} \end{bmatrix} \tag{F.39}$$

The initial states correspond to an error in y of $3.5m$ initially. This corresponds to the lane width on

Parameter	Value	Unit
m	1200	kg
a	0.92	m
b	1.38	m
C_f	120000	N/rad
C_r	80000	N/rad
v_x	20	m/s

Table F.1: Vehicle model parameters

the road. The vehicle is assumed to be in steady state, meaning that all other states should be (close to) 0. Since the constraint matrix should be invertible, the initial states are chosen to be not exactly 0.

The vehicle model is discretized applying the zero-order hold (zoh) method with a sample time $T_s = 0.05s$. The obtained matrices A_d and B_d are used into the set of LMI's of Theorem F.4.1 (F.36a). For (F.36b) the following is used:

$$C(k)C^T(k) = \Gamma(k), \quad k \in [k_0+1, k_0+2, ..., N] \tag{F.40}$$

Hence (F.36b) can be written as:

$$\begin{aligned} Q(k) &< \Gamma^{-1}(k), \quad k \in [k_0+1, k_0+2, ..., N] \\ C^T(k)Q(k)C(k) &< I, \quad k \in [k_0+1, k_0+2, ..., N] \end{aligned} \tag{F.41}$$

For the evasive manoeuvre, two constraints are posed on the system. First one for the lateral position and the second one for the maximum steering angle. Limiting the steering angle will indirectly constrain the lateral acceleration to prevent the vehicle for a roll-over. Since these constraints are fully independent, the constraint is split into two weighting matrices: $\Gamma_1(k)$ and $\Gamma_2(k)$. Following the methodology in (F.40), the weighting matrices can be split into $C_1(k)$ and $C_2(k)$. The first matrix poses an exponential constraint on the lateral position:

$$C_1(k) = diag\left(10^{-6}, 10^{-6}, \frac{1}{y_{max}} e^{\frac{kT_s}{\gamma}}, 10^{-6}, 10^{-6}\right), \quad k \in [k_0+1, k_0+2, ..., N]. \tag{F.42}$$

The parameter y_{max} and γ are tunable parameters and are set to 30 and 0.5 respectively. The second constraint C_2 poses a constraint on the steering angle.

$$C_2 = diag\left(10^{-6}, 10^{-6}, 10^{-6}, 10^{-6}, \frac{1}{\delta_{max}}\right), \quad k \in [k_0+1, k_0+2, ..., N]. \tag{F.43}$$

Tunable parameter δ_{max} is chosen to be 0.66rad, which would result in a steady state lateral acceleration of 2.5m/s^2.

For the third inequality in Theorem F.4.1 (F.36c), the following is defined:

$$R^{-1} = \frac{c_1}{c_2}\Gamma^{-1}(k_0) \tag{F.44}$$

and

$$R = diag(1./x_0)diag(1./x_0)^T. \tag{F.45}$$

Hence (F.36c) can alternatively be written as:

$$\begin{aligned} Q(k_0) &> \frac{c_1}{c_2}\Gamma^{-1}(k_0) \\ Q(k_0) &> R^{-1} \\ diag(x_0)^T Q(k_0) diag(x_0) &> I \end{aligned} \tag{F.46}$$

The LMI's are solved using the Matlab Robust Control Toolbox, using a horizon of $3s$ ($N = 61$). The calculated per state controller gains $K_d(k)$ are shown in Fig F.1. These controller gains are first applied to

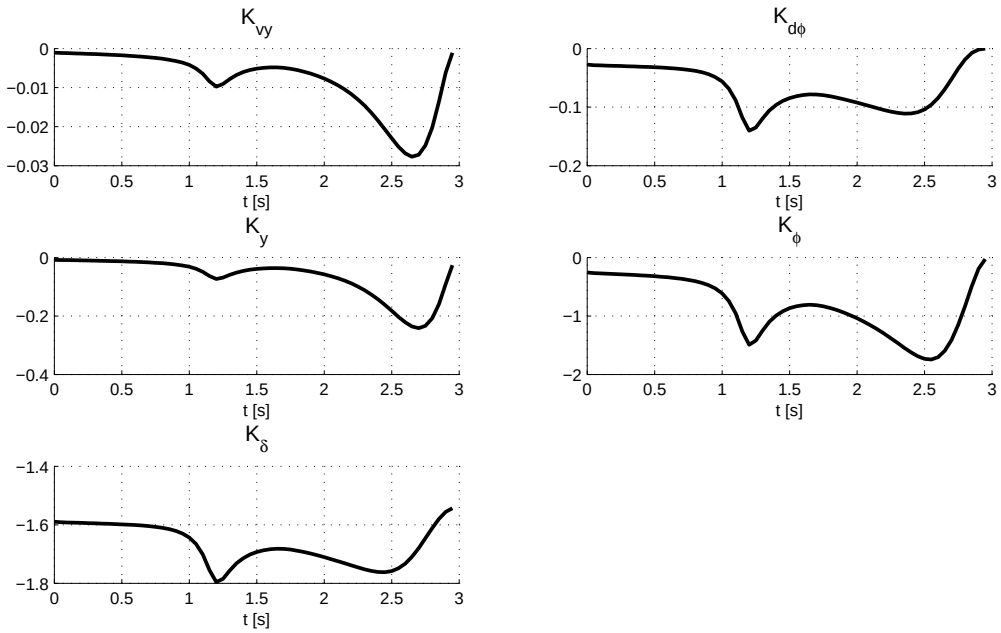

Fig F.1: Control gains for state feedback for System (F.35)

the discrete time system. The response is depicted by the blue line in Fig F.2. Some slight deviations are shown applying the same gains to the continuous system, represented by the red line. The deviations will become smaller when reducing the sample time of the discrete time system. However this will increase the number of LMI's, making the set of LMI's unsolvable by the solver.

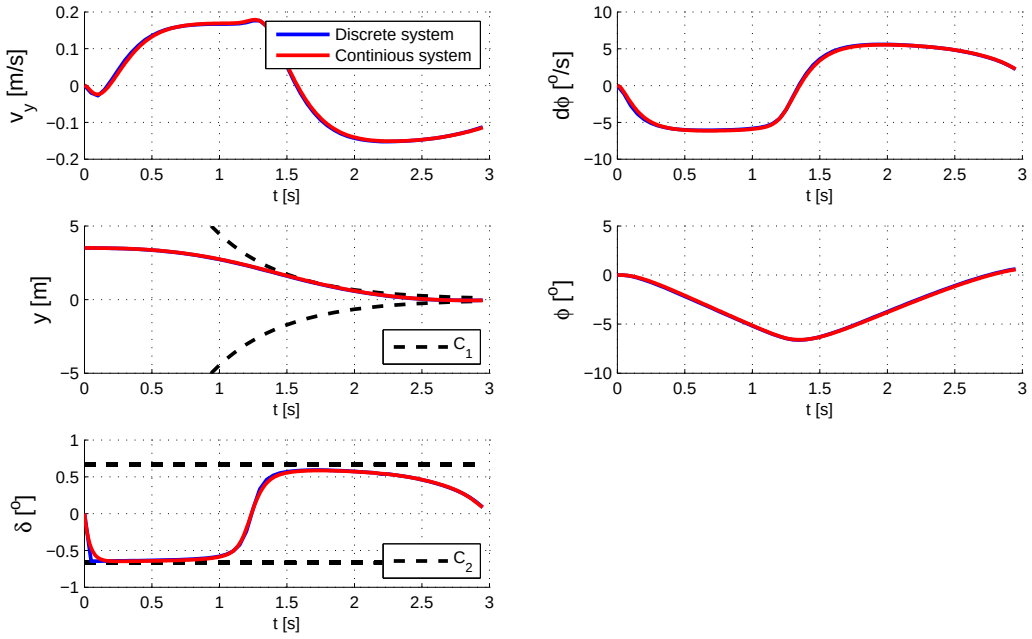

Fig F.2: System state variable response applying the control gains in Fig F.1

Appendix G

Sliding mode controller background

This appendix will elaborate on the Sliding Mode Control (SMC) concept for lateral collision avoidance. In SMC, a discontinuous control law is chosen such that all trajectories converge towards the sliding surface in finite time, and remain on the surface afterwards. This principle is illustrated in Fig G.1. The control law could look like:

$$u_y(t) = -u_{y,lim}\text{sign}(s_y(t)) \tag{G.1}$$

where u_y is the control variable and $u_{y,lim}$ the limit on the control input. On both sides of the surface maximum control effort is applied to direct the trajectories in finite time to the surface. The control variable could be for instance the steering angle. In ideal SMC the trajectories will start to slide on the surface once they hit the surface. However, actuator dynamics and time delays will prevent the system from ideal sliding. Instead, the trajectories will start chattering around the surface within a region around the surface. The limits of the chattering region should remain within prescribed bounds, as for FTS.

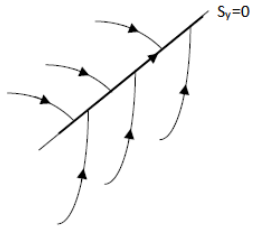

Fig G.1: The sliding mode of a system: all trajectories converge to the sliding surface [57]

.

Main difficulty is finding an appropriate sliding surface that can be reached by the control input u_y, and can be followed once the trajectories hit the surface. Moreover, the lateral acceleration limit to prevent the vehicle for a roll-over should not be exceeded. In [23] a SMC approach for collision avoidance purposes is proposed with a linear surface. However, a linear surface will not constrain the lateral acceleration, and hence prevent roll-overs. The sliding surface could also be non-linear, for instance:

$$s_y(t) = \dot{y}(t) + \beta\sqrt{y(t)}, \tag{G.2}$$

which is illustrated by the solid line in Fig G.2 and describes a constant lateral acceleration $\bar{a}_y$ surface, with

$$\beta = \sqrt{|2\bar{a}_y|}\text{sign}(\bar{a}_y). \tag{G.3}$$

The constant acceleration could be the roll-over constraint of the vehicle. However, this constraint is only valid on the sliding surface. In the reaching phase, the lateral acceleration is only limited by the control input. The control limit $u_{y,lim}$ in control law (G.1) should however be chosen as large as possible to follow the constant acceleration trajectory once the trajectories reach the surface. These are two contradictory requirements. Alternatively, the sliding surface can be constructed out of the segments,

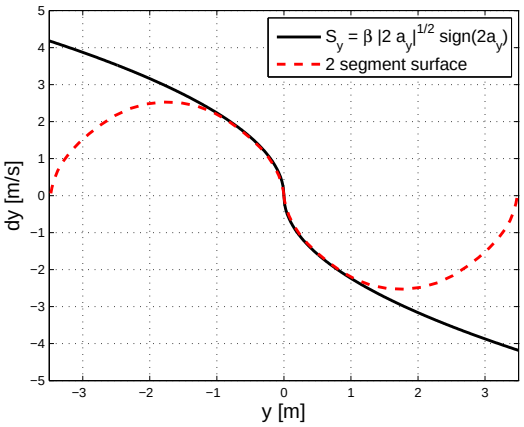

Fig G.2: Non-linear second order manifold and the two segment constant acceleration manifold

which is illustrated by the dotted line in Fig G.2. This will limit the duration of the reaching phase, such that sliding occurs faster. The result is a surface consisting out of two constant acceleration segments. However, as mentioned in Section 4.2.3 are constant acceleration profiles not feasible to follow by vehicles. Alternatively, a constant acceleration surface with limited jerk can be constructed. Before elaborating on this, first look at the sliding behaviour on a constant acceleration surface. On the sliding surface, s_y is zero. To remain on the surface, $\dot{s}_y$ should be 0. From (G.2) the derivative of the sliding variable can be determined:

$$\dot{s}_y(t) = \ddot{y}(t) + \frac{\beta}{2}\frac{\dot{y}(t)}{\sqrt{y(t)}}. \tag{G.4}$$

Substitution of System (6.4) into (G.4) and choosing s_y to be zero, results in the following equation for the control input on the sliding surface:

$$\delta_{eq}(t) = -\frac{1}{b_1 + l_s b_2}\left(f_1\left(v_y(t), \dot{\Phi}(t), \dot{\phi}(t), \phi(t)\right) + \frac{\beta}{2}\frac{\dot{y}(t)}{\sqrt{y(t)}}\right). \tag{G.5}$$

When choosing control input u_y to be the steering angle, the steering angle in (G.5) is also referred as equivalent control input: the required control effort on the sliding surface to remain on the sliding surface. Equivalent control is the effective control effort applied by the discontinuous control law (G.1). But as can be seen from (G.5), contains the equivalent control equation a term $\dot{y}/\sqrt{y}$. This results in high gains around the origin. For an ideal system without actuator dynamics or time delay this is not a problem. However, for a system with time delay or actuator dynamics this will introduce severe chattering.

In the previous paragraph, the need for different segments in the sliding surface was stated. The non-linear surface caused severe chattering due to time delay and actuator dynamics. A linear surface can not incorporate the lateral acceleration constraints. An equivalent approach is a path generator, generating a path which should be followed. This circumvents the problem of big initial condition errors and hence a long reaching phase; consequently a linear surface can be applied. In that case the surface is a function of error coordinates instead of absolute coordinates:

$$s_y(t) = \dot{y}_e(t) + k_y y_e(t), \tag{G.6}$$

where error coordinate y_e is defined as:

$$y_e(t) = y(t) - y_{ref}(t), \tag{G.7}$$

where y is the lateral position of the vehicle and y_{ref} the reference position determined by the path generator. The path generator is part of the Situation Awareness block and is discussed in Appendix C. The previous discussion showed the potential of SMC and its limitations. Part of the limitations of SMC can be circumvented by adding a path generator to the controller design. Requirement is of course that the error to the path can be measured or calculated.

Appendix H

Uncertainty analysis for the lateral SMC

This appendix shows a simulation study of the lateral SMC. The controller is applied to the linear lateral vehicle model presented in Section 3.2.2. The model parameters are shown in Appendix A.1 and the SMC parameters in Table 6.2. Note that all time delays are neglected. First the nominal system behaviour will be discussed. Then the influence of system uncertainties, initial errors and sensor noise is investigated. Finally, a brief analysis of the actuator delay influence will be shown.

Nominal behaviour

Fig H.1 shows the behaviour of the nominal system for a lane change. The top left plot shows the reference and actual value for the lateral position, the top right plot the lateral acceleration, the bottom right plot the sliding variable and the bottom right plot the reference steering angle. The sliding variable stays well within the boundary layer during the manoeuvre, implying the limited jerk path is tracked sufficiently accurate.

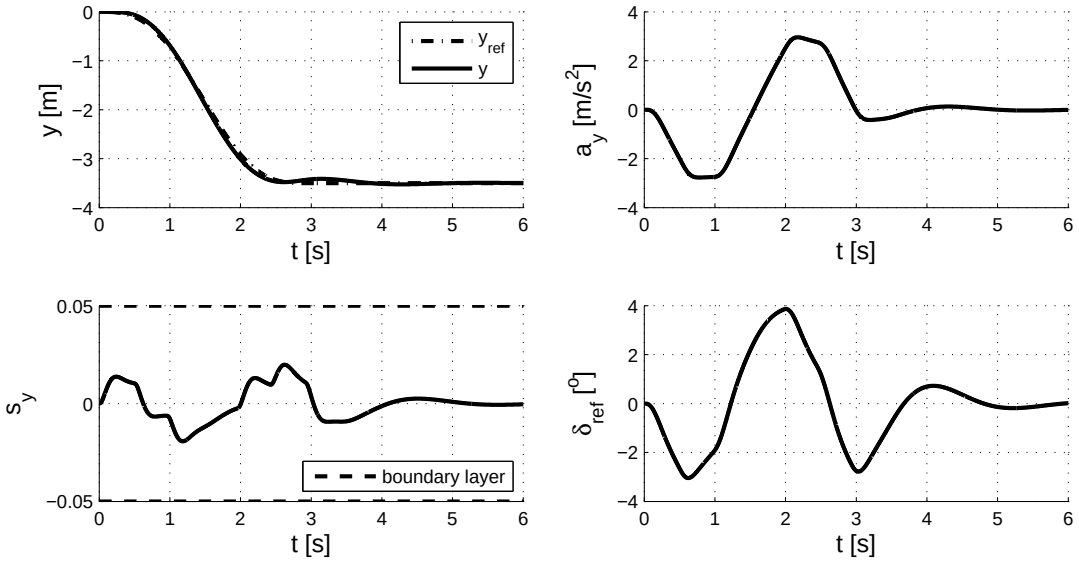

Fig H.1: Simulation results of a lane change with the nominal system

Uncertain normalized cornering stiffness

Fig H.2 shows the same plot as in the previous paragraph, but now for a system with uncertain parameters. The blue line represents the system behaviour for a normalized cornering stiffness of 25% of the nominal value; the red line for 200%. Both track the desired path. However, for a low normalized cornering stiffness the sliding variable exceeds the limits of the defined boundary layer. Moreover, the sliding variable deviations become larger in the second part of the manoeuvre. This implies the system is not able to settle in between the constant jerk path segments. Actuator dynamics, which were neglected in the design phase are causing this behaviour. Increasing the boundary layer or decrease the jerk limit in the path generator are possible solutions. However, this would increase the transition time of the manoeuvre. Alternatively, the steering rate limit can be increased in case this is possible within the steering actuator constraints.

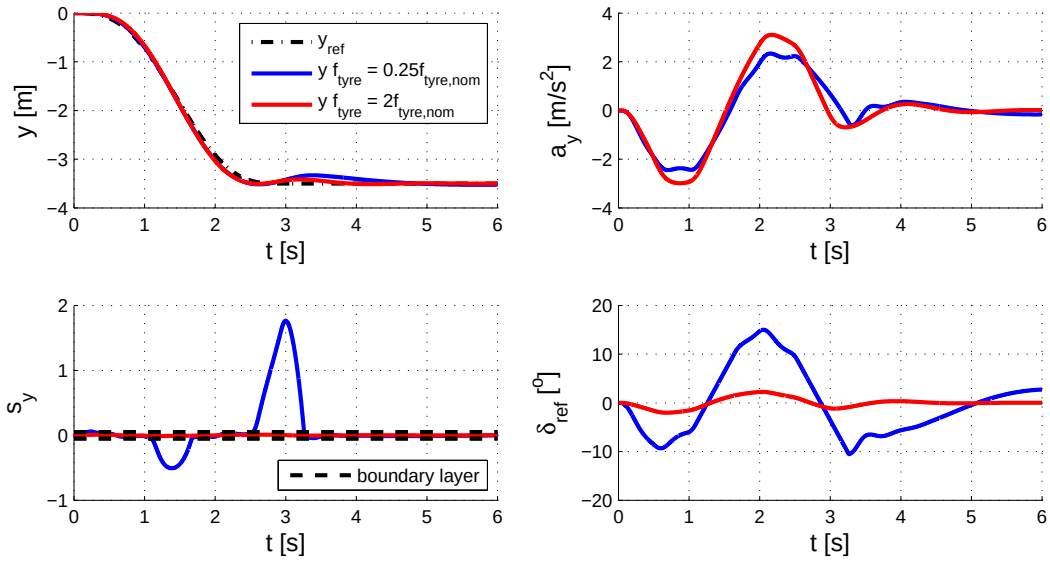

Fig H.2: Simulation results of uncertain system parameters

Initial errors

The system behaviour with an initial position error of 30cm is shown in Fig H.3. The sliding variable in the bottom left plot convergences quickly to the boundary layer. The lateral position in the top left plot requires more time to converge to zero. Because the surface poles λ_y in (6.12) are chosen to respond slow, the trajectories converge slowly to the origin on the sliding surface. However, a faster surface would lead to unstable behaviour since the vehicle dynamics are relatively slow.

Sensor noise

Gaussian sensor noise is added to the lateral vehicle position measurement. The noise has a standard deviation σ_y of 0.03rad/s with a sample time of 1ms. The controller behaviour is heavily influenced by this sensor noise. The system is still able to follow the reference path, although the sliding variable shows very noisy behaviour. Clearly, sensor noise is one of the most critical effects. Increasing the smoothing factor of the observer will result in better filtering properties. However, this would introduce additional phase lag possible resulting in an unstable system.

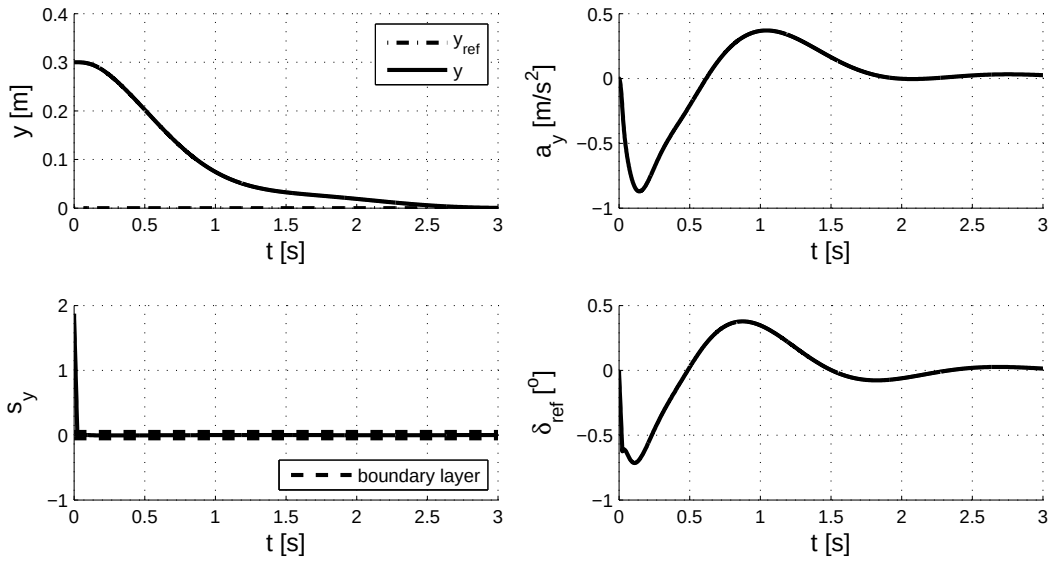

Fig H.3: Simulation of initial error response

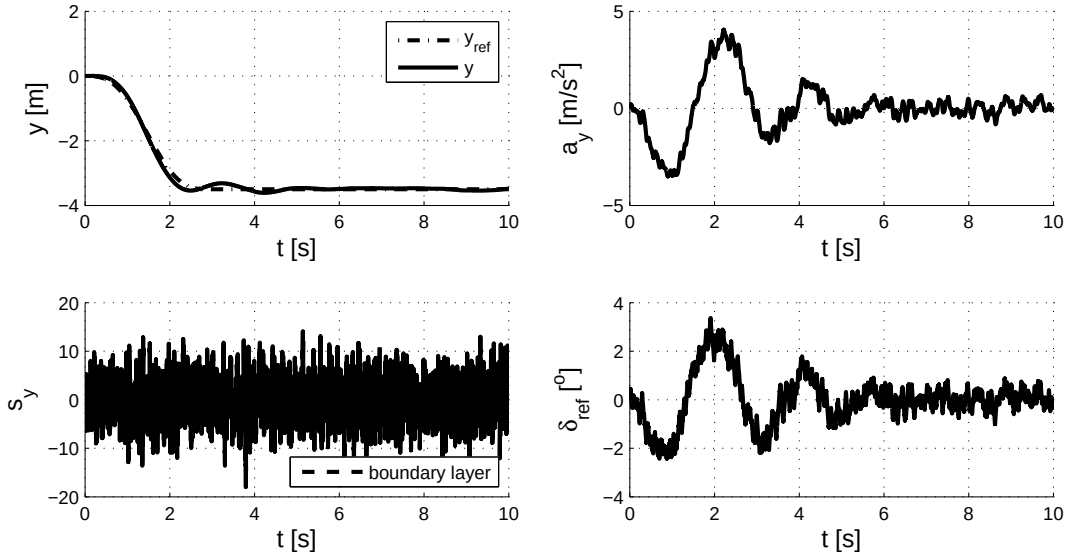

Fig H.4: Influence of sensor noise

Time delay

The previous simulations assumed the system without time delay. However, time delay is an important limiting factor for a SMC approach. This paragraph will concentrate on actuator delay and not measurement delay which is inherently present as well. Fig H.5 shows simulations with 5ms and 10ms steering actuator time delay. The path tracking for an actuator delay of 5ms still performs well. However, for 10ms actuator delay severe chattering occurs. Possibly a state predictor as proposed in [57] can be added to the controller design to compensate for the time delay. Alternatively, [53] uses a Kalman filter to estimate the lateral position from a lateral accelerometer and yaw rate sensor.

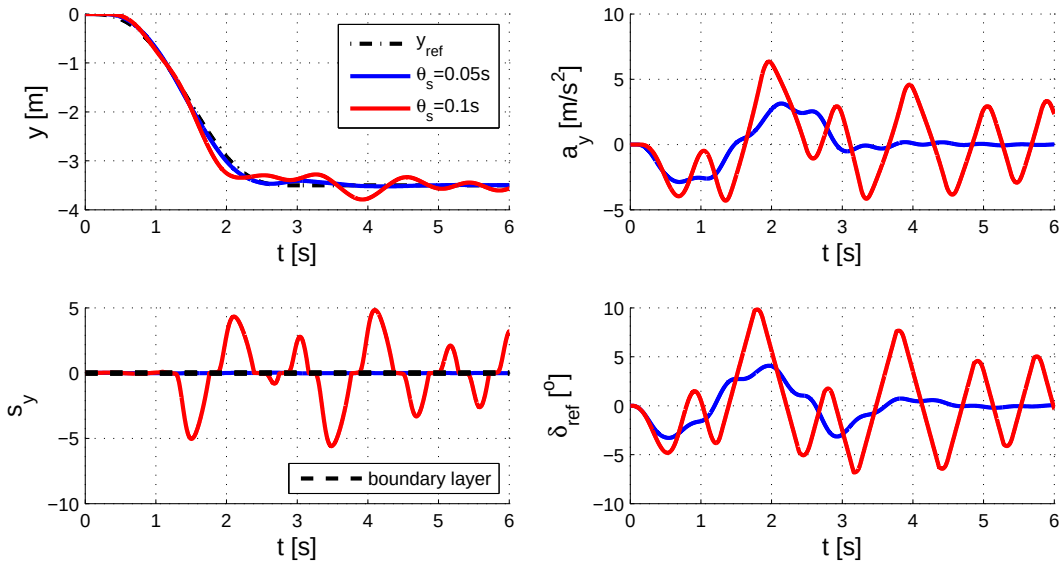

Fig H.5: Influence of steering actuator time delay